Numerical Investigation of Hydrogen Sonic Jet With Real Gas Model

Reza Khaksarfard

A Thesis

in

the Department

of

Mechanical and Industrial Engineering

Presented in Partial Fulfillment of the Requirements
for the Degree of Doctor of Philosophy (Mechanical Engineering) at
Concordia University
Montreal, Quebec, Canada

August 2011

CONCORDIA UNIVERSITY
SCHOOL OF GRADUATE STUDIES

This is to certify that the thesis prepared

By: **Reza KHAKSARFARD**

Entitled: **Numerical Investigation of Hydrogen Sonic Jet with Real Gas Model**

and submitted in partial fulfillment of the requirements for the degree of

Doctor of Philosophy (Mechanical Engineering)

Complies with the regulations of the University and meets the accepted standards with respect to originality and quality.

Signed by the final examining committee:

Dr. O. A. Mohamed	Chair
Dr. A. Straatman	External Examiner
Dr. R. Zmeureanu	External to Program
Dr. A. Dolatabadi	Examiner
Dr. H.D. Ng	Examiner
Dr. M. Paraschivoiu	Thesis Supervisor

Approved by _____
Chair of Department or Graduate Program Director

mm/dd/yyyy _____
Dean of Faculty

ABSTRACT

NUMERICAL INVESTIGATION OF HYDROGEN SONIC JET

WITH REAL GAS MODEL

Reza Khaksarfard

Hydrogen is combustible at a very wide range of concentration (4% - 75%) and may ignite by a small amount of energy. Furthermore, the small amount of energy per unit volume of hydrogen requires a very high pressure reservoir to have sufficient amount of fuel. This increases the risk of failure of the tank valve which can lead to the release of high pressure hydrogen and explosion. Therefore, safe storage of hydrogen is an issue if it is stored at high pressures. Sudden release of hydrogen from a high pressure tank is numerically investigated here-in by Computational fluid dynamics (CFD). A three dimensional in-house code is developed to simulate this flow. A transport equation is added to solve and find the concentration of Hydrogen-air mixture in the domain. A very small mesh, especially near the release area, is required to capture all the shocks and features of the flow, therefore parallel computation is used to overcome memory problems and to decrease the computation time. High pressure hydrogen requires a real gas equation of state to be accurate. Two equations of state, Beattie-Bridgeman and Abel-Noble are applied as the real gas equation. The results show that the real

gas model is necessary to accurately capture this flow. In reality, the release hole is not fixed and enlarges in time. In this work, a moving mesh is developed and used to enlarge the release area in time. The impact on the flow is analyzed. The boundaries of the release area move in time and all the nodes are moved accordingly based on the spring method to have a good mesh quality. The code is capable to solve the flow after sudden release which can help the industries to investigate different safety scenarios.

ACKNOWLEDGMENTS

I would like to thank my supervisor, Professor Marius Paraschivoiu for all his support and help throughout this research and also my friend, Doctor Kaveh Mohamed for all his suggestions.

TABLE OF CONTENTS

LIST OF FIGURES

LIST OF TABLES

LIST OF SYMBOLS

a	Sound speed
c	Concentration of air
C_v	Constant volume specific heat of real gas
$\widetilde{C}_v$	Constant volume specific heat of ideal gas
C_P	Constant pressure specific heat of real gas
D	Diameter of the release area
E	Total energy
F	Flux
H	Total enthalpy
i	Internal energy
J	Jacobian
k_i	Spring constant
P	Pressure
Q	Primitive variables
R	Specific ideal gas constant
s	Entropy
T	Temperature
t	Time
U	Conservative variables
u	x-component of velocity

v	y-component of velocity
w	z-component of velocity
Z	Distance from the release hole in the z direction
ΔA	Surface area of the control volume
Δt	Time step
Δx	Displacement of a node
ζ	Compressibility factor
γ	Ratio of specific heats
ρ	Density

Chapter 1

INTRODUCTION

1-1 Hydrogen production, storage and safety

The pollution problems and global warming due to carbon dioxide and other emissions increase the need for a cleaner source of energy such as hydrogen. Hydrogen is an affordable, low-polluting, renewable and efficient energy and is a good replacement for rapidly depleting fossil fuels. Hydrogen use as fuel is growing fast and countries are investing in hydrogen industries to reduce the cost of hydrogen production, storage and safety. Hydrogen is also an energy carrier and can be stored in gaseous and liquid form.

Hydrogen can be produced by hydrocarbons, water and biomass. Steam reforming is the common way to produce hydrogen by hydrocarbons, mostly methane and natural gas. Currently hydrocarbons are the main source of hydrogen. Since hydrogen is supposed to replace the current fossil fuels, this method is not a good way to produce hydrogen. Hydrogen can be produced by water through electrolysis in which water is decomposed into hydrogen and oxygen. Unfortunately this method requires a large amount of energy and the electricity needed is more valuable than the hydrogen produced. Hydrogen can be produced by biomass. Biomass is derived from garbage, wood or waste and is the best way to produce hydrogen since is not using hydrocarbons and is not as expensive as

electrolysis. In one method of producing hydrogen through biomass, cellulosic materials can be used to produce hydrogen through a stoichiometric reaction. The biomass method is the most efficient method and is the future of hydrogen production.

Hydrogen can be stored as compressed, liquid or slush hydrogen. Liquefaction of hydrogen imposes a large amount of energy loss and the tank of storage should be well insulated to avoid temperature rise. Compressed hydrogen has good amount of energy by weight but poor amount of energy by volume and it required a larger tank to store. Figure (1-1) shows compressed and liquid hydrogen tanks. Car manufacturers such as Honda and Nissan are using compressed hydrogen of 350 or 700 bar. BMW has worked on liquid hydrogen and BMW hydrogen 7 is the model.

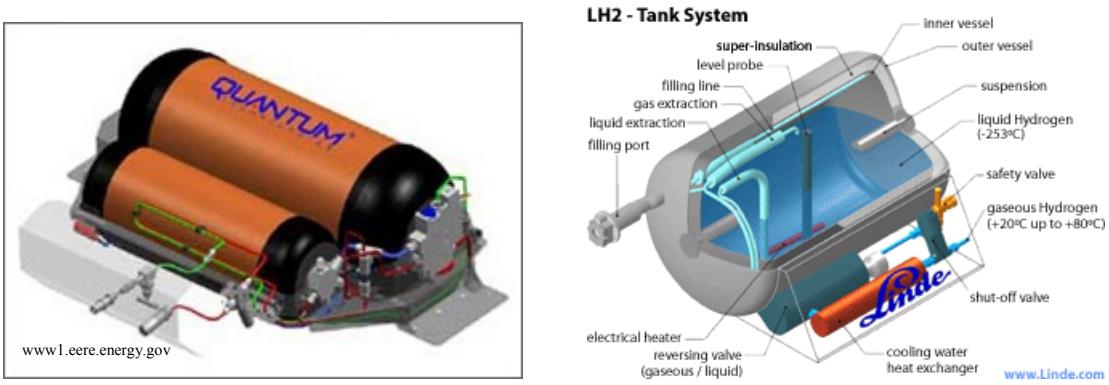

Figure (1-1) – Compressed (left) and Liquid (right) hydrogen tanks

The main drawback of extensive use of hydrogen is insufficient hydrogen fuel stations. Therefore countries like USA, Canada, Japan and some European countries like Norway are investing lots of money on building hydrogen fuel stations. A total of 12 hydrogen fuel stations are built in 11 different cities of Japan and they plan to create a

total 100 by 2015. In March 2007, Stephen Harper, Canadian Prime Minister announced funding of almost $200 million for environmental projects in British Columbia including the hydrogen highway from Vancouver to Whistler. Today, 20 local Whistler buses in British Columbia are using hydrogen fuel cell which accounts for 70 percent of the total local buses. Figure (1-2) shows one of theses buses. Hydrogen fuel stations began to be built in California in 1999. There are currently between 25 and 30 hydrogen stations in California, mostly in and around Los Angeles.

Figure (1-2)- Hydrogen fuel cell bus in Whistler, British Columbia

Investigating the parameters related to combustibility of hydrogen shows that hydrogen is combustible at concentrations between 4% and 74%. Furthermore, Hydrogen flame speed is very high in comparison with other gases such as methane. Also hydrogen

needs lower ignition energy. Therefore safety of hydrogen is important for an increased use in industries such as the automobile transportation industry.

Hydrogen has low-energy content per unit volume and it has to be stored in high pressure tanks to store sufficient amount of energy. Computational Fluid Dynamics (CFD) is used to simulate the hydrogen release in case of sudden failure of the tank as it can become an effective approach to investigate many safety relevant scenarios. The objective of this work is to develop an accurate simulation tool for the flow of hydrogen in air, to understand the physics regarding the sudden release of hydrogen from a high pressure reservoir and to analyze the sonic jet of hydrogen near the exit of the reservoir. High pressure of the tank causes choked flow at the exit which causes maximum flow rate possible. The sonic flow quickly becomes supersonic after release to the environment and shock occurs in the near field of the sonic jet. In this situation the flame front moves at a supersonic speed and a strong shockwave propagates. Explosion related to the development of a shock wave is called detonation which is the most dangerous type of explosion. Figure (1-3) shows the flow of a highly under expanded jet and the resulting shocks [1]. The mach disk is a strong normal shock which changes regime to subsonic. The barrel shock is not as strong as this normal shock mach. The pressure ratio of the tank to the external environment makes a very high gradient flow which requires a stable code along with a high quality mesh to be accurately captured. More description of under expanded jets can be found in [2-7].

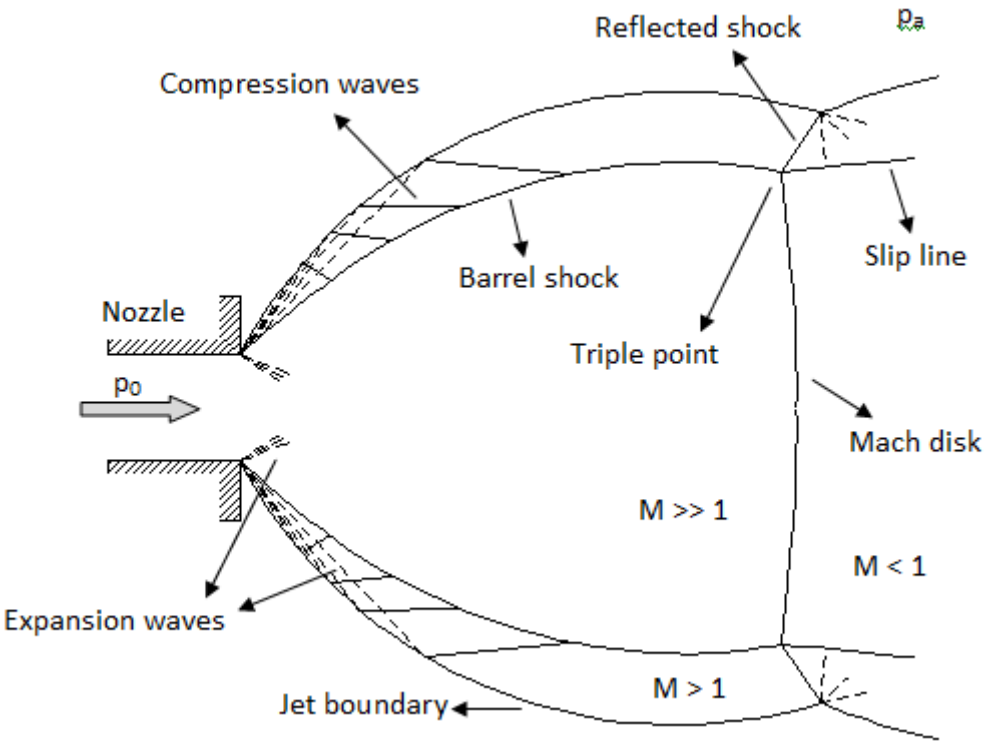

Figure (1-3) the flow structure of a highly under expanded jet [1]

1-2 In-house code features

Navier-Stokes equations are the general governing equations for the numerical simulation of fluid flows. These equations consider the convective terms and viscous terms as well as body forces like gravity. The equations consist of a continuity equation, three momentum equations for three dimensional problems and the energy equation. (Navier-Stokes equations are the three momentum equations but usually all five equations are call Navier-Stokes equations). Euler equations are the simpler form of Navier-stokes equations where viscosity and heat conduction are zero. Euler equations are applied for an inviscid flow. In our cases, the governing equations are Euler equations, since the near exit flow is at high speeds and viscous terms can be assumed

negligible compared to convective terms. All these equations require a state equation to be completed. This equation is either an ideal gas or real gas equation of state.

In order to accurately simulate the near jet flow, the numerical code has to include the real gas model. High pressure hydrogen deviates from ideal gas law. The in-house code employs a real gas model. Beattie-Bridgeman equation of state with five constants, Van der waals with two constants or Abel Noble with only one constant are samples of real gas equations of states. In this work, Beattie-Bridgeman and Abel Noble equations are applied as real gas equations and the difference is discussed. To apply these equation the Jacobian matrices and flux calculating methods are modified.

Since the area of release is very small relative to the whole domain, the elements near the jet exit are much smaller than the elements near the far field. This situation increases the total number of elements which increases the memory. Parallel processing is used to overcome the memory requirements. Also the small size elements decrease the time steps and the convergence time becomes very large. Parallel use of processors allows decreasing the total computational time. METIS software is used for grid partitioning needed for parallel processing.

The mesh used is a three-dimensional tetrahedral grid which is generated with GAMBIT. A three-dimensional simulation is necessary since in the future gravity effects will be considered and the flow can not be simulated by a two-dimensional axisymmetric mesh. Second order accuracy in space is applied to accurately simulate the flow and an

implicit scheme is used. Van Leer limiter is used in the M.U.S.C.L. (Monotone Upwind Scheme for Conservation Laws) procedure.

After release, hydrogen is mixed with air in the low-pressure environment and a mixture of hydrogen and air exists in the flow. A transport equation is applied to find the concentration of the hydrogen-air mixture. More of multi-species flows can be found in [1,8].

In reality the exit is gradually opening, since the failure of the tank or the pipes results in a hole with increasing diameter. All the research in this field deal with a fixed diameter exit and a fixed mesh is applied in the release area. A moving mesh is required to accurately simulate the flow. In this work, the boundary nodes are moved and all the other nodes are moved accordingly based on the spring method to have the best quality.

The final code will be a tool which solves the three-dimensional flow of sudden release of Hydrogen into air. The hazards related to the sudden release are predicted by using this code and it can be used in industry as a safety tool to replace the present fuels with hydrogen.

1-3 Literature Review

Swain et al. [9] divide the hydrogen release in three main types: hydrogen release in enclosed spaces, partially enclosed and unenclosed spaces. When hydrogen is released

into an enclosed space the volume of hydrogen accumulating in the space is of great importance, while for an unenclosed space the release velocity is the important parameter. For a semi-enclosed space which is usually an enclosed space with vents, both the hydrogen volume and flow velocity are important. The explosion in an enclosed space can be delayed because the volume of hydrogen gradually increases and reaches the minimum volume required to have an explosion. Hydrogen explosion can occur if the volume of hydrogen is higher than 4.1% and lower that 75% of the space. This wide range of flammability confirms the hazardous of hydrogen release. The explosion in an enclosed space is more likely to happen in a garage. When the vehicle is parked and there is release from the reservoir, hydrogen accumulates in the garage and has potential of explosion. Breitung et al. [10] numerically investigate the hydrogen release in a garage with CFD simulations. In their work hydrogen releases into air and the flammability of the mixture according to the volume percentage of the hydrogen and the flame acceleration is discussed. Also a criterion for deflagration to detonation transition probability is given.

Mukai et al. [11] simulate the diffusion of Hydrogen in a tunnel, an underground parking lot and a multistory parking garage with CFD simulations. The leak hole is a square with sides of 5 cm. The 3D Navier-Stokes flow is solved by STAR-CD and standard k-epsilon model is used to model turbulence. Results show that in all cases the flammable region is restricted to the small region near the leakage hole. Effects of tunnel length for the case of tunnels are presented. Also for the case of parking lot, effects of

two leaking vehicle are compared with one leaking vehicle. For the case of multistory garage, effects of the position of vehicle are discussed.

Agranat et al. [12] simulate the hydrogen release into a partially enclosed space which is an enclosed space with two vents. The gases are treated as ideal gases. The hydrogen concentration is compared with experimental results. Near the outlets (vents) the results of the numerical model used are 10 percent different from the experimental results, while the results are 20 percent different near the inlet.

In an unenclosed space the flow velocity has an important role in the explosion. In this case hydrogen does not accumulate. The pressure ratio of reservoir to environment and the release velocity determine the probability of explosion. Hydrogen release into an unenclosed space causes a strong shock which may lead to detonation which is the most dangerous type of explosion. An explosion occurred in March 1983 in Stockholm, Sweden shows the dangers regarding the release of hydrogen. Venetsanos et al. [13] model this explosion with CFD. The accident occurred because of the sudden release of hydrogen from a rack of 18 connected vessels with the pressure of 200bar. The 18 vessels are modeled by just one reservoir with the same number of openings. In this accident 16 people were killed and 10 vehicles were damaged. To model this accident, a real gas model has been used. The model uses enthalpy as function of temperature and pressure, and equation of state $\zeta = \zeta(T, P) = P/\rho RT$. The numerical results are largely compatible with the reported accident, both in near and far fields damages.

Experimental work about hydrogen release is rare in the literature but can be found in [14]. Golub et al. [15] experimentally investigate the self-ignition of release of hydrogen through a tube of 65-185 mm in length and the cross section area of 20 mm^2 into a semi-confined space. They have tried both round and rectangular cross sections. The pressure in the chamber is increased up to 10MPa. They conclude the self-ignition in the tubes of 20 mm^2 in cross section is possible when hydrogen is released from a high pressure reservoir of 4MPa and higher.

Schefer et al. [16] experimentally discuss the vertical jet into open space. Hydrogen is released from eight high pressure hydrogen tubes with the volume of 0.6 m^3 into a stagnation chamber and then is release into air through a jet nozzle. The pressure is increased up to 40MPa and the release hole diameter is almost 5mm. The flow pattern is discussed for longer times after release in the order of seconds. The flame length is almost 9 m after the test initiation. It takes 500s for the tank pressure to reach near atmospheric pressure.

Shirvill et al. [17] experimentally investigate the jet release of hydrogen. The results are recorded by video cameras. Unignited and ignited releases are tested. The maximum release pressure is 130 bars from an orifice diameter of 3 mm.

Dubois [18] discuss the release experimentally in case of a free subsonic jet, free supersonic jet and subsonic jet in the presence of an obstacle. Helium is applied for the experimental tests. An optical technique, BOS (Background Oriented Schlieren), is used

to get the images. For the free subsonic jet, four release area diamteres of 1, 2, 3 and 8 mm are tested. The results are in 10% difference from the literature simulation for Helium subsonic free jet. For the free supersonic jet, the release diameter is fixed at 1 mm and the pressure is in the approximate range of 3 to 12 MPa. The experiment is done with helium and based on a law resulted from the experiment, hydrogen results are provided. It is concluded that the result of BOS for helium are different from the results of hydrogen based on a developed law.

Computational fluid dynamics has been very helpful in this field. Many results achieved have been done by using Computational fluid dynamics [19-23]. Cheng et al. [24] simulate the hydrogen release from a reservoir of 400 bars. The differences between using ideal and real gas models are presented. The release hole is 6 mm. For high pressure release the difference between ideal gas and real gas is not negligible. The Abel-Noble equation of state was used to model the real gas. This equation deviates from the ideal gas law by a compressibility factor. The difference between ideal gas and real gas results increases by increasing the pressure and reducing the temperature. The results show that ideal gas law overestimates the mass flow rate by 30% in the first 10 seconds and 35% in the first 25 seconds of release compared to real gas model. The choked release lasts 50 seconds by real gas model compared to 47.7 seconds for ideal gas law.

Xu et al. [25] simulate numerically highly under-expanded hydrogen jet. The vessel pressure and temperature is set as 20 MPa and 300 K, respectively and the orifice diameter is 1 cm. The release pressure, temperature and velocity are 10.6 MPa, 251 K

and 1020 m/s, respectively. LES is selected to model turbulence in this problem. A 45-degree slice domain with diameter of 50D and length of 80D is used. The second order accuracy is employed but it is changed locally to a first order upwind to avoid non-physical oscillations. The maximum Mach number and velocity are 9 and 2700 m/s respectively.

Liu et al. [26] use direct numerical simulation to investigate the high pressure hydrogen jet. Two dimensional Euler equations are used and due to symmetry of the problem, axisymmetric equations are applied. Hydrogen ignition and combustion are simulated by using chemical mechanisms. The exit diameter is 1 mm and the tank pressures of 10, 40 and 70 MPa are employed. The stagnation temperature is 300 K. the computational domain is a rectangle. The results show that an ignition source is required to generate a hydrogen flame.

Pedro et al. [27] simulate the hydrogen release from a vessel of pressure of 100 atm by using FLUENT. Ideal gas law is used and the reservoir is also simulated. A second order upwind scheme is used for continuity and momentum equations. The energy equation is resolved by a first order upwind scheme. Time has also the second order accuracy. Nozzle diameter is 5 mm. Adaptation is used to reduce the computational time and capture the shocks better. The time steps used are lower than 10e-8 seconds.

Radulescu et al. [28] numerically investigate highly under-expanded slit and round jets. The results are compared with the existing experimental results. An adaptive code is

used to solve the two dimensional axisymmetric equations and ideal gas law is used. The code uses a second order Godunov scheme. Axisymmetric coordinates are used due to symmetry of the problem. The pressure ratio of reservoir to environment is between 100 and 1000. The Reynolds number is assumed high in order to restrict the viscous effects to regions with high gradients. Therefore in regions without these high gradients, the results are similar to results of Euler equations.

To simulate the real gas, the equation of state for the real gas should be known. This equation can be found by equation $\zeta = \zeta(T, P) = P/\rho RT$. In this definition, Real gases are different from ideal gases by a factor ζ in the ideal gas law and is a function of temperature and pressure. The pressure derivatives are found by using this equation. For hydrogen, ζ increases by increasing the pressure at a constant temperature. A more accurate model of ζ leads to a more accurate equation of state.

In another approach pressure is directly defined as a function of two independent variables. Montagne et al. [29] defines pressure as a function of density and internal energy. Mohamed et al. [30] uses Beattie-Bridgeman state equation, in this equation pressure is a function of temperature and specific volume. The required derivatives are found by this equation and thermodynamics properties.

Recall that hydrogen has a high potential to auto ignite. The possibility of ignition is high in front of the hydrogen-air contact surface where the flow is heated by the lead shock. Several ignition mechanisms have been tried in the literature including diffusion ignition,

sudden adiabatic compression, hot surface ignition, etc. [25] Xu et al. focus on the diffusion ignition which was first introduced in [31]. In this mechanism, ignition is caused by the diffusion between hydrogen and heated oxygen. Oxygen is heated by the lead shock. Since the ignition is cause by diffusion, this mechanism is called diffusion ignition. Xu et al. [25] show that when hydrogen is released through a tube, if the tube is long enough and the hydrogen pressure is high enough, hydrogen will auto ignite. It is presented that the pressure of almost 4 MPa does not lead to auto ignition since the lead shock is not strong enough, while the pressure of almost 7 MPa results in auto ignition and when the tube length is increased from 2 cm to 6 cm, hydrogen and air have more time to mix and auto ignition is more likely to happen. Melguizo-Gavilanes et al. [32] study the shock-induced ignition in details. The case is studied by the reactive Euler equations. The simulation is performed in one dimension and a transformed coordinate system is applied. Liang et al. [33] discuss the detonation structure and Bedard-Tremblay et al. [34] investigate the detonation and also deflagration to detonation transition (DDT) after the accidental release. The simulation is two-dimensional which causes confinement compared to an actual three-dimensional case.

In this work, ignition is not discussed. More of ignition can be found in [35-38]. The numerical results achieved in this research will be used by ignition people to be discussed in term of different forms of ignition. For example, the pressure on the contact surface at different times is important for ignition models. This is one of the outputs of our in-house code to be applied for further ignition investigations.

1-4 Methodology

The ultimate goal of the work is to have a code which accurately models the release of hydrogen into air. Since strong shocks occur in micro seconds after release, a very accurate tool is needed to capture all the features of the flow. To achieve this, it is needed to have an accurate three-dimensional code.

An existing three-dimensional Euler parallel code is modified to simulate the flow. The first task is to apply the real gas model. Since Hydrogen is stored in a high pressure tank, ideal gas model can not accurately capture the characteristics of the flow. The real gas model is needed to simulate the hydrogen release from a high pressure reservoir. In this work, Beattie-Bridgeman and Abel Noble equations are applied as real gas equations and the difference is discussed. All Jacobian matrices and flux calculating methods are modified for real gas simulation.

The second task is to increase the accuracy from first order to second order. A modified Van Leer limiter is used in the M.U.S.C.L. (Monotone Upwind Scheme for Conservation Laws) procedure to have the second order accuracy in space.

The third task is to add a transport equation to find out the concentration of hydrogen-air mixture. Soon after release hydrogen is mixed with the air and a contact surface is generated. The transport equation is solved at each iteration to find out the concentration of each species.

The fourth task is to add the moving mesh capability to the code. In reality the release hole expands by time, therefore a simulation with a fixed diameter hole is not accurate. A moving mesh is required to simulate this scenario. Spring-based method is added to the code. Boundary nodes are moved and all the other nodes are moved accordingly based on the spring method.

The final code is able to model the hydrogen jet. This will help us to examine where and when the probability of explosion exists and what should be done to avoid it to happen. The novelty of this code is that it considers all the detailed features of the flow and it can be used in industry as a tool to safely use Hydrogen as a fuel. Commercial codes do not offer this level of accuracy. This tool uses real gas model which is necessary to accurately simulate the release of high pressure hydrogen into air. Commercial codes are not capable of applying the real gas equation for this flow. High gradients caused by the high pressure ratio result in high instability which commercial codes are not able to handle. Application of second order accuracy to this simulation is really a challenge due to high gradients in the flow. Note that the flow can reach Mach number of about 9. The code uses a transport equation which is capable of finding out the concentration of hydrogen or air in the mixture after releasing the high pressure hydrogen into ambient air. This tool also considers the fact that the release area is expanding in time by adding the moving mesh feature. The moving mesh method maintains the quality of the mesh at each step of enlarging the release area. These features of the code make it powerful to accurately simulate the flow and have precise results close to what happens in real cases.

To be more specific this research wants to make the following contributions:

- Real gas model
  - Two real gas equations of state, Beattie-Bridgeman and Abel Noble are implemented in the code. Results show the real gas model is necessary for the simulation.
- Second order accuracy
  - A modified limiter is used to apply the second order accuracy since high gradients in the flow make the second order accuracy hard to be applied.
- Transport equation
  - A transport equation is added to code to predict the concentration of each specie in the hydrogen-air mixture happening soon after release.
- Moving mesh
  - In reality the release area is expanded by time and is not fixed. Spring-based method is used to move the mesh to make the simulation as real as possible.

Chapter 2

GOVERNING EQUATIONS

The near exit flow is high speed therefore viscous terms can be assumed negligible compared to convective terms. For high gradient areas like shock regions viscous effects become higher but the flow can still be treated as inviscid and Euler equations give accurate results. Therefore Euler equations are used to simulate this flow:

$$\frac{\partial U}{\partial t} + \nabla . F = 0 \tag{2-1}$$

where,

$$U = \begin{bmatrix} \rho \\ \rho u \\ \rho v \\ \rho w \\ \rho E \end{bmatrix} \quad , \quad F = \left\{ \begin{bmatrix} \rho u \\ \rho u^2 + P \\ \rho uv \\ \rho uw \\ \rho uH \end{bmatrix} \begin{bmatrix} \rho v \\ \rho vu \\ \rho v^2 + P \\ \rho vw \\ \rho vH \end{bmatrix} \begin{bmatrix} \rho w \\ \rho wu \\ \rho wv \\ \rho w^2 + P \\ \rho wH \end{bmatrix} \right\} \tag{2-2}$$

$$H = E + \frac{P}{\rho} \quad , \quad E = i + \frac{1}{2}(u^2 + v^2 + w^2)$$

For an ideal gas state equation, pressure is related to the energy as follows:

$$P = \rho RT = \rho R\frac{i}{C_v} = \rho R\frac{i}{R/(\gamma-1)} = \rho(\gamma-1)i \tag{2-3}$$

For a real gas this relation will be discussed in section 2-1-2

The implicit finite-volume discretization is as follows:

$$|V|\frac{U^{n+1}-U^n}{\Delta t} + \sum_{surface} F^{n+1}.n\,\Delta A = 0 \tag{2-4}$$

$$F^{n+1} = F^n + (\frac{\partial F}{\partial U})^n (U^{n+1}-U^n) = F^n + J^n(U^{n+1}-U^n)$$

where J is the flux-Jacobian.

Roe's averaging method is used to calculate Fluxes [39]. Conservative jacobians are found by primirive jacobians. The Jacobians can be achieved easily if primitive variables are used. Primitive variables are $Q^T = [\rho \quad u \quad v \quad w \quad P]$. The jacobians of primitive variables are not a function of equation of state. In other words, the primitive jacobians are the same for ideal gas and real gas. So to find conservative jacobians, it is much easier to find them by using primirive jacobians. The numerical code uses conservative variable but the jacobians are first found by primitive variables and then conservative jacobians are calculated by the help of $\partial U/\partial Q$ which is needed to transform between the primitive and conservative variables. $\partial U/\partial Q$ is as follows:

$$M = \frac{\partial U}{\partial Q} = \begin{bmatrix} 1 & 0 & 0 & 0 & 0 \\ u & \rho & 0 & 0 & 0 \\ v & 0 & \rho & 0 & 0 \\ w & 0 & 0 & \rho & 0 \\ H-\rho\frac{P_\rho}{P_i}-\frac{P}{\rho} & \rho u & \rho v & \rho w & \frac{\rho}{P_i} \end{bmatrix} \tag{2-5}$$

Equation (2-6) shows this relation between primitive Jacobian and conservative Jacobian.

$$J_P = M^{-1} J_c M \tag{2-6}$$

In the same way the left and right eigenvector matrices of conservative Jacobian can be found by left and right eigenvector matrices of primitive Jacobian.

$$L_c{}^T = L_p{}^T M^{-1} \tag{2-7}$$

$$R_c = M R_p \tag{2-8}$$

The conservative left and right eigenvector matrices are as follows:

$$L = \begin{bmatrix} \frac{-P_i}{\rho a^2}(V^2 - H) & \frac{uP_i}{\rho a^2} & \frac{vP_i}{\rho a^2} & \frac{wP_i}{\rho a^2} & \frac{-P_i}{\rho a^2} \\ \frac{un_z}{\rho} - \frac{wn_x}{\rho} & \frac{-n_z}{\rho} & 0 & \frac{n_x}{\rho} & 0 \\ \frac{-un_y}{\rho} + \frac{vn_x}{\rho} & \frac{n_y}{\rho} & \frac{-n_x}{\rho} & 0 & 0 \\ -\frac{un_x}{\rho} - \frac{vn_y}{\rho} - \frac{wn_z}{\rho} & & & & \\ + \frac{a}{\rho} + \frac{P_i}{\rho^2 a}(V^2 - H) & \frac{n_x}{\rho} - \frac{uP_i}{\rho^2 a} & \frac{n_y}{\rho} - \frac{vP_i}{\rho^2 a} & \frac{n_z}{\rho} - \frac{wP_i}{\rho^2 a} & \frac{P_i}{\rho^2 a} \\ \frac{un_x}{\rho} + \frac{vn_y}{\rho} + \frac{wn_z}{\rho} & & & & \\ + \frac{a}{\rho} + \frac{P_i}{\rho^2 a}(V^2 - H) & -\frac{n_x}{\rho} - \frac{uP_i}{\rho^2 a} & -\frac{n_y}{\rho} - \frac{vP_i}{\rho^2 a} & -\frac{n_z}{\rho} - \frac{wP_i}{\rho^2 a} & \frac{P_i}{\rho^2 a} \end{bmatrix}$$

$$R=\begin{bmatrix} 1 & 0 & 0 & \frac{\rho}{2a} & \frac{\rho}{2a} \\ u & -\rho n_z & \rho n_y & \frac{\rho u}{2a}+\frac{\rho n_x}{2} & \frac{\rho u}{2a}-\frac{\rho n_x}{2} \\ v & -\frac{\rho n_y n_z}{n_x} & -\frac{\rho(n_z^2+n_x^2)}{n_x} & \frac{\rho v}{2a}+\frac{\rho n_y}{2} & \frac{\rho v}{2a}-\frac{\rho n_y}{2} \\ w & \frac{\rho(n_y^2+n_x^2)}{n_x} & \frac{\rho n_y n_z}{n_x} & \frac{\rho w}{2a}+\frac{\rho n_z}{2} & \frac{\rho w}{2a}-\frac{\rho n_z}{2} \\ H-\frac{\rho a^2}{P_i} & -\rho u n_z-\frac{\rho v n_y n_z}{n_x}+\frac{\rho w(n_y^2+n_x^2)}{n_x} & \rho u n_y+\frac{\rho w n_y n_z}{n_x}-\frac{\rho v(n_z^2+n_x^2)}{n_x} & \frac{\rho H}{2a}+\frac{\rho u n_x}{2}+\frac{\rho v n_y}{2}+\frac{\rho w n_z}{2} & \frac{\rho H}{2a}-\frac{\rho u n_x}{2}-\frac{\rho v n_y}{2}-\frac{\rho w n_z}{2} \end{bmatrix}$$

where,

$$P_i=\left(\frac{\partial P}{\partial i}\right)_\rho=\left(\frac{\partial P}{\partial T}\right)_\rho\left(\frac{\partial T}{\partial i}\right)_\rho+\left(\frac{\partial P}{\partial \rho}\right)_T\left(\frac{\partial \rho}{\partial i}\right)_\rho=\left(\frac{\partial P}{\partial T}\right)_\rho\left(\frac{\partial T}{\partial i}\right)_\rho \tag{2-9}$$

$$a^2=\left(\frac{\partial P}{\partial \rho}\right)_s=\left(\frac{\partial P}{\partial i}\right)_\rho\left(\frac{\partial i}{\partial \rho}\right)_s+\left(\frac{\partial P}{\partial \rho}\right)_i\left(\frac{\partial \rho}{\partial \rho}\right)_s=\left(\frac{\partial P}{\partial i}\right)_\rho\left(\frac{\partial i}{\partial \rho}\right)_s+\left(\frac{\partial P}{\partial \rho}\right)_i \tag{2-10}$$

$$P_\rho=\left(\frac{\partial P}{\partial \rho}\right)_i=\left(\frac{\partial P}{\partial T}\right)_\rho\left(\frac{\partial T}{\partial \rho}\right)_i+\left(\frac{\partial P}{\partial \rho}\right)_T\left(\frac{\partial \rho}{\partial \rho}\right)_i=\left(\frac{\partial P}{\partial T}\right)_\rho\left(\frac{\partial T}{\partial \rho}\right)_i+\left(\frac{\partial P}{\partial \rho}\right)_T \tag{2-11}$$

From [40]:

$$di=Tds-Pd\upsilon=Tds+\frac{P}{\rho^2}d\rho \tag{2-12}$$

and for an isentropic process:

$$di=\frac{P}{\rho^2}d\rho \tag{2-13}$$

therefore,

$$\left(\frac{\partial i}{\partial \rho}\right)_s = \frac{P}{\rho^2} \tag{2-14}$$

And

$$a^2 = P_\rho + \frac{PP_i}{\rho^2} \tag{2-15}$$

2-1 Real gas models

High pressure hydrogen deviates from the ideal gas law. In order to simulate the flow more accurately, a real gas equation of state is added to the in-house code. There are several real gas equations. Van der Waals is a well known equation which uses two parameters a and b as follows:

$$(P + {}^{a}\!/_{V_m{}^2})(V_m - b) = RT$$

where V_m is the molar volume.

Another two parameters equation is the Redlich-Kwong equation which is more accurate than the Van der Waals:

$$(P + \frac{a}{V_m(V_m + b)T^{1/2}})(V_m - b) = RT$$

A three parameter state equation is Clausius equation :

$$(P + \frac{a}{(V_m + c)^2 T})(V_m - b) = RT$$

The Wohl equation is another three parameter equation which is more accurate and complex:

$$(P+\frac{a}{V_m(V_m-b)T}-\frac{c}{T^2V_m{}^3})(V_m-b)=RT$$

There are also other two parameters equations like Dieterici or Berthelot.

In this paper, three parameters Beattie-Bridgeman and one parameter Abel-Noble equations of state explained in sections 2-1-1 and 2-1-2 are implemented as real gas models. In the case of hydrogen in hydrogen both equations are studied but for the case of hydrogen in air only the Abel-Noble is examined. It will be shown that these two equations have almost the same accuracy for the case of hydrogen in hydrogen. Therefore it is pointless to use Beattie-Bridgeman for the case of hydrogen in air release. Furthermore the latter suffers from stability problems for the case of hydrogen in air and also it requires higher solution time since it is more complicated and uses more constants.

2-1-1 Beattie-Bridgeman

This equation is relatively complicated since it uses five constants.

$$P=\frac{RT}{\upsilon}+\left(\frac{-cR}{T^2}+B_\circ RT-A_\circ\right)\frac{1}{\upsilon^2}+\left(-\frac{B_\circ cR}{T^2}-B_\circ bRT+\alpha A_\circ\right)\frac{1}{\upsilon^3}+\frac{B_\circ bcR}{T^2}\frac{1}{\upsilon^4} \qquad (2\text{-}16)$$

In table (2-1) the constants are given [40]. This equation is used for the case of hydrogen in hydrogen.

Table (2-1) -constants of Beattie-Bridgeman equation for hydrogen

$A_\circ$ (m5/Kg.s2)	$10^{+3}\alpha$ (m3/Kg)	$10^{+2}B_\circ$ (m3/Kg)	$10^{+2}b$ (m3/Kg)	$10^{-2}c$ (m3 .K3/ Kg)
4924	-2.510	1.034	-2.162	2.500

$$P = f(T,v) = \frac{RT}{v} + (\frac{-cR}{T^2} + B_0 RT - A_0)\frac{1}{v^2} + (\frac{-B_0 cR}{T^2} - B_0 bRT + \alpha A_0)\frac{1}{v^3} + \frac{B_0 bcR}{T^2}\frac{1}{v^4} \quad (2\text{-}17)$$

P_i and P_ρ are calculated as follows [41]:

$$P_i = \frac{f_T}{i_T} \quad (2\text{-}18)$$

$$P_\rho = v^2(\frac{f_T i_v}{i_T} - f_v) \quad (2\text{-}19)$$

where

$$f_T = \frac{R}{v} + (\frac{2cR}{T^3} + B_0 R)\frac{1}{v^2} + (\frac{2B_0 cR}{T^3} - B_0 bR)\frac{1}{v^3} - \frac{2B_0 bcR}{T^3}\frac{1}{v^4}$$

$$i_T = \widetilde{C}_v - \frac{6cR}{T^3}(\frac{1}{v^0} - \frac{1}{v}) - \frac{6B_0 cR}{T^3}(\frac{1}{2v^{02}} - \frac{1}{2v^2}) + \frac{6B_0 bcR}{T^3}(\frac{1}{3v^{03}} - \frac{1}{3v^3})$$

$$f_v = -\frac{RT}{v^2} - (-\frac{cR}{T^2} + B_0 RT - A_0)\frac{2}{v^3} - (-\frac{B_0 cR}{T^2} - B_0 bRT + aA_0)\frac{3}{v^4} - \frac{B_0 bcR}{T^2}\frac{4}{v^5}$$

$$i_v = (\frac{3cR}{T^2} + A_0)\frac{1}{v^2} + (\frac{3B_0 cR}{T^2} - aA_0)\frac{1}{v^3} - \frac{3B_0 bcR}{T^2}\frac{1}{v^4}$$

$A_0 = 4924$, $B_0 = 1.034 \times 10^{-2}$

$a = -2.51 \times 10^{-3}$, $b = -2.162 \times 10^{-2}$, $c = 250$

$\widetilde{C}_v$ and v^0 are specific heat at constant volume and specific volume at pressure of 0.1 MPa.

For the ideal gas, P_i and P_ρ are simply calculated by using ideal gas law:

$$P_i = \rho(\gamma - 1) \quad (2\text{-}20)$$

$$P_\rho = (\gamma - 1)i \quad (2\text{-}21)$$

2-1-2 Abel-Noble

This equation is much simpler compared to Beattie-Bridgeman since it employs only one constant:

$$P = \frac{RT}{(\upsilon - b)} = \frac{\rho RT}{(1 - b\rho)} = (1 - b\rho)^{-1} \rho RT = \zeta \rho RT \tag{2-22}$$

where $b = 0.00775 \ m^3/kg$

The deviation from ideal gas equation can be illustrated by plotting the compressibility factor ζ . The compressibility factor for an ideal gas equals one while it changes for a real gas. In figure (2-1), the compressibility factor is compared for an ideal gas and Abel-Noble real gas for hydrogen at temperature of 300 K. It is always one for ideal gas but for the real gas it increases for increasing pressure. The difference may be negligible up to pressure of 10 MPa but for higher pressures ideal gas is not accurate enough and the real gas is necessary. For example the compressibility factor is almost 1.6 for pressure of 100 MPa. For compressed hydrogen, the pressure in the reservoir can reach up to 70 MPa and a real gas equation is required to capture the flow pattern accurately.

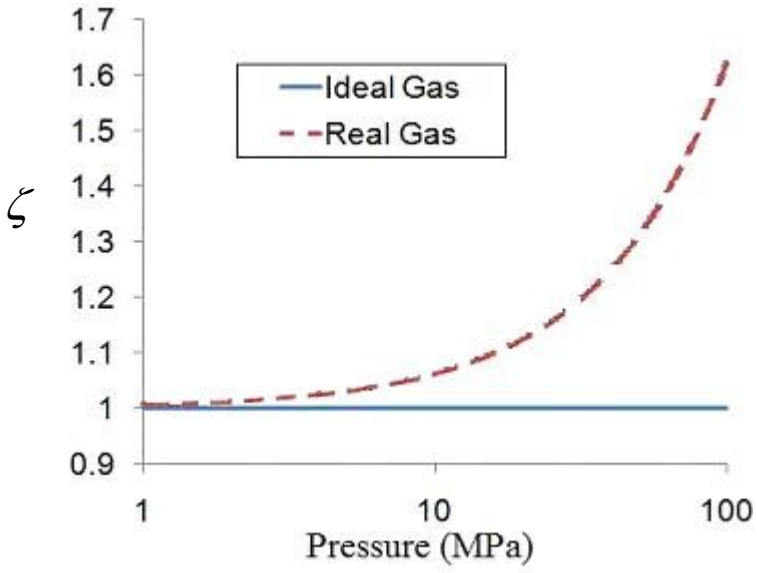

Figure (2-1)- Hydrogen Compressibility factor at Temperature of 300 K

To close the Euler equations the following relations are used:

$$H = E + \frac{P}{\rho} \tag{2-23}$$

$$i = E - \frac{1}{2}(u^2 + v^2 + w^2) \tag{2-24}$$

$$i = C_v T = \frac{R}{\gamma - 1} T \Rightarrow RT = (\gamma - 1)i \tag{2-25}$$

$$P = \frac{RT}{(\upsilon - b)} = \frac{(\gamma - 1)}{(\upsilon - b)} i = \frac{(\gamma - 1)}{(\upsilon - b)} \left[E - \frac{1}{2}(u^2 + v^2 + w^2) \right] = \frac{(\gamma - 1)\rho}{(1 - b\rho)} \left[E - \frac{1}{2}(u^2 + v^2 + w^2) \right] \tag{2-26}$$

P_i and P_ρ are calculated as follows:

$$P = f(T, \upsilon) = \frac{RT}{(\upsilon - b)} = \frac{\rho RT}{(1 - b\rho)} \tag{2-27}$$

$$P_i = \frac{f_T}{i_T} = \frac{\dfrac{R}{(\upsilon - b)}}{C_v} = \frac{\dfrac{R}{(\upsilon - b)}}{\dfrac{R}{(\gamma - 1)}} = \frac{(\gamma - 1)}{(\upsilon - b)} \tag{2-28}$$

$$P_\rho = \frac{RT(1 - b\rho) + b\rho RT}{(1 - b\rho)^2} = \frac{(\gamma - 1)}{(1 - b\rho)^2} \left[E - \frac{1}{2}(u^2 + v^2 + w^2) \right] \tag{2-29}$$

According to these relations, pressure and the derivatives are a function of ratio of the specific heats. Therefore if the species of a mixture have the same ratio of the specific heats, the equations are closed without updating the gas constant *R* of the mixture. Hydrogen and air have the same ratio of specific heats, so the equations are closed and do not need the updating the gas constant of the mixture.

2-1-3 Analytical solutions for choked flow

For the Abel Noble gas model, the choked flow in the release area is related to the stagnation state in the tank [16]. Release density is found by following equation:

$$\left(\frac{\rho_0}{1-b\rho_0}\right)^{\gamma} = \left(\frac{\rho_e}{1-b\rho_e}\right)^{\gamma}\left[1+\left(\frac{\gamma-1}{2(1-b\rho_e)^2}\right)\right]^{\gamma/\gamma-1} \tag{2-30}$$

Where ρ_0 is the stagnation density in the tank, ρ_e is the density at the release area, b is the Abel-Noble constant and γ is the ratio of specific heats. Knowing the stagnation density in the tank gives the release density. Temperature at the release area is related to the stagnation temperature by

$$T_0 = T_e\left[1+\left(\frac{\gamma-1}{2(1-b\rho_e)^2}\right)\right] \tag{2-31}$$

where T_0 is the stagnation temperature in the tank and T_e is the release temperature. Stagnation temperature found from the initial condition and the release density found from the equation (2-30) give the release temperature. The release pressure can now be found by Abel-Noble equation of state:

$$P_e = \frac{\rho_e R T_e}{1-b\rho_e} \tag{2-32}$$

And finally the release velocity which is the sound velocity in the release area is given by

$$u_e = \frac{1}{1-b\rho_e}\sqrt{\gamma R T_e} \tag{2-33}$$

For an ideal gas these equations are simpler as follows:

$$\rho_e = \rho_0\left(\frac{2}{\gamma+1}\right)^{\frac{1}{\gamma-1}} \tag{2-34}$$

$$T_e = \frac{2T_0}{\gamma+1} \tag{2-35}$$

$$P_e = \rho_e R T_e \tag{2-36}$$

$$u_e = \sqrt{\gamma R T_e} \tag{2-37}$$

2-1-4 Specific heats and speed of sound

The specific heats and ratio of specific heats are found by the following equations [30]:

$$C_\upsilon = \widetilde{C}_\upsilon + \int_{\upsilon^\circ}^{\upsilon} \left(\frac{\partial C_v}{\partial v} \right)_T d\upsilon \tag{2-38}$$

$\widetilde{C}_\upsilon$ is the specific heat at reference pressure of 0.1 MPa where ideal gas assumptions are valid.

$$\left(\frac{\partial C_v}{\partial v} \right)_T = T \left(\frac{\partial^2 P}{\partial T^2} \right)_v \Rightarrow C_\upsilon = \widetilde{C}_\upsilon + \int_{\upsilon^\circ}^{\upsilon} T \left(\frac{\partial^2 P}{\partial T^2} \right)_v d\upsilon \tag{2-39}$$

$$C_p = C_\upsilon - T \left(\frac{\partial P}{\partial T} \right)_v^2 \Big/ \left(\frac{\partial P}{\partial v} \right)_T \tag{2-40}$$

$$a(T,\upsilon) = \sqrt{-\upsilon^2 \frac{C_P}{C_v} \left(\frac{\partial P}{\partial v} \right)_T} \tag{2-41}$$

Assuming $P = f(T,\upsilon)$ the sound speed and specific heats are as follows:

$$C_\upsilon(T,\upsilon) = \widetilde{C}_\upsilon + \int_{\upsilon^\circ}^{\upsilon} T f_{TT}(T,\upsilon) d\upsilon \tag{2-42}$$

$$C_P(T,\upsilon) = C_\upsilon(T,\upsilon) - T \frac{f_T^2(T,\upsilon)}{f_\upsilon(T,\upsilon)} \tag{2-43}$$

$$a(T,\upsilon) = \sqrt{-\upsilon^2 \frac{C_P}{C_v} f_\upsilon(T,\upsilon)} \tag{2-44}$$

Beattie-Bridgeman equation of state

$$P = f(T,\upsilon) = \frac{RT}{\upsilon} + \left(\frac{-cR}{T^2} + B_\circ RT - A_\circ \right) \frac{1}{\upsilon^2} + \left(-\frac{B_\circ cR}{T^2} - B_\circ bRT + \alpha A_\circ \right) \frac{1}{\upsilon^3} + \frac{B_\circ bcR}{T^2} \frac{1}{\upsilon^4}$$

gives the following values for f_T, f_v and $\int_{v^\circ}^{v} Tf_{TT}(T,\upsilon)d\upsilon$:

$$f_T = \frac{R}{\upsilon} + \left(\frac{2cR}{T^3} + B_\circ R\right)\frac{1}{\upsilon^2} + \left(\frac{2B_\circ cR}{T^3} - B_\circ bR\right)\frac{1}{\upsilon^3} - \frac{2B_\circ bcR}{T^3}\frac{1}{\upsilon^4} \tag{2-45}$$

$$f_\upsilon = -\frac{RT}{\upsilon^2} - \left(\frac{-cR}{T^2} + B_\circ RT - A_\circ\right)\frac{2}{\upsilon^3} - \left(-\frac{B_\circ cR}{T^2} - B_\circ bRT + aA_\circ\right)\frac{3}{\upsilon^4} - \frac{B_\circ bcR}{T^2}\frac{4}{\upsilon^5} \tag{2-46}$$

$$\int_{v^\circ}^{v} Tf_{TT}(T,\upsilon)d\upsilon = \frac{6cR}{T^3}\left(\frac{1}{\upsilon} - \frac{1}{\upsilon^\circ}\right) + \frac{3B_\circ cR}{T^3}\left(\frac{1}{\upsilon^2} - \frac{1}{\upsilon^{\circ 2}}\right) - \frac{2B_\circ bcR}{T^3}\left(\frac{1}{\upsilon^3} - \frac{1}{\upsilon^{\circ 3}}\right) \tag{2-47}$$

By substituting these values into equations (2-42 to 2-44) specific heats and sound speed are found.

Abel-Noble equation of state $P = f(T,\upsilon) = \frac{RT}{(\upsilon - b)}$ gives the following values for f_T, f_v and $\int_{v^\circ}^{v} Tf_{TT}(T,\upsilon)d\upsilon$:

$$f_T = \frac{R}{\upsilon - b} \tag{2-48}$$

$$f_\upsilon = -\frac{RT}{(\upsilon - b)^2} \tag{2-49}$$

$$\int_{v^\circ}^{v} Tf_{TT}(T,\upsilon)d\upsilon = 0 \tag{2-50}$$

By substituting these values into equations (2-42 to 2-44) specific heats and sound speed are simplified as follows:

$$C_\upsilon = \widetilde{C}_\upsilon \tag{2-51}$$

$$C_P = C_\upsilon - T\frac{\left(\frac{R}{\upsilon - b}\right)^2}{-\frac{RT}{(\upsilon - b)^2}} = C_\upsilon - R \tag{2-52}$$

$$a(T,\upsilon)=\sqrt{-\upsilon^2\frac{C_P}{C_v}f_\upsilon(T,\upsilon)}=\sqrt{\upsilon^2\frac{C_P}{C_v}\frac{RT}{(\upsilon-b)^2}}=\frac{v}{v-b}\sqrt{\frac{C_P}{C_v}RT} \tag{2-53}$$

Therefore in the Abel-Noble code, specific heats are found by ideal gas law and are function of R and a constant ratio of specific heats while equations (2-45 to 2-47) show that in the Beattie-Bridgeman specific heats are different from ideal gas and the ratio of specific heats cannot be assumed constant.

2-2 Transport Equation

After release, hydrogen is mixed with air in the low-pressure environment and a mixture of hydrogen and air exists in the flow. A transport equation is applied to find the concentration of the hydrogen-air mixture [1]:

$$\frac{\partial(\rho c)}{\partial t}+\frac{\partial(\rho cu)}{\partial x}+\frac{\partial(\rho cv)}{\partial y}+\frac{\partial(\rho cw)}{\partial z}=0 \tag{2-54}$$

The air concentration is given by c and varies between 0 and 1. Initially the concentration is zero in the tank where there is no air while it is one in the low-pressure environment where there is no hydrogen. Soon after release hydrogen mixes with air and c changes in the mixture regions. The transport equation is solved separately at the end of each time step solution, with the same numerical approach as the Euler equations. R of the mixture is averaged with respect to concentration as follows:

$$R_{mix}=R_{H_2}(1-c)+R_{Air}c \tag{2-55}$$

where $R_{H_2}=4124(J/kgK)$ and $R_{Air}=287(J/kgK)$

2-3 Temperature Calculation

After computing R, Temperature is simply found by

$$T = \frac{P(1-b\rho)}{\rho R_{mix}} \tag{2-56}$$

For Abel-Noble equation of state, this is the end of the calculation at each iteration. The updated R will not be used in the next iteration since the pressure is only dependent on the specific heat. Since air and hydrogen have the same specific heat ratio, the information found by the transport equation is not used in the next time step and is only useful to find the temperature. If the mixture contains a substance with a different specific heat ratio, the concentration of each specie has an impact on the next time step and our method should be modified.

2-4 Moving Mesh

When the computational mesh moves, Euler equations are changed [42]:

$$U = \begin{bmatrix} \rho \\ \rho u_x \\ \rho u_y \\ \rho u_z \\ \rho E \end{bmatrix} \quad , \quad F = \left\{ \begin{bmatrix} \rho(u_x - w_x) \\ \rho(u_x - w_x)u_x + P \\ \rho(u_x - w_x)u_y \\ \rho(u_x - w_x)u_z \\ \rho(u_x - w_x)E + u_x P \end{bmatrix} \begin{bmatrix} \rho(u_y - w_y) \\ \rho(u_y - w_y)u_y \\ \rho(u_y - w_y)u_y + P \\ \rho(u_y - w_y)u_z \\ \rho(u_y - w_y)E + u_y P \end{bmatrix} \begin{bmatrix} \rho(u_z - w_z) \\ \rho(u_z - w_z)u_x \\ \rho(u_z - w_z)u_y \\ \rho(u_z - w_z)u_z + P \\ \rho(u_z - w_z)E + u_z P \end{bmatrix} \right\} \tag{2-57}$$

Where w is the velocity of each node in case of movement. The discretization is changed to the following equation:

$$\frac{U^{n+1}V^{n+1} - U^n V^n}{\Delta t} + \sum_{surface} F^{n+1}.n\,\Delta A = 0$$

which includes the volume of the control volume before and after each time step.

The transport equation is also changed to

$$\frac{\partial(\rho c)}{\partial t}+\frac{\partial(\rho c(u_x-w_x))}{\partial x}+\frac{\partial(\rho c(u_y-w_y))}{\partial y}+\frac{\partial(\rho c(u_z-w_z))}{\partial z}=0$$

The mesh is moved based on the spring method [43-45], in which the boundary nodes are moved forcing the interior nodes to move accordingly to reach the equilibrium state. Each edge acts like a spring. A movement on the boundary nodes causes a force along the edges connected to the node, This force based on the Hook's law is found as:

$$F=\sum k_i\ (\Delta x_i-\Delta x) \tag{2-58}$$

Where Δx , Δx_i are the node displacement and the displacements of neighbouring nodes. The total force on the each node is the sum of all forces along the edges connected to it. k_i is the stiffness of the edge and is found as follows:

$$k_i=\frac{1}{Edge\ \ Length} \tag{2-59}$$

Since the force on each node should be zero at equilibrium, the following iterative equation is solved:

$$\Delta x=\frac{\sum k_i\Delta x_i}{\sum k_i} \tag{2-60}$$

Finally the new position of each node is calculated by adding the displacement:

$$x^{n+1}=x^n+\Delta x \tag{2-61}$$

2-5 Second order accuracy in space

The code uses second order accuracy in space and van Leer - Van Albada limiter is used [46]:

$$f(x,y)=\begin{Bmatrix} 0 & if\ xy<0 \\ \dfrac{(y^2+\varepsilon)x+(x^2+\varepsilon)y}{x^2+y^2+2\varepsilon} & else \end{Bmatrix}$$

This limiter is modified to avoid the instability problems. The limiter switches the accuracy to first order in locations very near to exit area ($|Z|<D/10$, where D is the release area diameter) or the locations of high Mach number gradient.

Chapter 3

SIMULATION

A three-dimensional code is developed to simulate the release of high pressure hydrogen into ambient air by computational fluid dynamics. The pressure ratio of the hydrogen in the tank to the ambient air should be as high as 700 in order to have sufficient fuel in the tank. This high pressure ratio results in a very unstable simulation. First of all a very high quality mesh with high number of nodes is required to capture all the features of this flow accurately. High gradients caused by the high pressure ratio results in a very high speed flow and strong shocks.

3-1 Computational fluid dynamics model

The geometry and mesh requirements are described in this section. GAMBIT is used to generate the mesh required for the numerical simulation. High pressure ratio needs a very fine mesh to capture all the complexities of the flow. Note that the flow variables are stored at nodes, the high number of nodes and elements requires significant memory and long computational time; therefore the code employs parallel processing to overcome memory requirements and to have much shorter computing time. Without parallel processing, it may take months to reach the results on one processor. Message Passing

Interface (MPI) method is used in the parallel code. METIS software and an in-house code are used for the grid partitioning needed for parallel processing. Cirrus which is one of the Concordia University supercomputers is used to run the parallel code. In this research, the maximum memory used on cirrus is almost 25GB for a 3 million nodes mesh divided into 64 partitions.

3-1-1 Fixed Mesh

Figure (3-1) shows the three-dimensional and two-dimensional views of the geometry and the mesh. The mesh uses three-dimensional tetrahedral elements. The symmetry of the problem allows us to model just a small part like a 60-degree or 90-degree slice of the geometry but the high aspect ratio of the elements reduces the mesh quality, so it was decided to model the whole geometry to have better elements. Furthermore we are interested in full three-dimensional results as to be used later to simulate ground effect on the jet. This mesh contains almost 11 million elements and 2 million nodes. The dimensions are given in the two-dimensional view. The low pressure outside environment is a cylinder which is 150 millimetres long and has a radius of 80 millimetres. The release hole diameter is 5 millimetres. The mesh is very dense in the release area and it becomes less dense as the distance from the release area increases. In the reservoir the mesh is comparatively coarse since the flow gradients in the reservoir are much smaller than flow gradients in the low pressure outside environment.

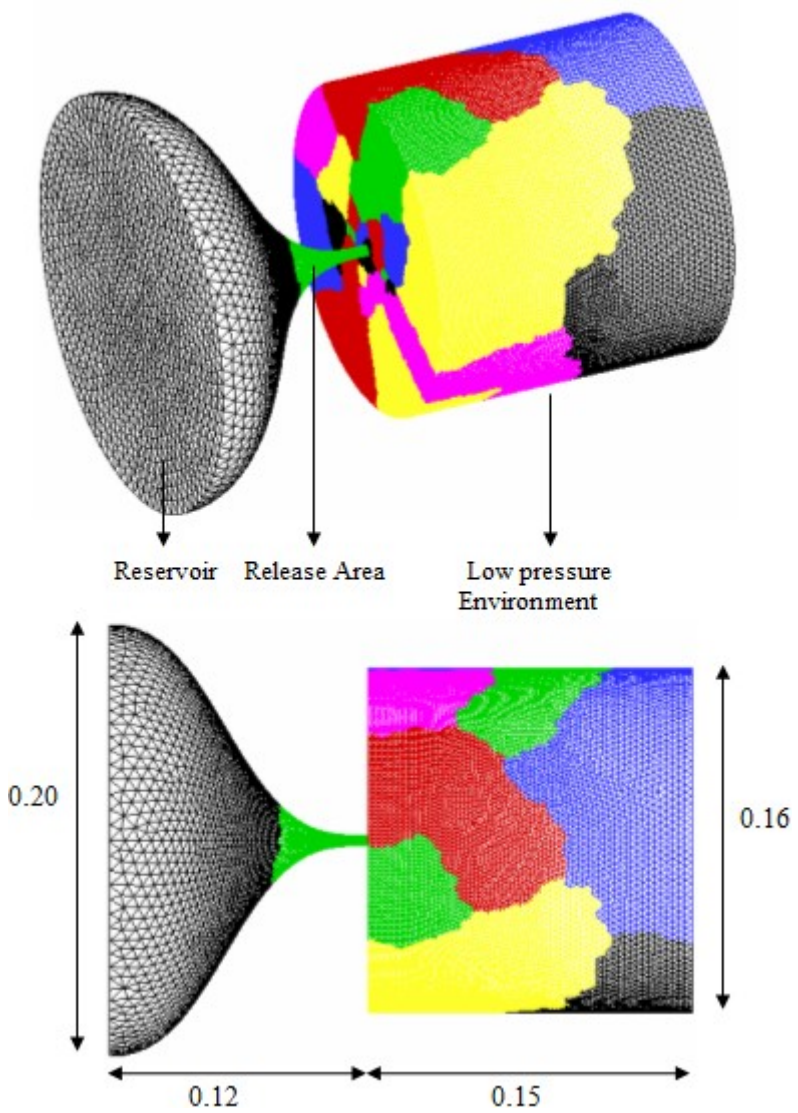

Figure (3-1) - 3D and 2D views of the fixed mesh (Units are in meters)

3-1-2 Moving Mesh

In reality the opening is not fixed and is expanding in time. Our results showed the main difference in the results happens in the very first few micro seconds, therefore it was decided to change the geometry focus more on the area close to the release area. In figure (3-2), the initial geometry and mesh for the initial release diameter of 2.0mm are given. It is noticed the external environment size is reduced to concentrate on the very first few

micro seconds after release. Three different meshes of different release area diameters are created with Gambit. The meshes have initial release diameters of 2.0mm, 1.5mm and 1.0mm. The geometry for all cases is similar except the release area. All three meshes include around 0.8 million nodes and 4 million tetrahedral elements. Each mesh is divided into 32 partitions. Boundary nodes are moved at each time step and all the other nodes are moving based on the spring method. In order to see the effect of mesh on the results, two fine meshes of 2 million and 3 million nodes with the same geometry are also tried for the moving mesh. These meshes are not shown here since the geometry is the same and the only difference is the high concentration of node numbers.

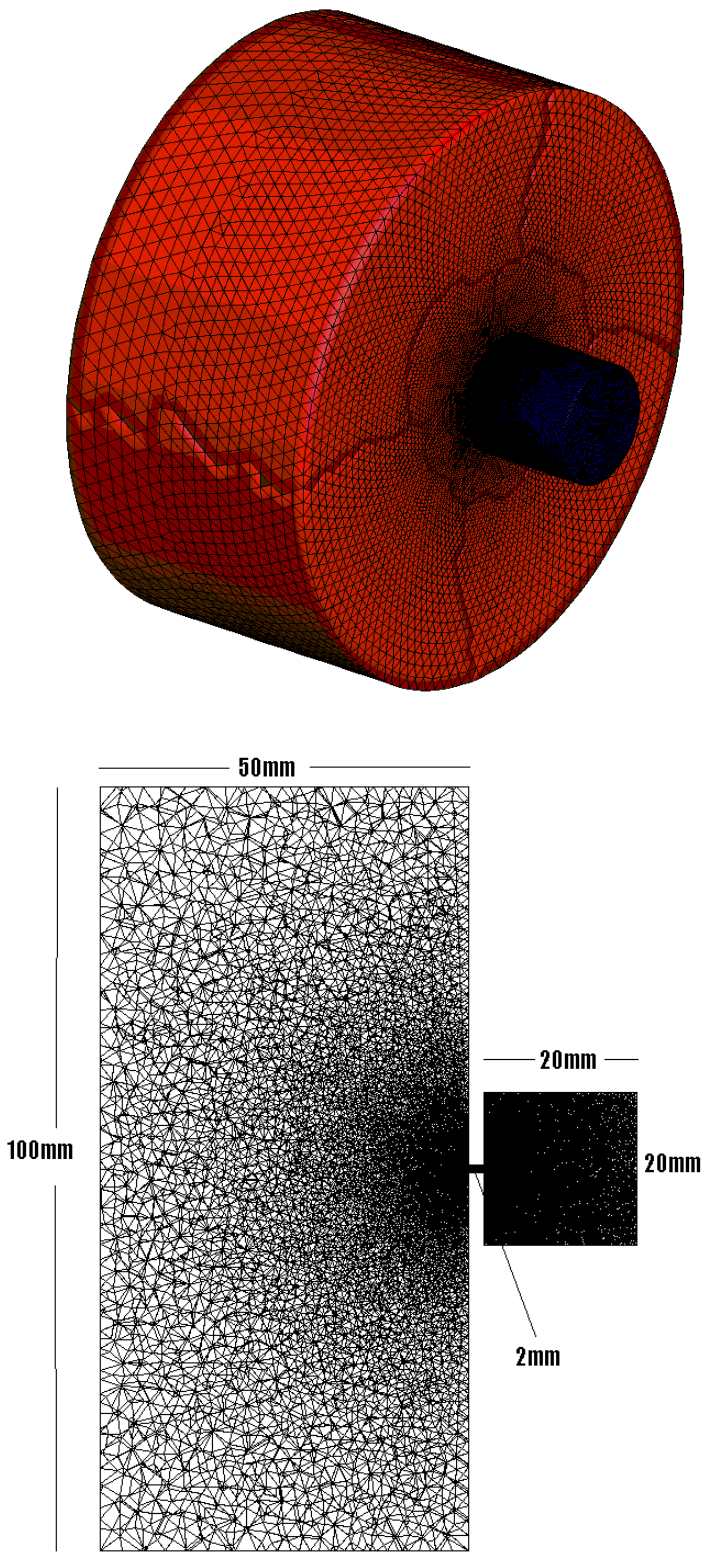

Figure (3-2) - 3D and 2D views of the moving mesh

3-2 Initial and boundary conditions

The reservoir and outside have the same temperature and velocity as the initial conditions. The velocity is zero and the temperature is 300 K. the pressure for the outside is 101325 Pa. The initial interface is always in the middle of the release area. The release area is 10 mm long for the cases of fixed mesh and 2 mm long for the moving mesh cases. The boundary conditions required are slip wall and non-reflecting far field as shown in figure (3-3). Boundaries are also adiabatic. Since after a certain amount of time there will be no choked flow in the release area and the velocity drops down, the reservoir should be included in the domain.

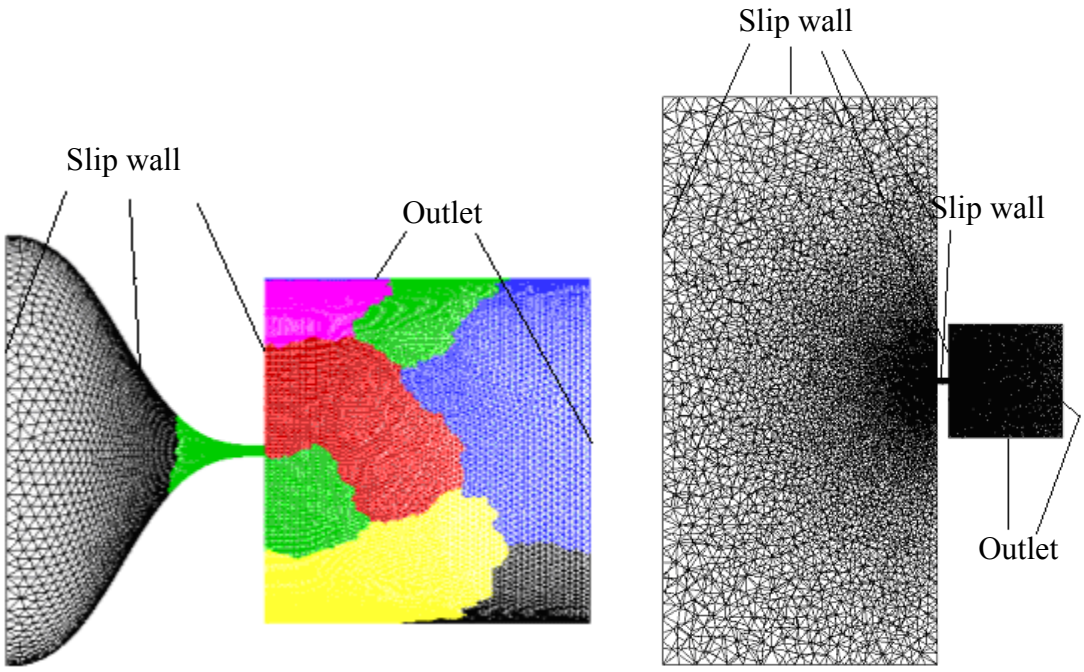

Figure (3-3) – Boundary condition for the fixed and moving mesh

Chapter 4

RESULTS

A three-dimensional in-house code is developed to simulate the release of hydrogen from a high pressure tank (up to 70 MPa) using both real and ideal gas models. Scenarios of hydrogen release in hydrogen and hydrogen release in air are examined. Euler equations are used since viscous terms can be neglected in this high speed and high Reynolds number (in the order of 10^7) flow. The code uses parallel processing to decrease the solution time and a transport equation to find out the concentration of each specie in the hydrogen-air mixture. The geometry consists of a cylinder-shaped reservoir, a tube-shaped release area and a cylinder-shaped external environment. Two scenarios of fixed mesh and moving mesh are discussed in the case of hydrogen release in air. For the fixed mesh the release area diameter is 5 mm. Three cases of tank pressure of 10MPa, 34.5MPa and 70MPa are examined up to the time of almost 100 micro seconds after release. For the moving mesh, three cases of initial diameter of 1.0 mm, 1.5 mm and 2.0 mm are considered. Each case is simulated up to the time of 3 micro seconds and three opening speed of 80m/s, 200m/s and 500m/s are tested.

4-1 Hydrogen release in hydrogen

The first case investigated is the release of hydrogen in hydrogen, i.e. high pressure hydrogen is released into low pressure hydrogen. Both Abel-Noble and Beattie-Bridgeman equation of states are examined for this case. Initially the tank pressure is 34.5 MPa and the pressure of the low pressure environment is ambient. The initial temperature is 300 K in the whole domain and the initial velocity is zero everywhere. The initial interface is at 5mm from the end of the release area.

4-1-1 Real gas simulations comparison

In table (4-1), the initial density of reservoir is given for ideal gas, Abel-Noble gas and Beattie-Bridgeman gas. The ideal gas result is considerably different from the real gas results. The difference between the real gas results is negligible.

Table (4-1)-Initial tank density at the pressure of 34.5 MPa

Equation of state	Ideal gas	Abel-Noble	Beattie-Bridgeman
Initial tank density	27.88	22.93	22.32

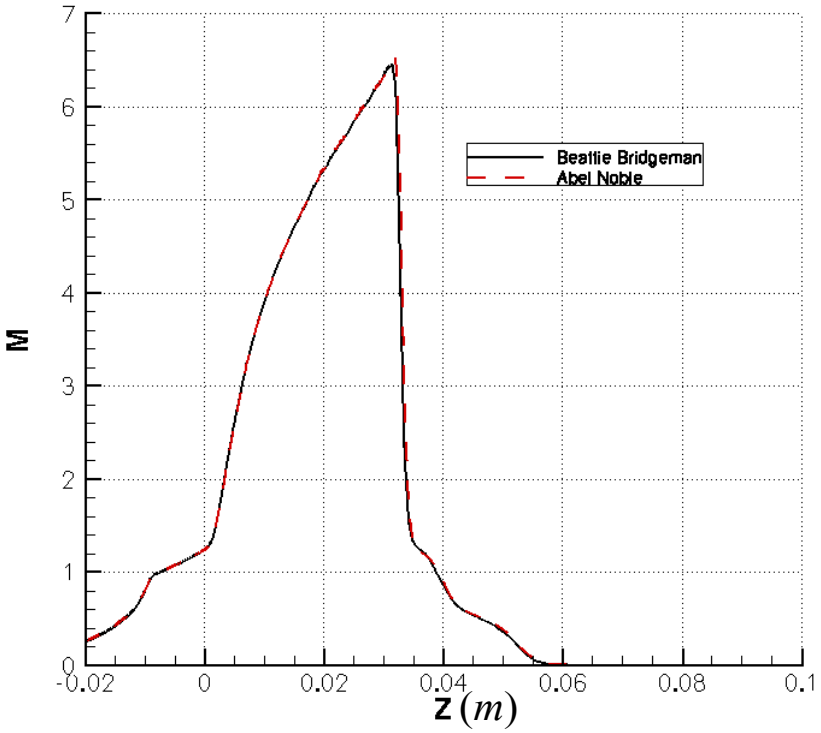

Figure (4-1) - Mach number along the centerline for pressure of 34.5 MPa at t=25 micro seconds

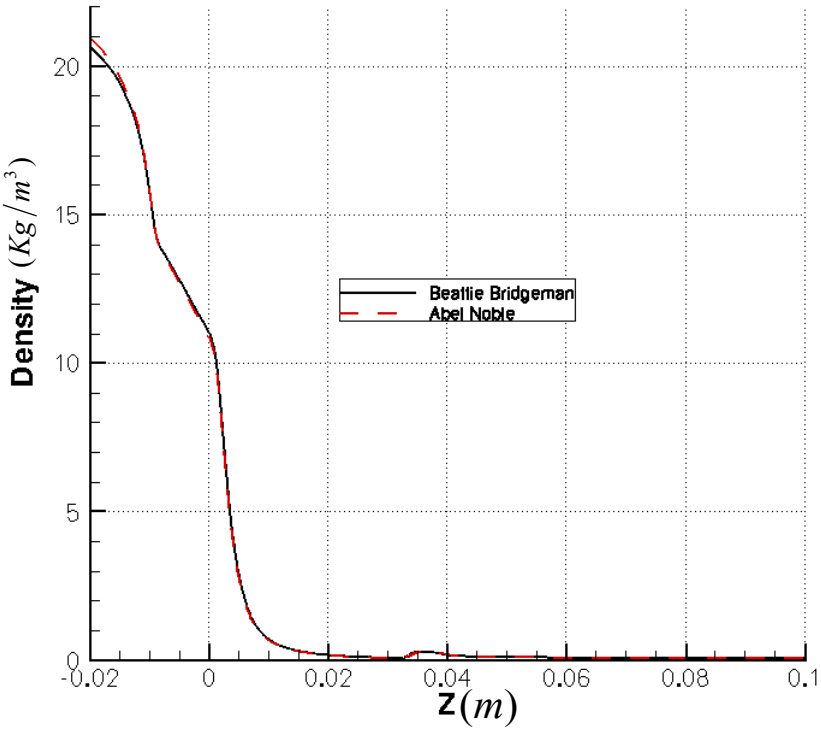

Figure (4-2) - Density along the centerline for pressure of 34.5 MPa at t=25 micro seconds

In figures (4-1) and (4-2), Mach number and density distribution along the centerline are given for Beattie-Bridgeman and Abel-Noble at 25 micro seconds. The maximum Mach number is almost 6.5 and the results are very close between the two models. To compare the ratio of specific heats for Beattie-Bridgeman and Abel-Noble, in figure (4-3) the ratio of specific heats of Beattie-Bridgeman is given. As mentioned earlier, for the Abel-Noble the ratio of specific heats is constant and equal to 1.40, therefore the maximum difference is less than 3 percent. It is noticed that the Abel-Noble and the Beattie-Bridgeman models give almost the same results while the Abel-Noble is more stable and is computationally faster.

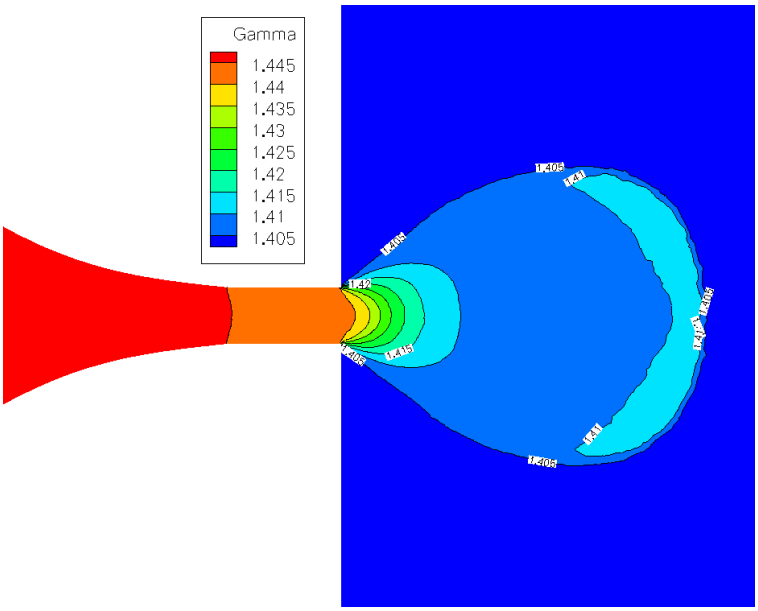

Figure (4-3) – ratio of specific heats for pressure of 34.5 MPa at t=25 micro seconds (Beattie-Bridgeman equation of state)

4-1-2 Validation of the Mach disk final location

Ashkenas et al. [47] propose an equation for the final location of the Mach disk as a function of pressure ratio. Although the unsteady jet is studied in this work, the Mach disk finally reaches a steady position and their equation can be used for the validation of

the code. According to the work of Ashkenas et al. [47], the final position of the Mach disk is given by:

$$Z/D = 0.67\,(P_0/P_1)^{1/2} \tag{4-1}$$

where Z is the final location of the Mach disk, D is the release area diameter, P_0 is the tank pressure and P_1 is the pressure of low pressure environment. This equation is valid for all ratios of specific heats in the range of $15 \le P_0/P_1 \le 17000$. Therefore it is valid for the cases reported herein.

In table (4-2), values from equation (4-1) are compared with results of our simulation for the real gas. Although the difference between these results is not negligible, it is still acceptable especially for the lowest pressure of 10 MPa. For the pressure of 70 MPa the difference is more than 10 percent. It can be concluded that equation (4-1) is not accurate enough for high pressures.

Table (4-2)-Final Mach disk location comparison

	10 MPa	34.5 MPa	70 MPa
Z/D (equation(4-1))	6.66	12.36	17.61
Z/D (simulation)	7.00	14.00	20.00

4-1-3 Comparison with FLUENT

To verify the accuracy of our code, simulation results are compared with previous work in the literature. Pedro et al. [27] used Fluent to simulate the high pressure release from a

10 MPa tank. Axisymmetric equations using ideal gas law are employed in their work. A two dimensional structured mesh is used and the mesh is adapted in critical areas. The release hole diameter is 5 mm. The mesh initially contains 70,000 quadrilateral elements. The external environment is 0.15 m long. Ideal gas was applied in their work. Ideal gas is accurate enough for the pressure of 10 MPa.

In our simulation the Abel-Noble equation is employed as the real gas equation of state. The mesh is a three-dimensional tetrahedral mesh which does not have the adaptation feature. Note that the Fluent simulation uses a two-dimensional mesh, therefore there is limited memory requirements and adaptation can be easily applied. In our work, more elements are used to make sure the same quality and accuracy is provided. In fact, in the future work it is expected to add the adaptation feature to avoid the high number of elements and decrease the solution time. Although the two-dimensional Fluent mesh seems better in terms of memory requirements and gives the same accuracy, the three-dimensional mesh used in our research is more flexible in terms of coarsening in less important areas like inside the tank and fining in areas like the release area. Overall a three-dimensional is is needed for future work for example when adding the ground effects. Most cases of interest can only be modeled by a three-dimensional mesh which is the ultimate goal of this research.

The Mach number along the centerline is given in figure (4-4) at four different times. Time is non-dimensionalized by diameter of the release area over sound speed of hydrogen for ideal gas at Temperature of 300 K. Comparison shows good agreement between these two results.

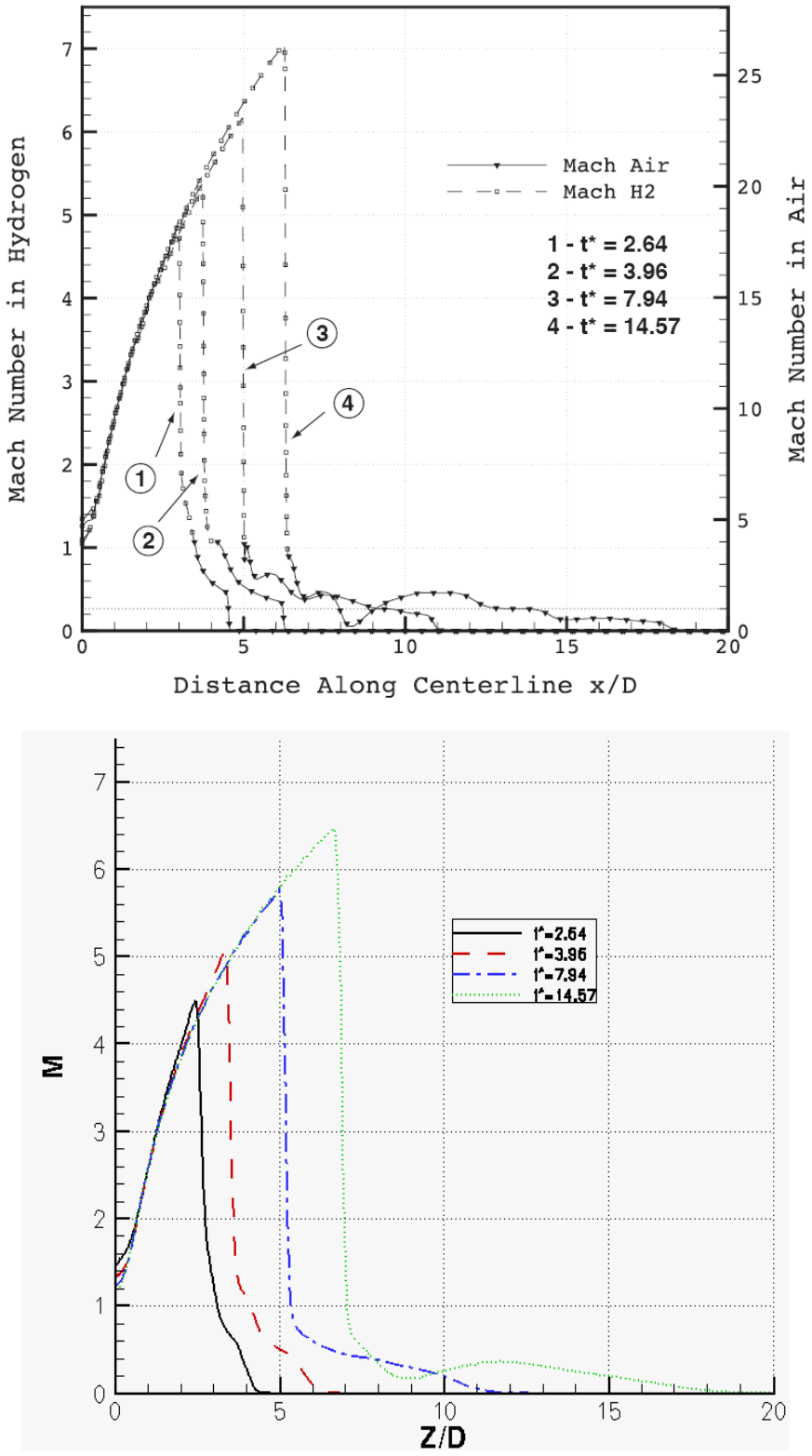

Figure (4-4) - Mach number along the centerline for pressure of 10 MPa (Top: results of [27], Bottom: present simulation)

4-2 Hydrogen release in air

In general, high pressure hydrogen is released in low pressure air so the rest of the thesis analyses this situation. The challenging difference is the hydrogen-air mixture caused after release in air since a contact surface between hydrogen and air is generated which moves in time and to capture this contact surface a new equation called transport equation should be added. Due to different properties of hydrogen and air there are more stability problems especially in more complicated situations like using Beattie-Bridgeman equation. In the previous section there was only one specie (hydrogen), now the transport equation is added to find the concentration of the hydrogen-air mixture. The Beattie-Bridgeman equation of state encountered stability problems for this case and since in the case of hydrogen release in hydrogen it has shown no advantage over the Abel Noble model, only the Abel Noble model is applied as the real gas equation.

4-2-1 The evolution of the flow

Three different tank pressures of 10 MPa, 34.5 MPa and 70 MPa are examined to investigate both low and high pressure ratios. In all cases the initial interface is at 5mm from the end of the release area. In figures (4-5) to (4-19) Mach, concentration, pressure, density and velocity contours are presented at six different times for the initial tank pressures of 10 MPa, 34.5 MPa and 70 MPa respectively. The initial temperature is 300K and the low pressure environment has initially ambient pressure. Shortly after release, a Mach disk and a barrel shock appear and the flow pattern remains the same at all times i.e. the Mach disk and the barrel shock exist in all figures. The sonic flow in the release area rapidly becomes supersonic after release. The jet gets stronger until it reaches the

Mach disk where it is changed to subsonic flow. The Mach disk is a very strong shock. The contact surface observed in the concentration contours is ahead of the Mach disk.

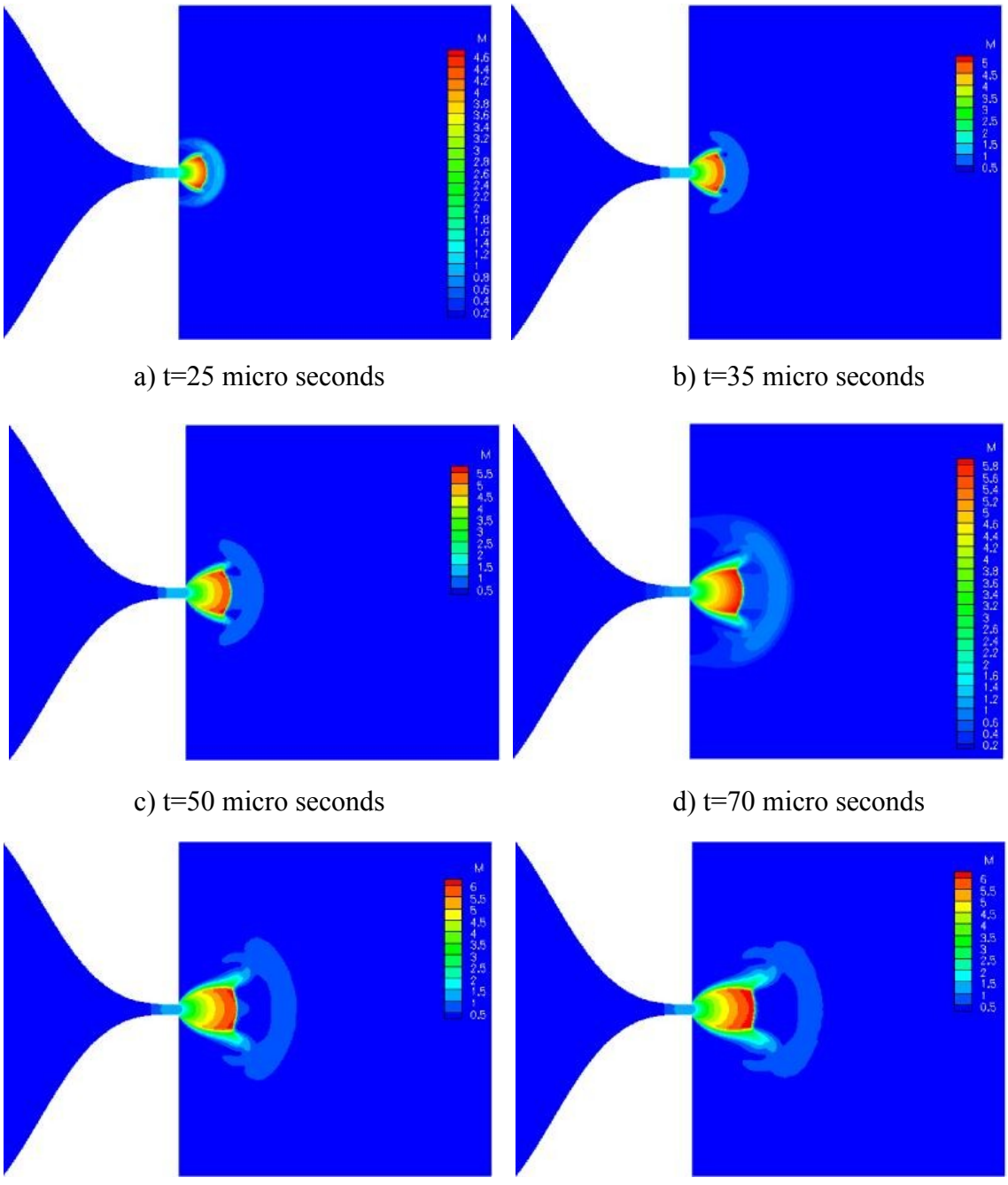

a) t=25 micro seconds

b) t=35 micro seconds

c) t=50 micro seconds

d) t=70 micro seconds

e) t=90 micro seconds

f) t=110 micro seconds

Figure (4-5)- Mach number for an initial tank pressure of 10 MPa at different times

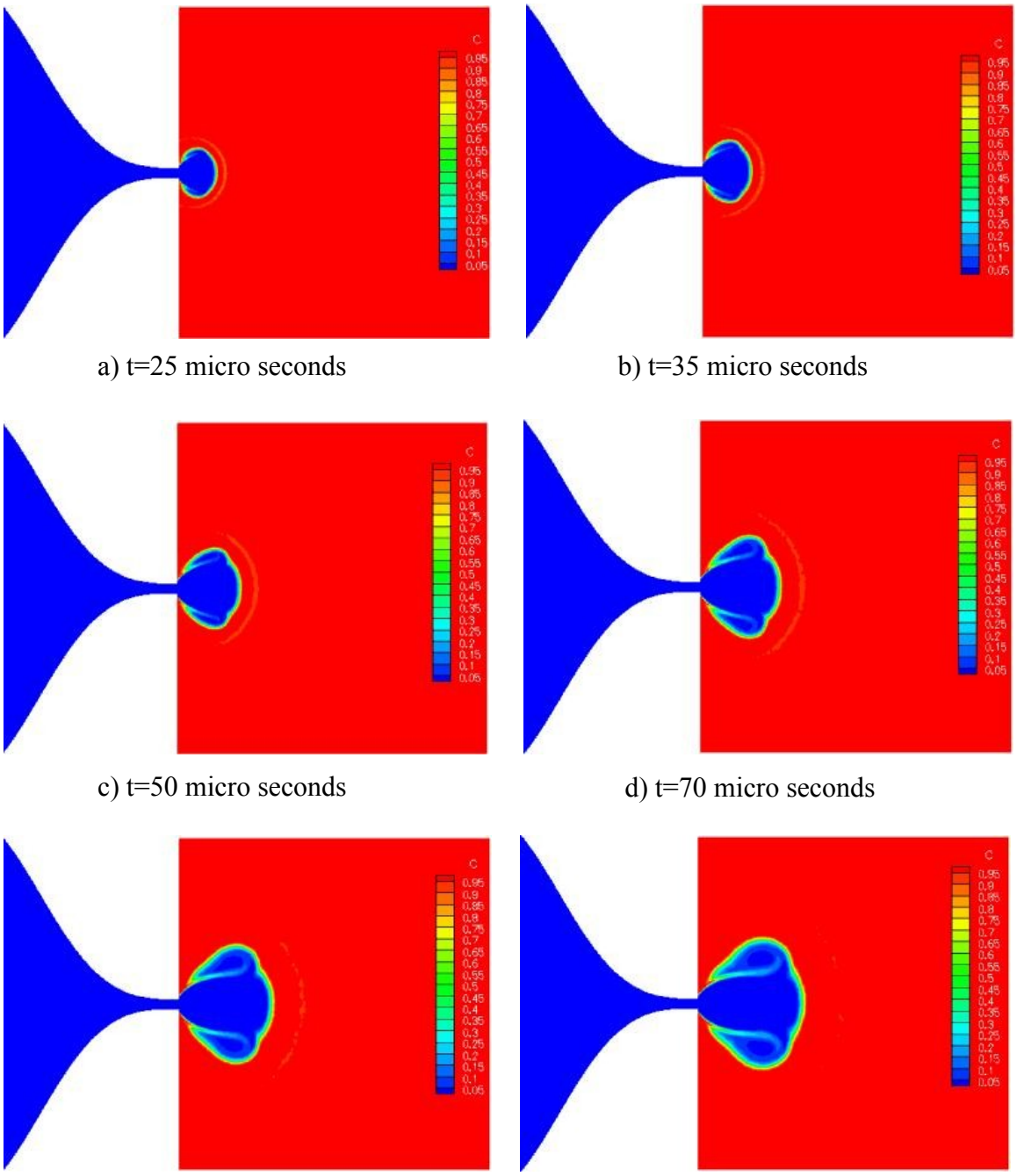

a) t=25 micro seconds

b) t=35 micro seconds

c) t=50 micro seconds

d) t=70 micro seconds

e) t=90 micro seconds

f) t=110 micro seconds

Figure (4-6)- Concentration contours for an initial tank pressure of 10 MPa at different times

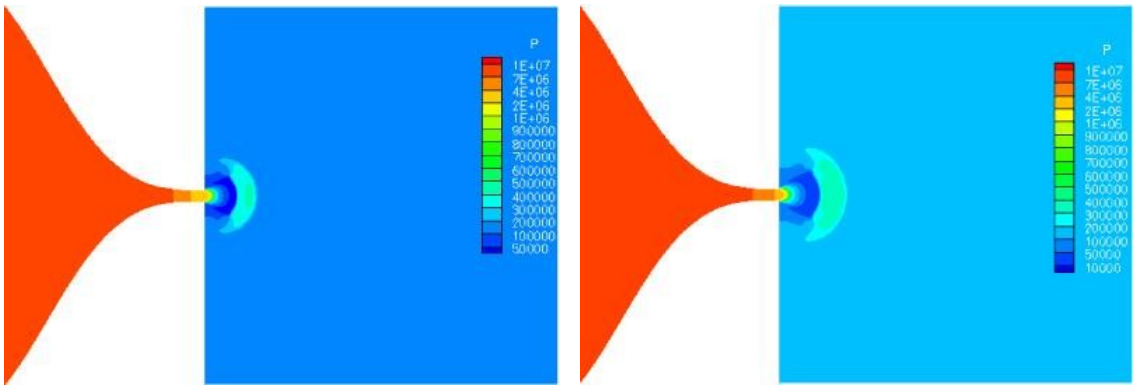

a) t=25 micro seconds

b) t=35 micro seconds

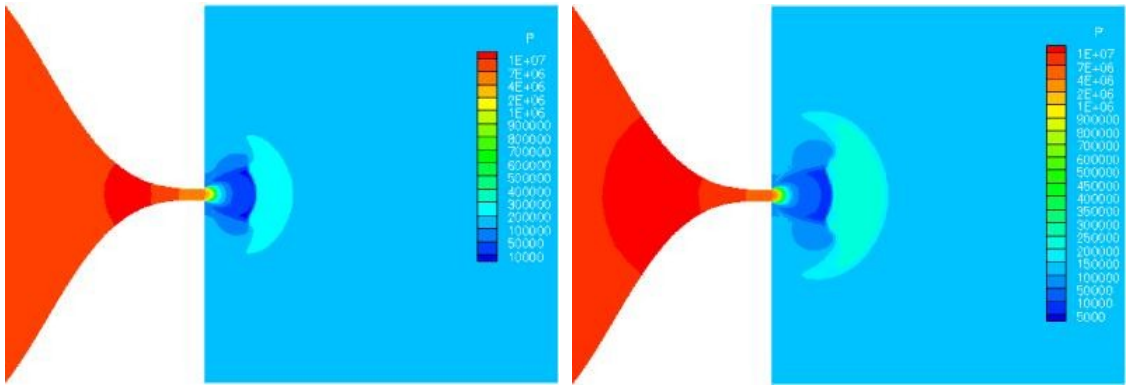

c) t=50 micro seconds

d) t=70 micro seconds

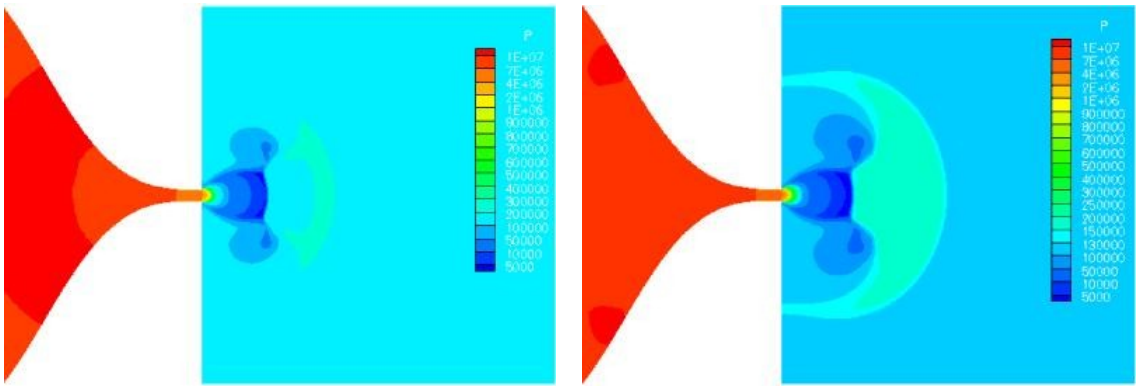

e) t=90 micro seconds

f) t=110 micro seconds

Figure (4-7)- Pressure for an initial tank pressure of 10 MPa at different times

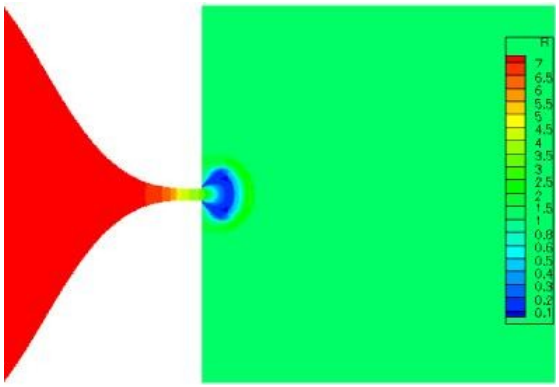

a) t=25 micro seconds

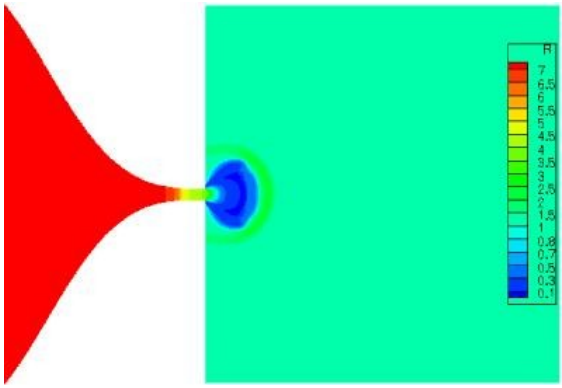

b) t=35 micro seconds

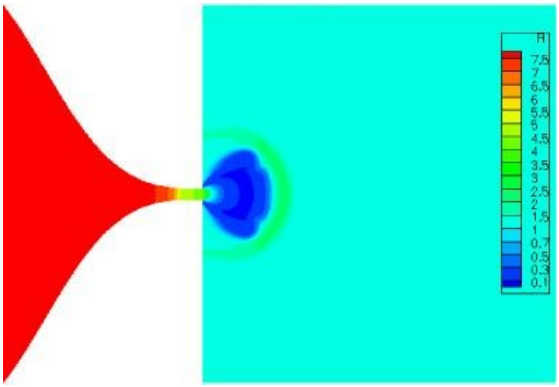

c) t=50 micro seconds

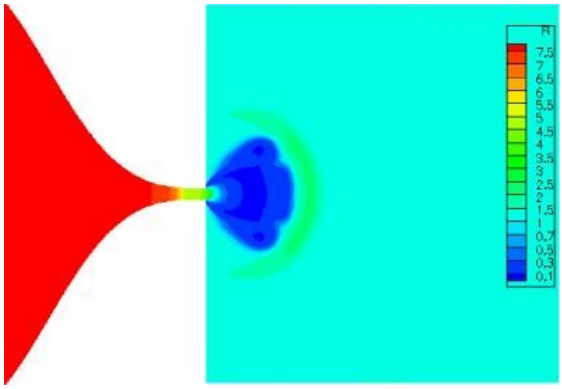

d) t=70 micro seconds

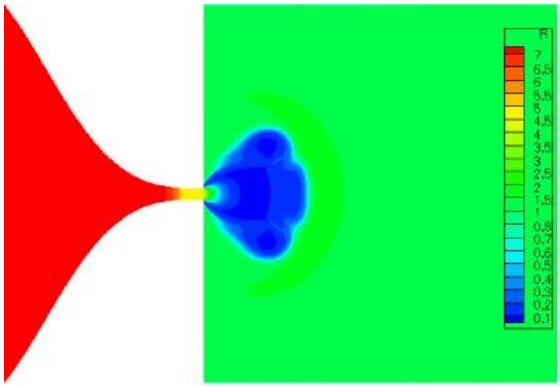

e) t=90 micro seconds

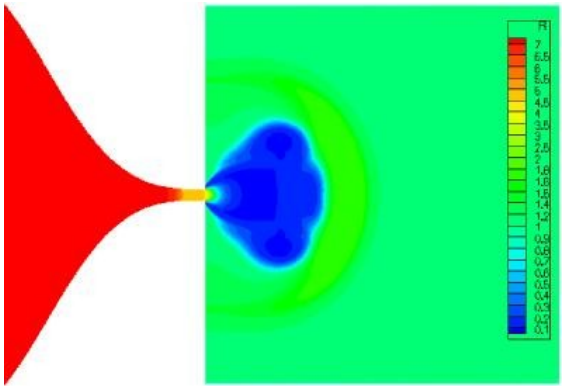

f) t=110 micro seconds

Figure (4-8)- Density for an initial tank pressure of 10 MPa at different times

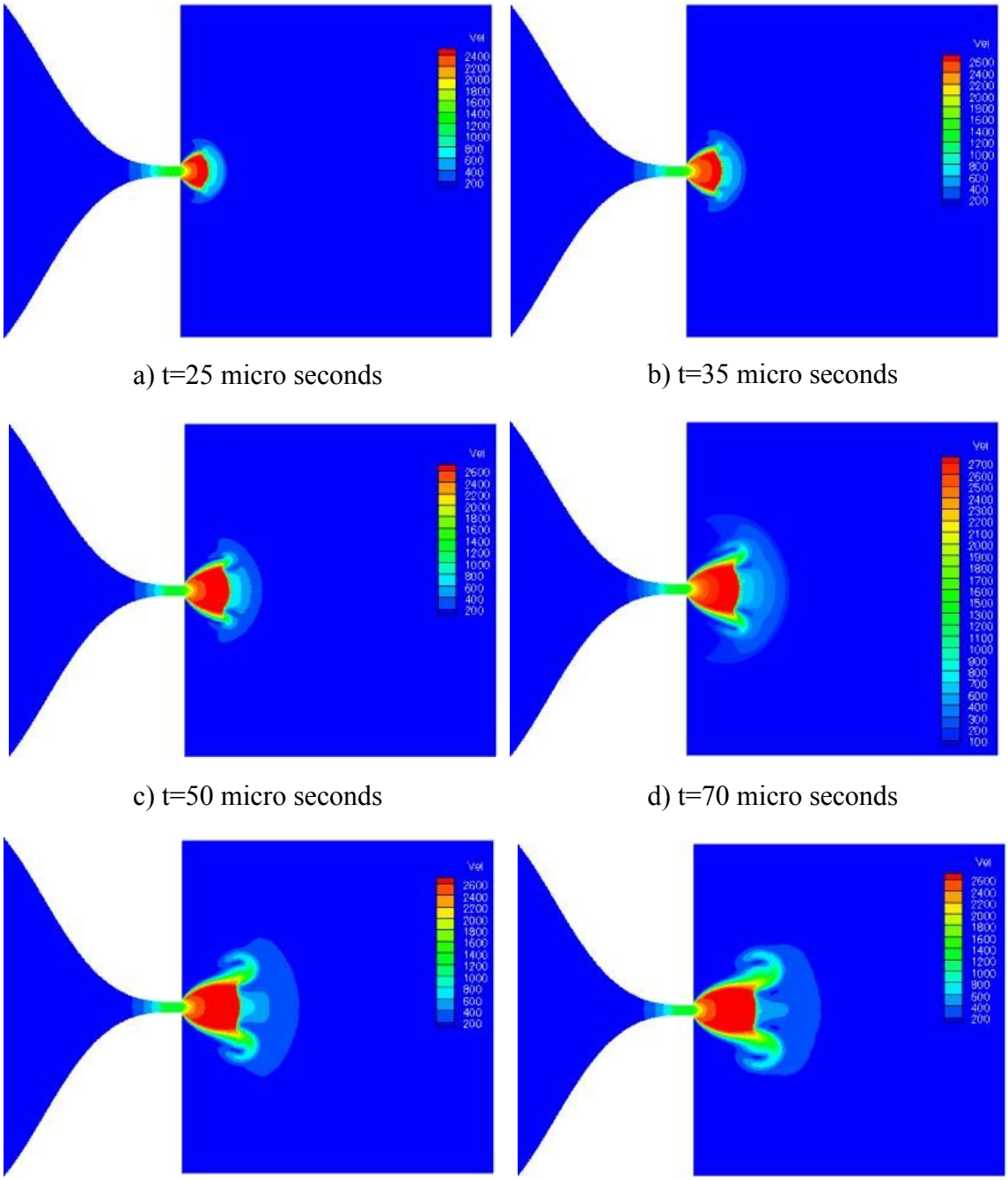

a) t=25 micro seconds

b) t=35 micro seconds

c) t=50 micro seconds

d) t=70 micro seconds

e) t=90 micro seconds

f) t=110 micro seconds

Figure (4-9)- Velocity for an initial tank pressure of 10 MPa at different times

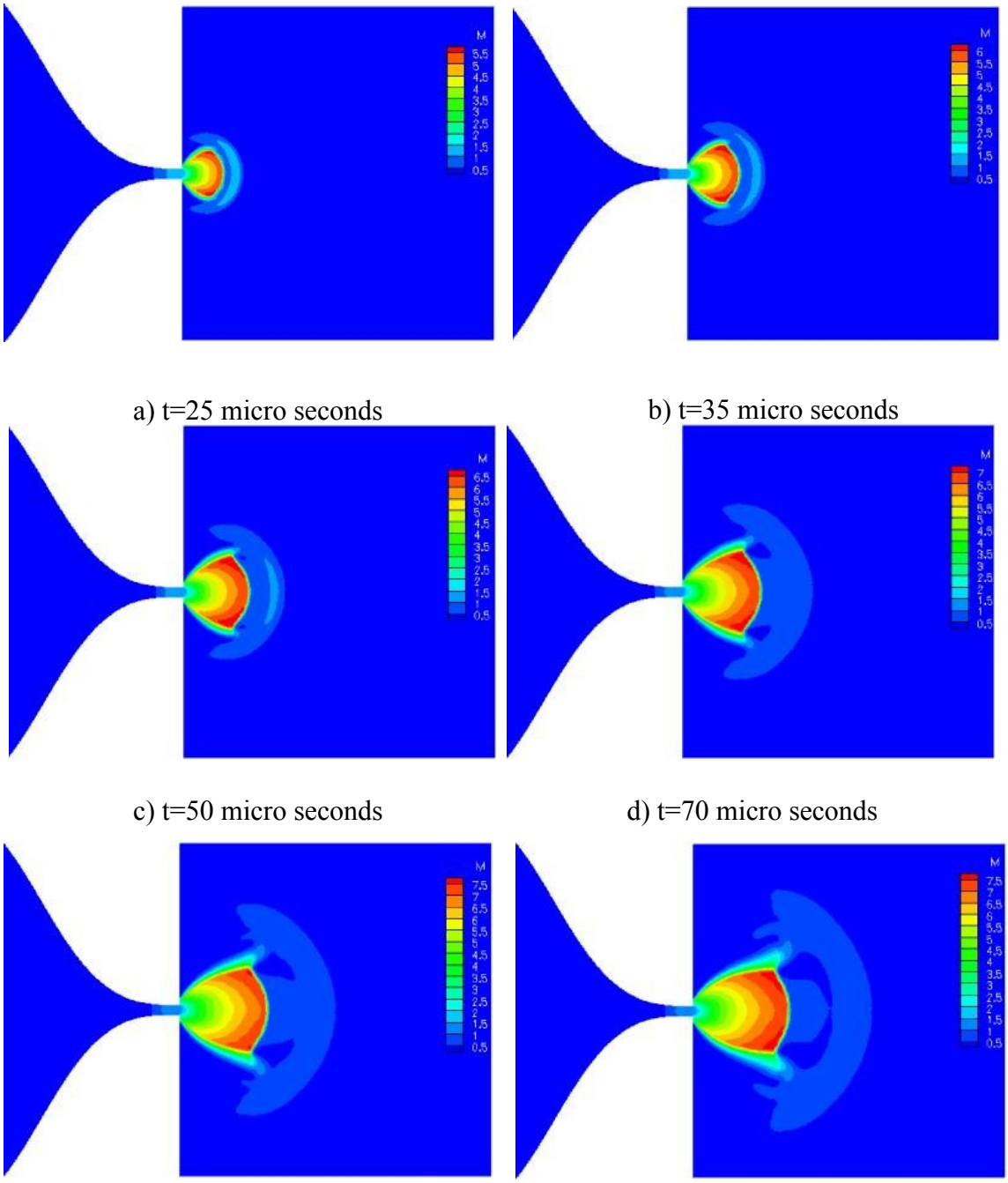

a) t=25 micro seconds

b) t=35 micro seconds

c) t=50 micro seconds

d) t=70 micro seconds

e) t=90 micro seconds

f) t=110 micro seconds

Figure (4-10)- Mach number for an initial tank pressure of 34.5 MPa at different times

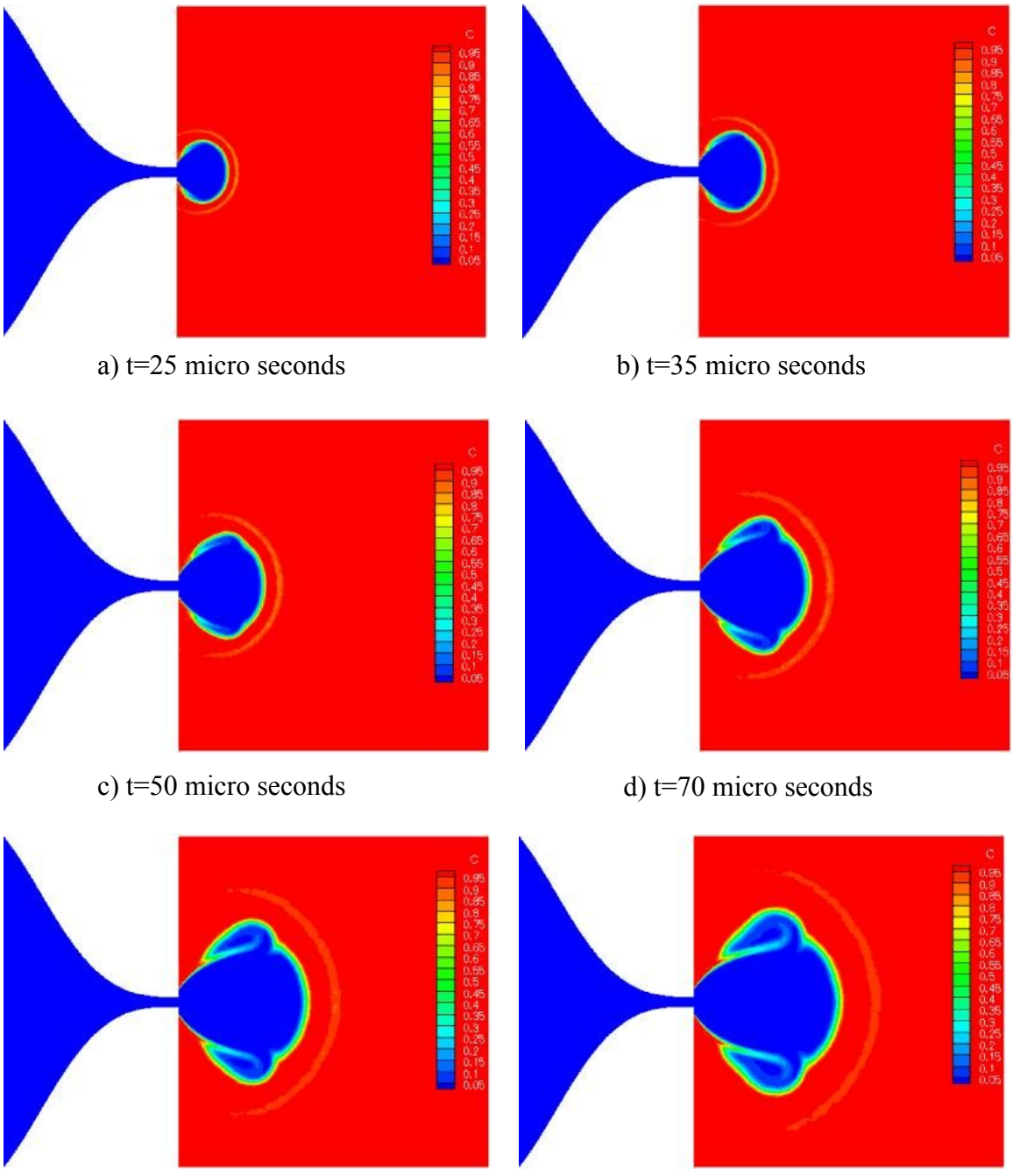

a) t=25 micro seconds

b) t=35 micro seconds

c) t=50 micro seconds

d) t=70 micro seconds

e) t=90 micro seconds

f) t=110 micro seconds

Figure (4-11)- concentration contours for an initial tank pressure of 34.5 MPa at different times

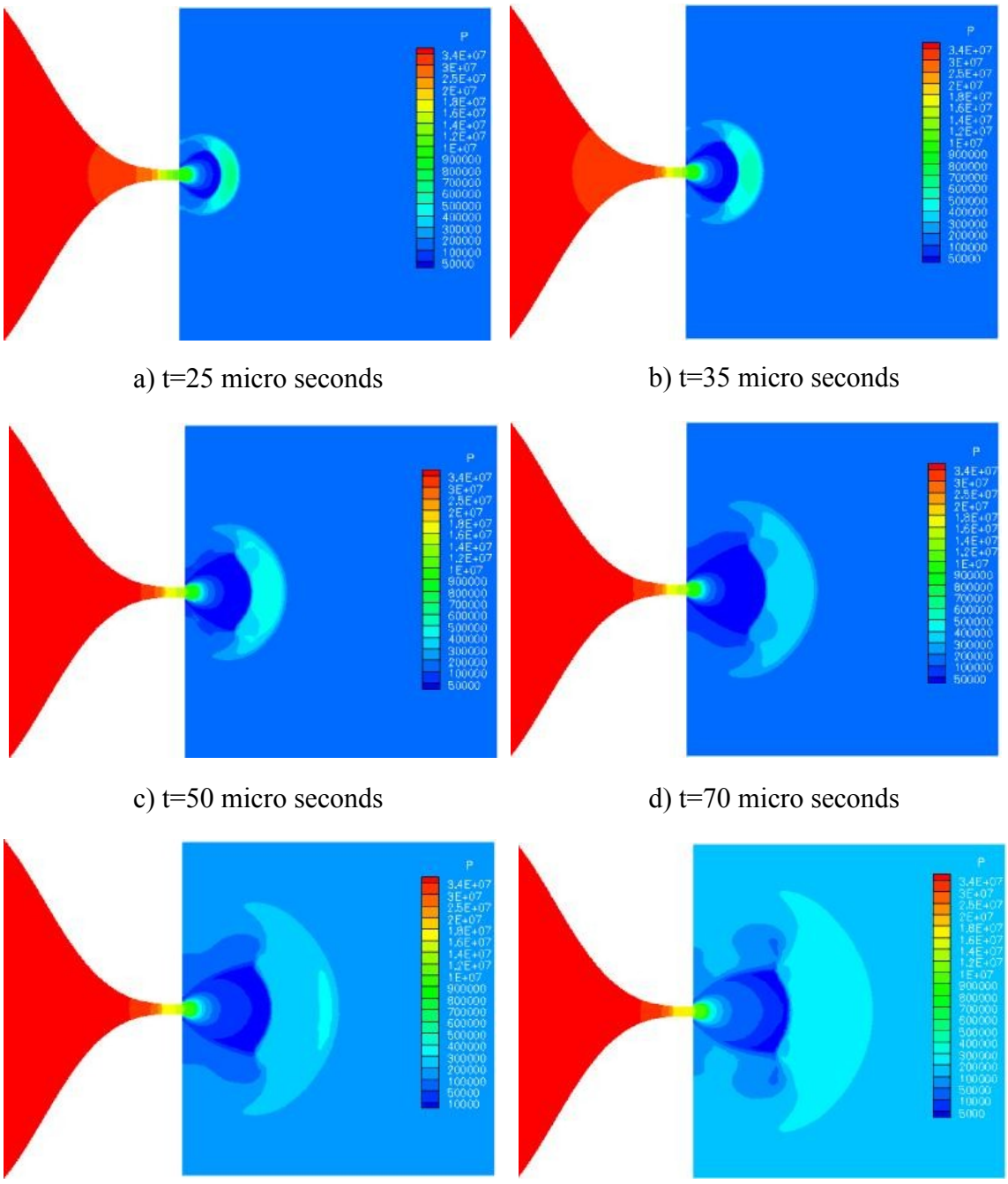

a) t=25 micro seconds

b) t=35 micro seconds

c) t=50 micro seconds

d) t=70 micro seconds

e) t=90 micro seconds

f) t=110 micro seconds

Figure (4-12)- Pressure for an initial tank pressure of 34.5 MPa at different times

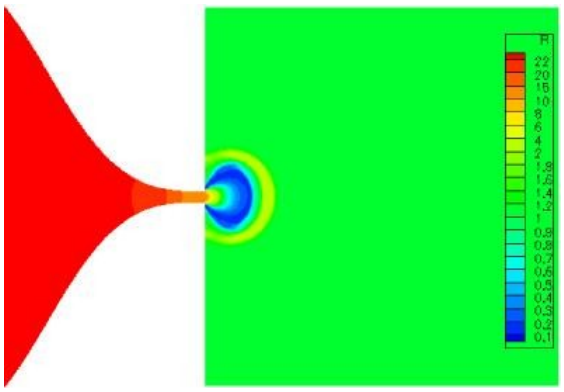

a) t=25 micro seconds

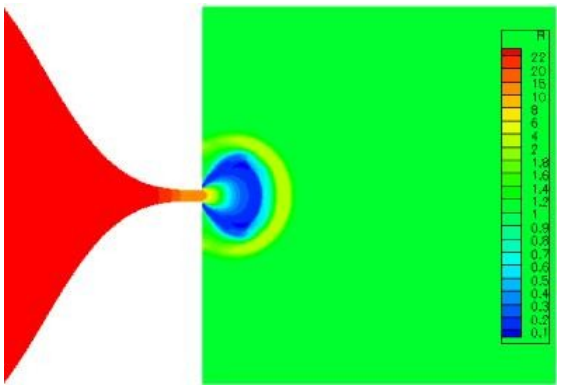

b) t=35 micro seconds

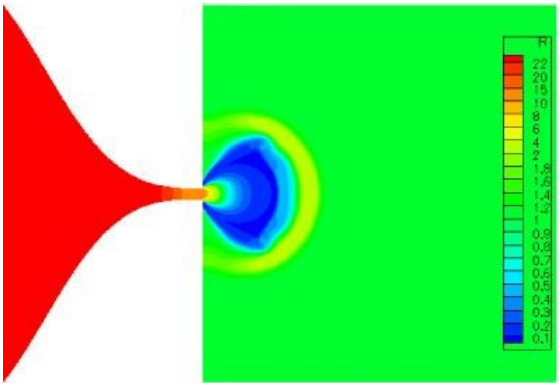

c) t=50 micro seconds

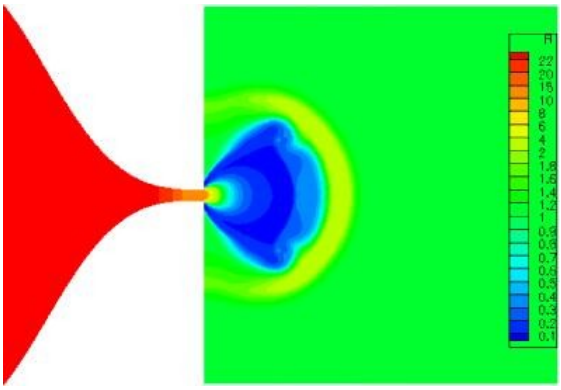

d) t=70 micro seconds

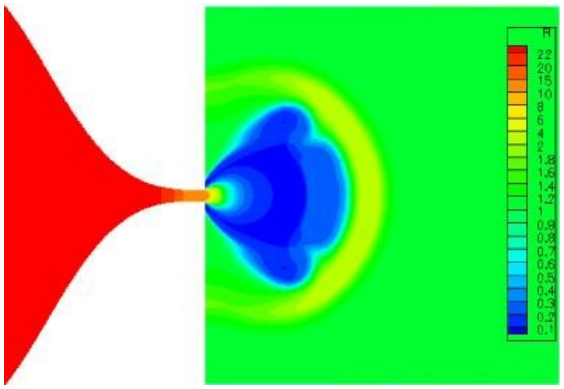

e) t=90 micro seconds

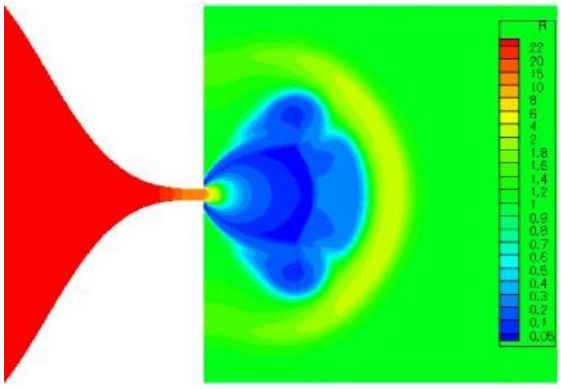

f) t=110 micro seconds

Figure (4-13)- Density for an initial tank pressure of 34.5 MPa at different times

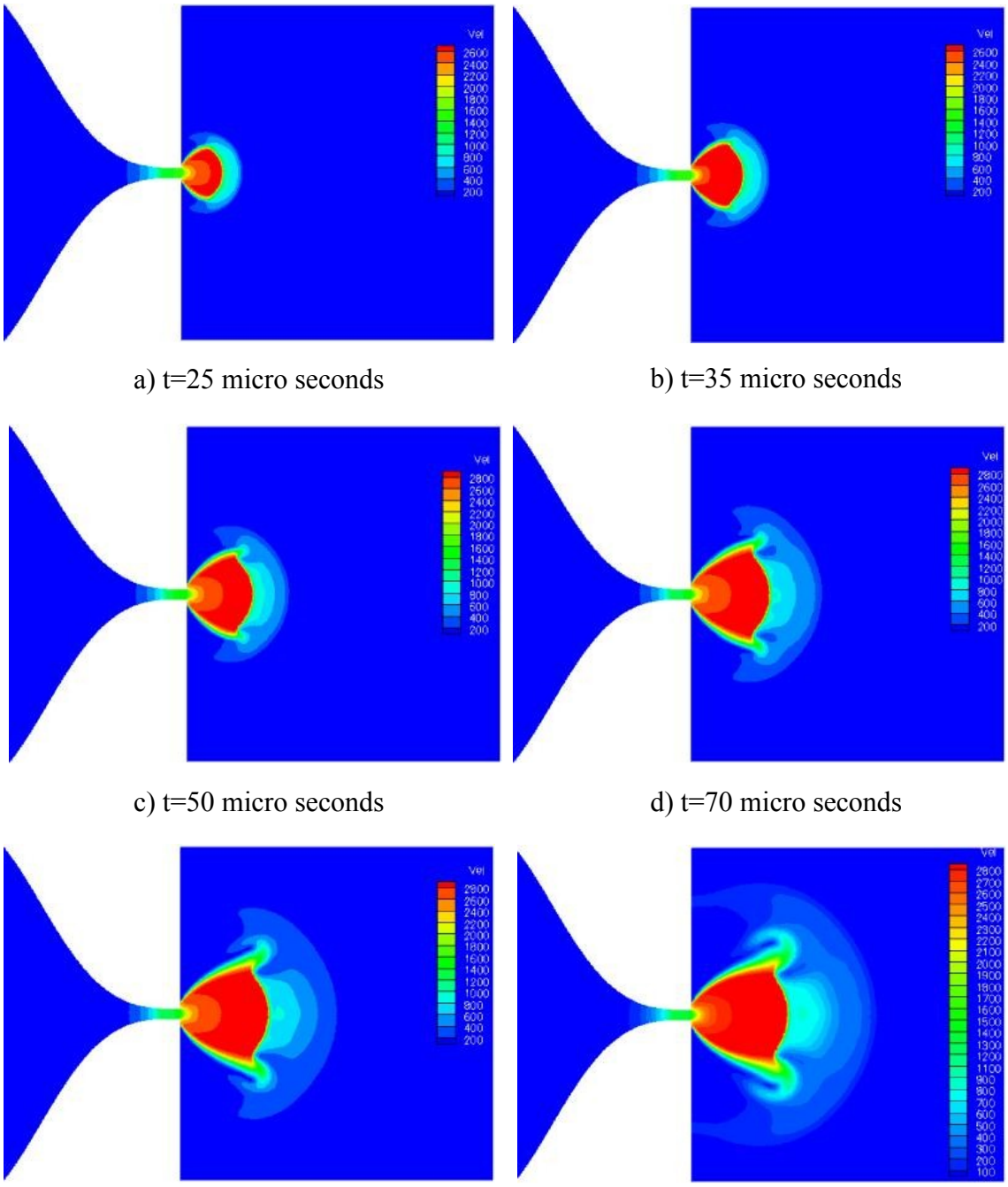

a) t=25 micro seconds

b) t=35 micro seconds

c) t=50 micro seconds

d) t=70 micro seconds

e) t=90 micro seconds

f) t=110 micro seconds

Figure (4-14)- Velocity for an initial tank pressure of 34.5 MPa at different times

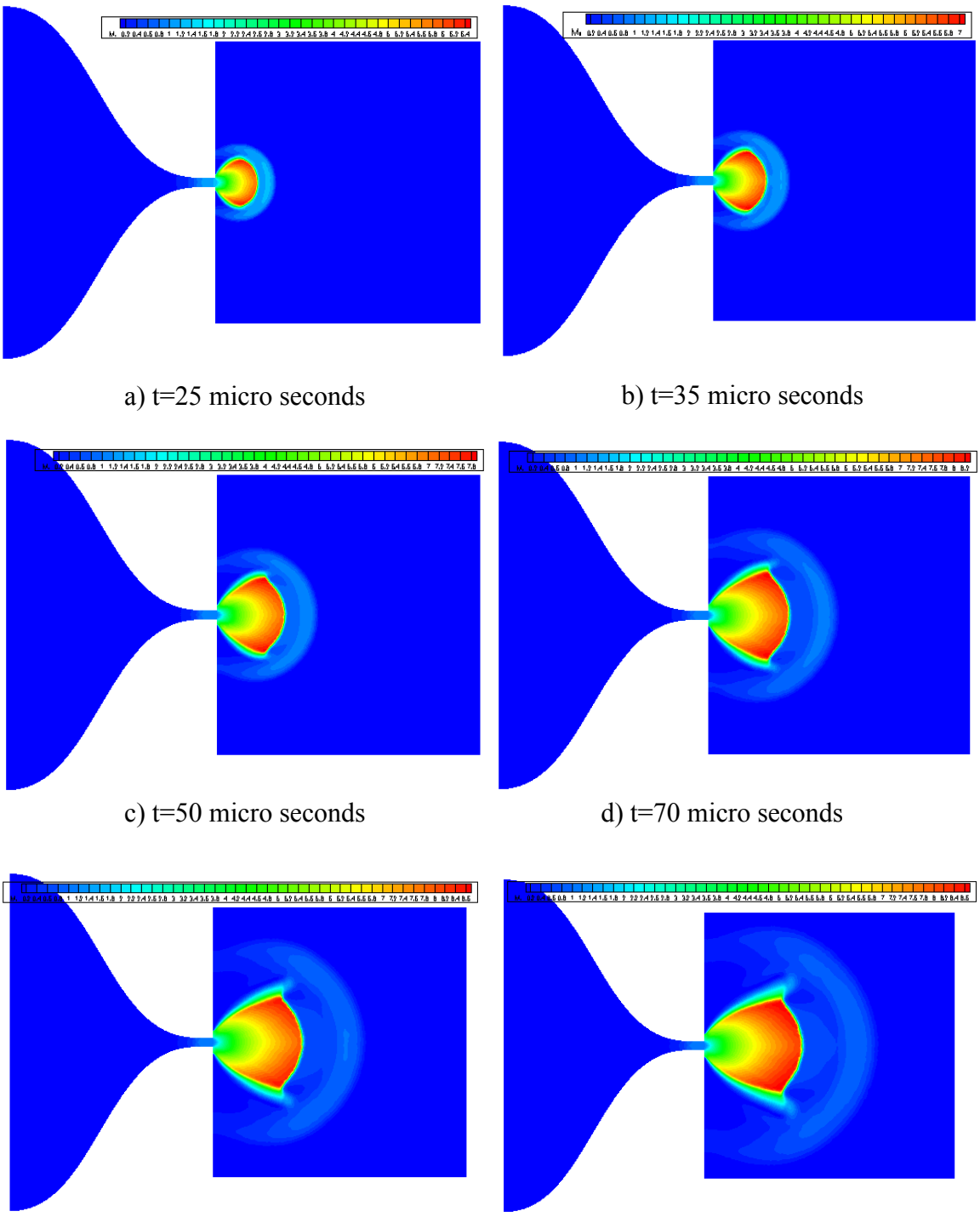

a) t=25 micro seconds

b) t=35 micro seconds

c) t=50 micro seconds

d) t=70 micro seconds

e) t=90 micro seconds

f) t=110 micro seconds

Figure (4-15)- Mach number for an initial tank pressure of 70 MPa at different times

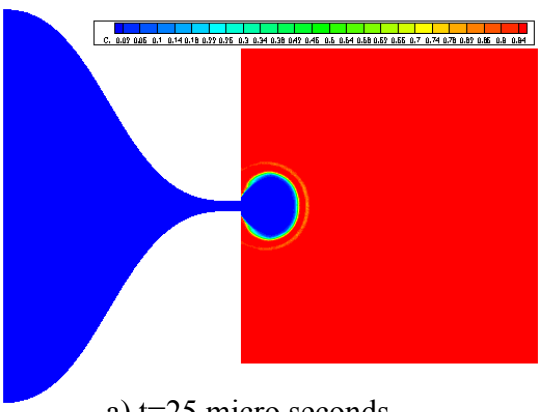

a) t=25 micro seconds

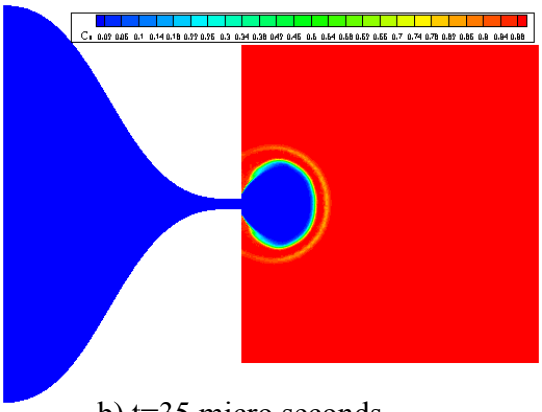

b) t=35 micro seconds

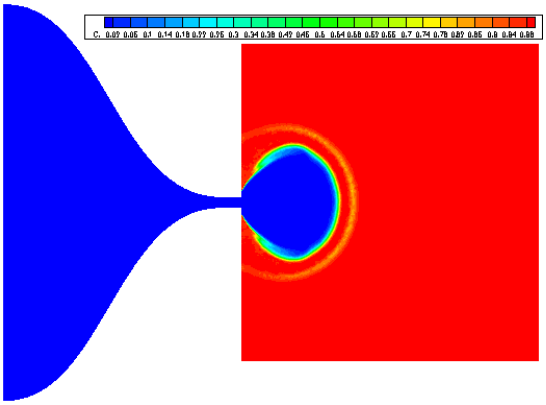

c) t=50 micro seconds

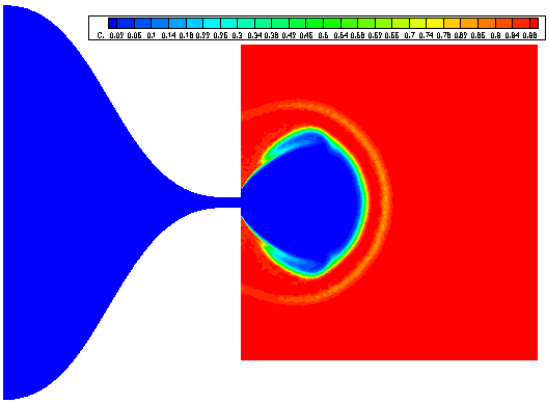

d) t=70 micro seconds

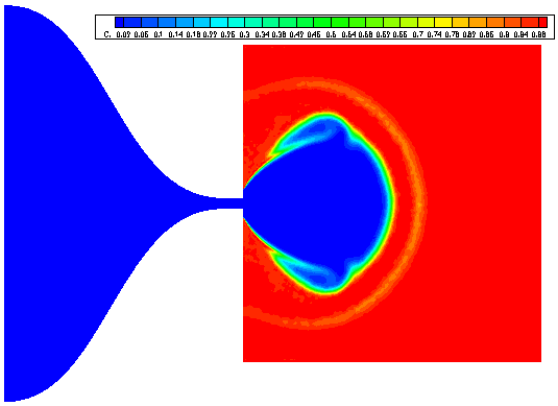

e) t=90 micro seconds

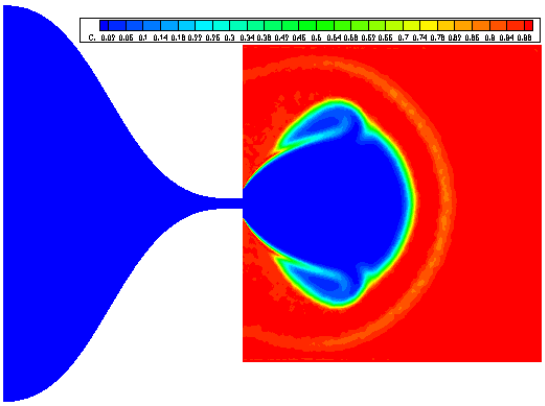

f) t=110 micro seconds

Figure (4-16)- concentration contours for an initial tank pressure of 70 MPa at different times

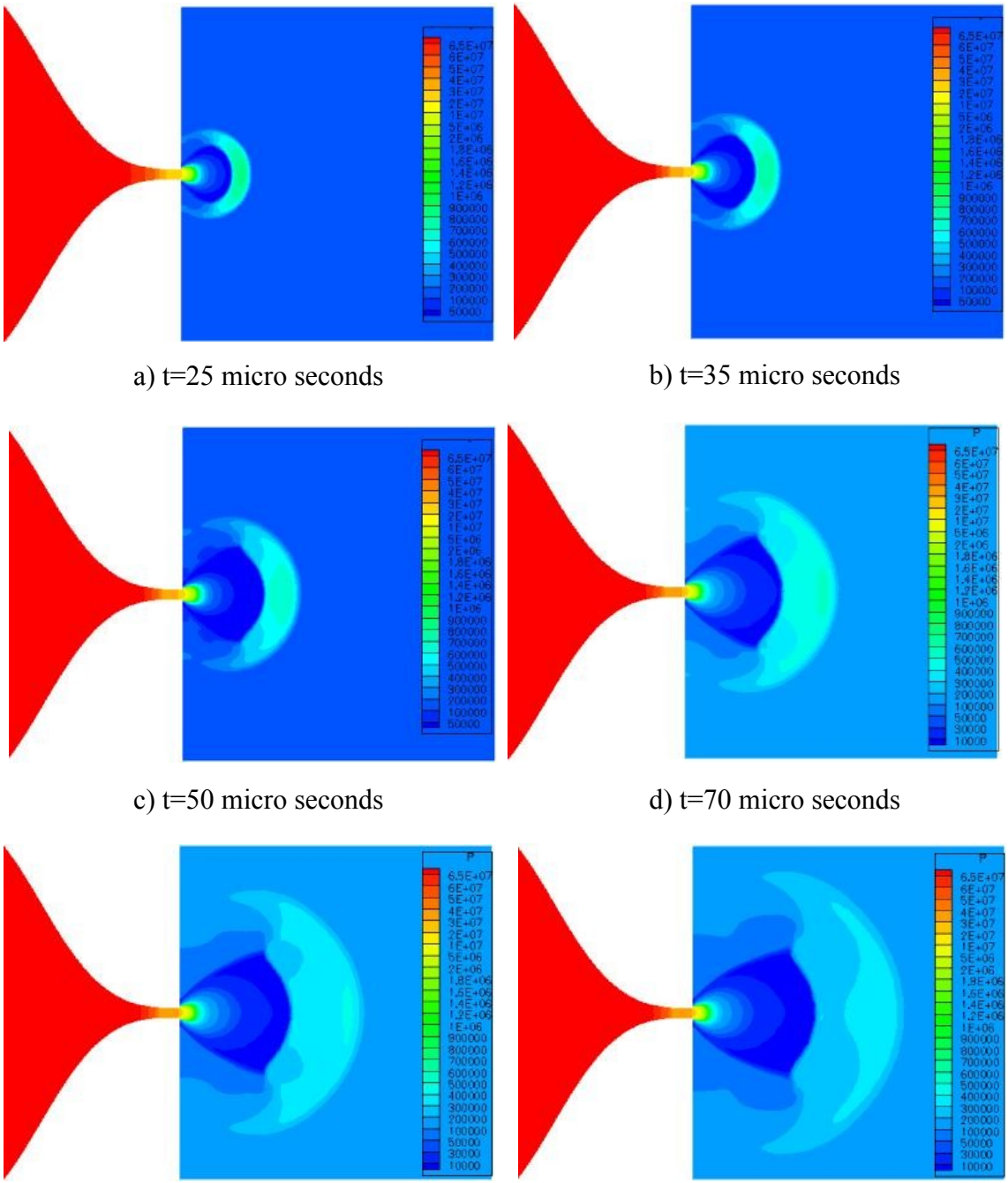

a) t=25 micro seconds

b) t=35 micro seconds

c) t=50 micro seconds

d) t=70 micro seconds

e) t=90 micro seconds

f) t=110 micro seconds

Figure (4-17)- Pressure for an initial tank pressure of 70 MPa at different times

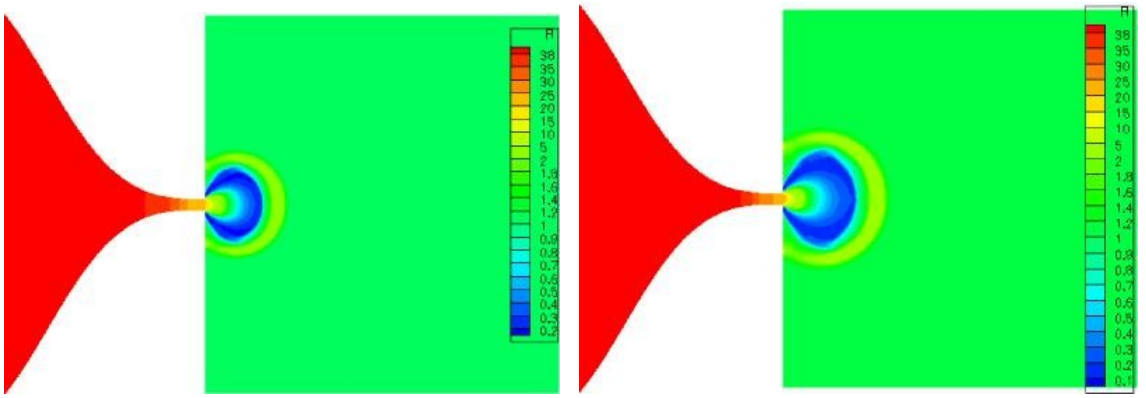

a) t=25 micro seconds

b) t=35 micro seconds

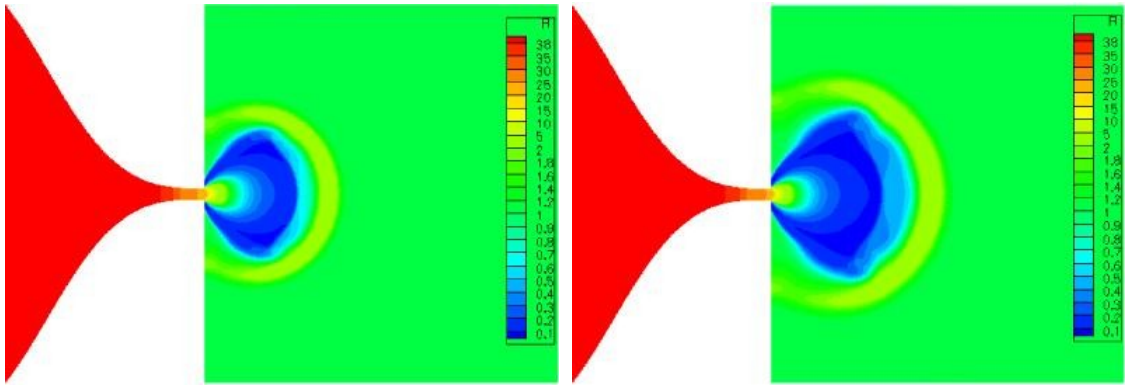

c) t=50 micro seconds

d) t=70 micro seconds

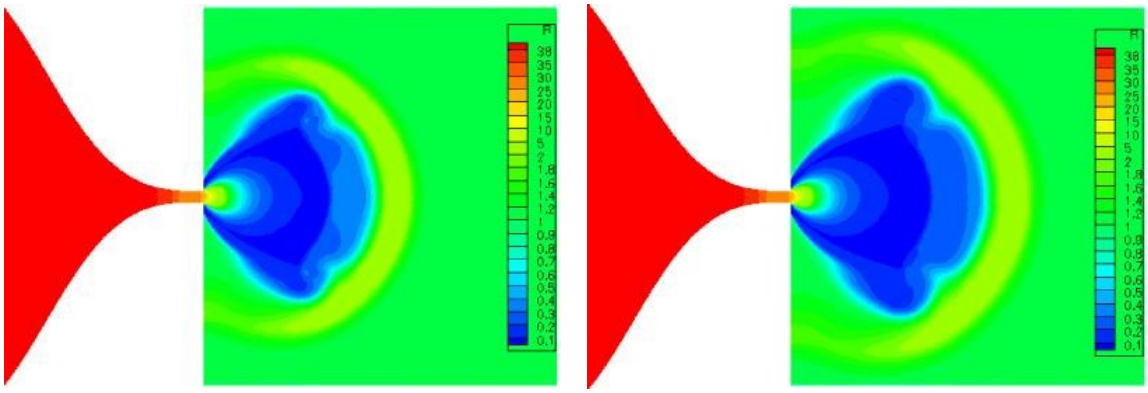

e) t=90 micro seconds

f) t=110 micro seconds

Figure (4-18)- Density for an initial tank pressure of 70 MPa at different times

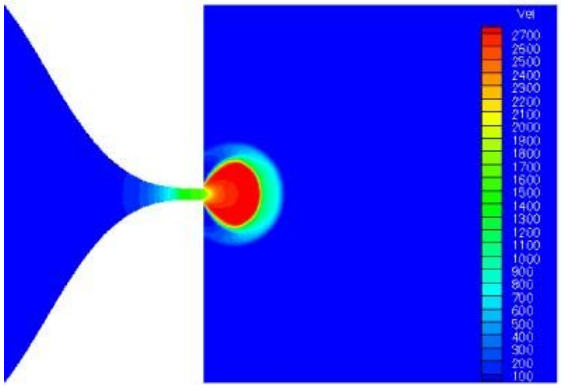

a) t=25 micro seconds

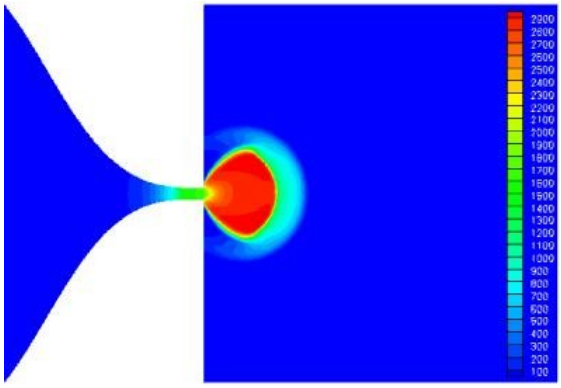

b) t=35 micro seconds

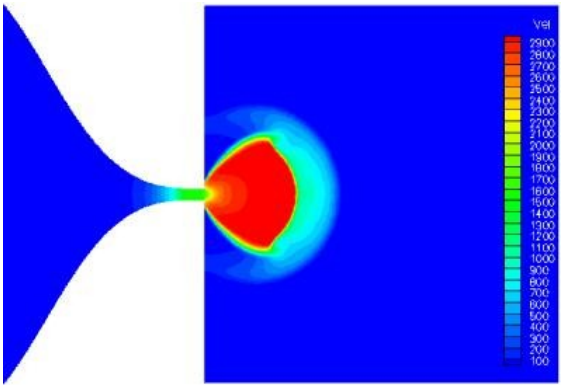

c) t=50 micro seconds

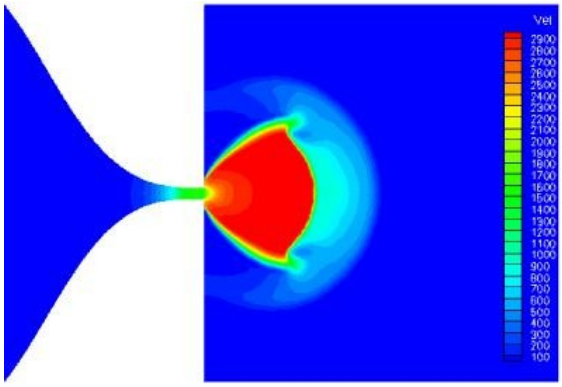

d) t=70 micro seconds

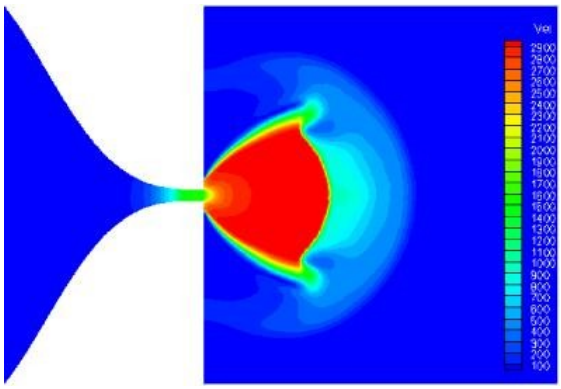

e) t=90 micro seconds

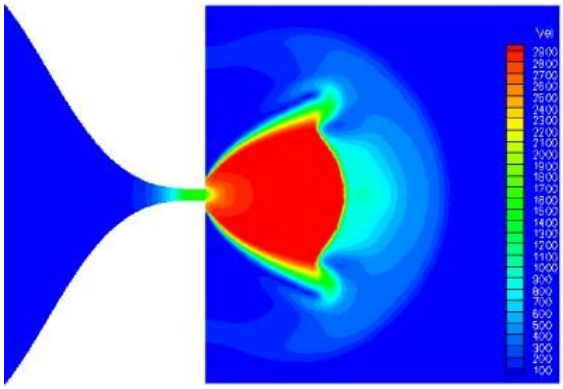

f) t=110 micro seconds

Figure (4-19)- Velocity for an initial tank pressure of 70 MPa at different times

In figures (4-20) to (4-37) Mach number, concentration, pressure, density, velocity and temperature along the centerline are plotted at six different times for the initial tank pressures of 10 MPa, 34.5 MPa and 70 MPa respectively. For the case of 10 MPa, at time of 110 micro seconds, the maximum Mach number along the centerline reaches 6.2 (figure(4-20)), for 34.5 MPa it is 7.4 (figure(4-26)) and for the case of 70 MPa it is 8.2 (figure(4-32)). The flow becomes stronger for higher pressures. Contact surface for the case of 10 MPa at the time of 110 micro seconds is located at 0.05 m (figure (4-21)), for the case of 34.5 MPa it is at 0.07 m (figure (4-27)) and for the case of 70 MPa it is at 0.085 m (figure (4-33)). The flow advances faster for higher pressures. Maximum velocity also increases by increasing the pressure but relatively it is increased slowly compared to Mach number and contact surface location. Maximum velocity at time of 110 micro seconds is 2750 m/s for the case of 10 MPa (figure (4-24)), it is 2900 m/s for the case of 34.5 MPa (figure (4-30)) and 3000 m/s for the case of 70 MPa (figure (4-36)). The flow advances very fast as the Mach number increases very rapidly. This shows the necessity of a stable code and a high quality mesh to accurately capture all the features of the flow. Also a very dense mesh which contains a high number of nodes and elements is required. This dense mesh requires a long computational time. Parallel processing helps to decrease the solution time. Without parallel processing, it may take months to have one solution. The gradients are very high so that the time step should be kept less than 10^{-8} seconds.

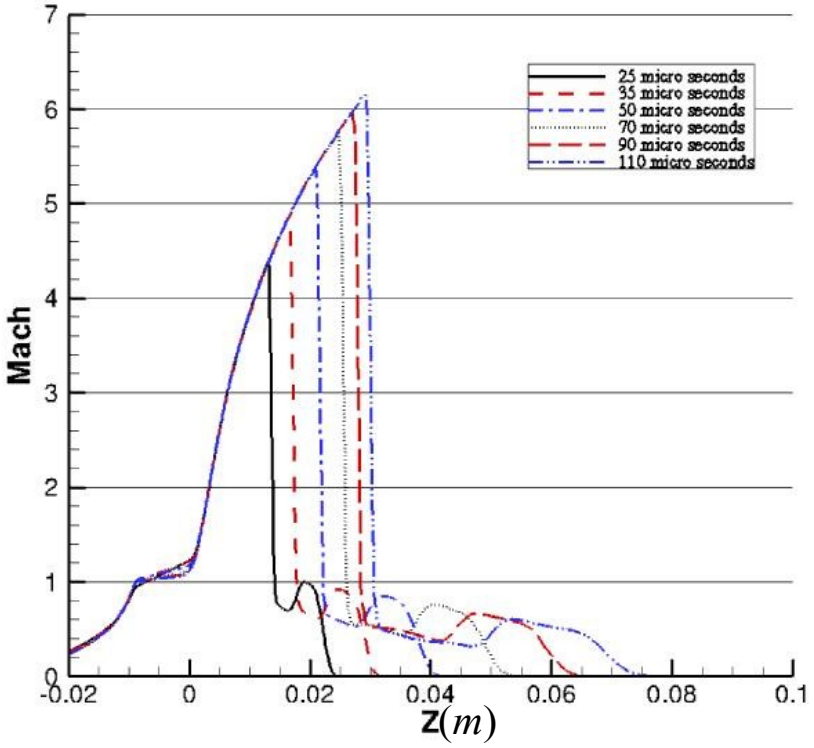

Figure (4-20)- Mach number along the centerline for tank pressure of 10 MPa

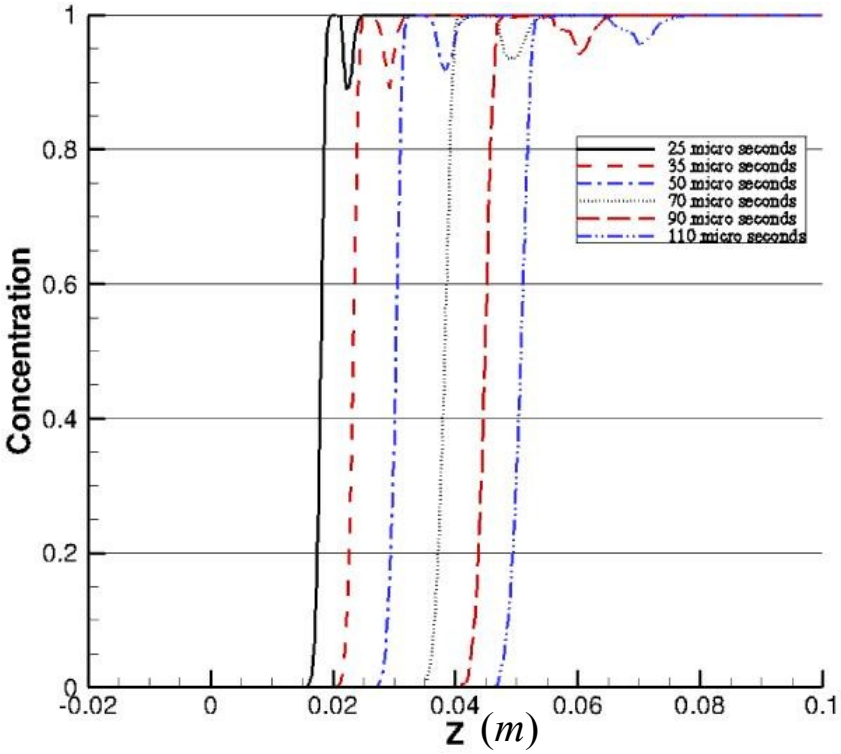

Figure (4-21)- Concentration along the centerline for tank pressure of 10 MPa

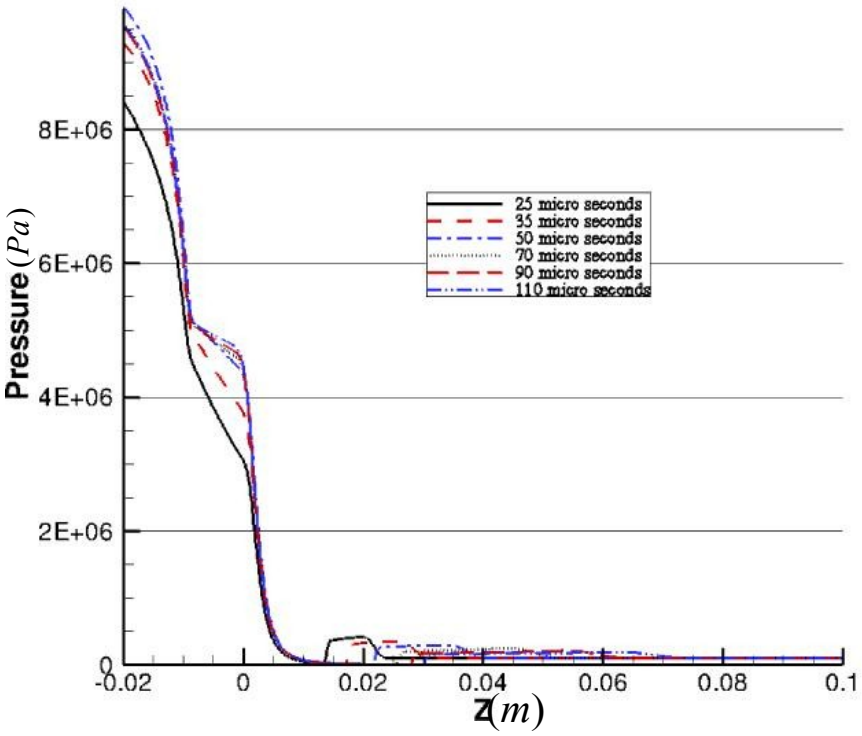

Figure (4-22)- Pressure along the centerline for tank pressure of 10 MPa

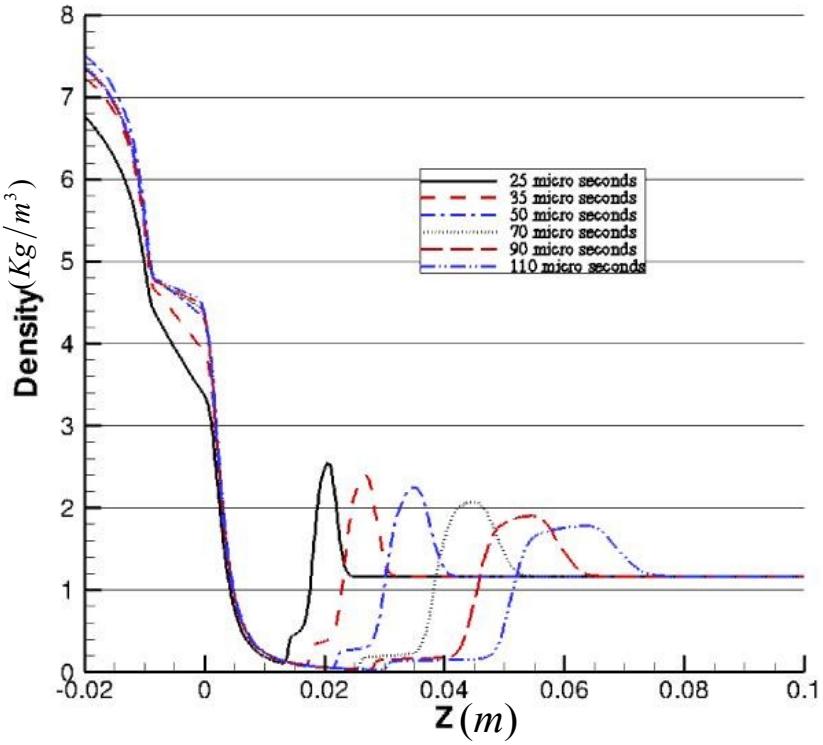

Figure (4-23)- Density along the centerline for tank pressure of 10 MPa

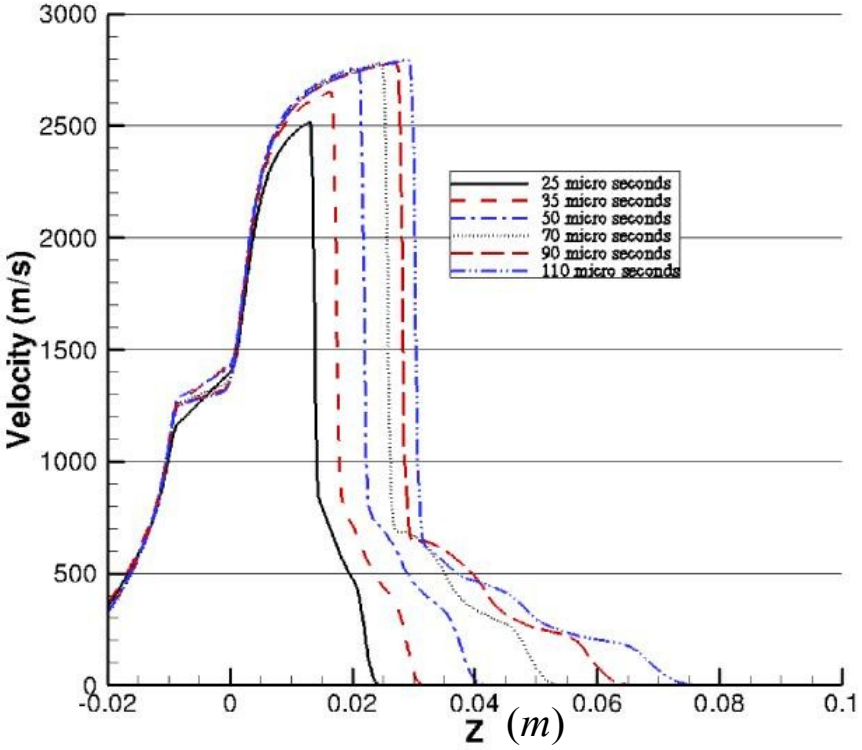

Figure (4-24)- Velocity along the centerline for tank pressure of 10 MPa

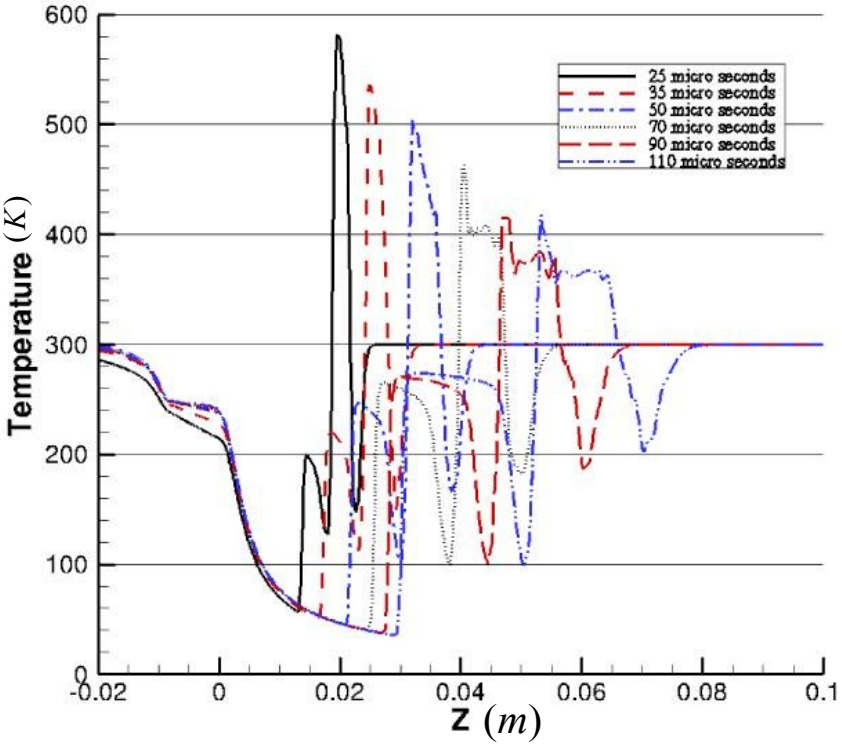

Figure (4-25)- Temperature along the centerline for tank pressure of 10 MPa

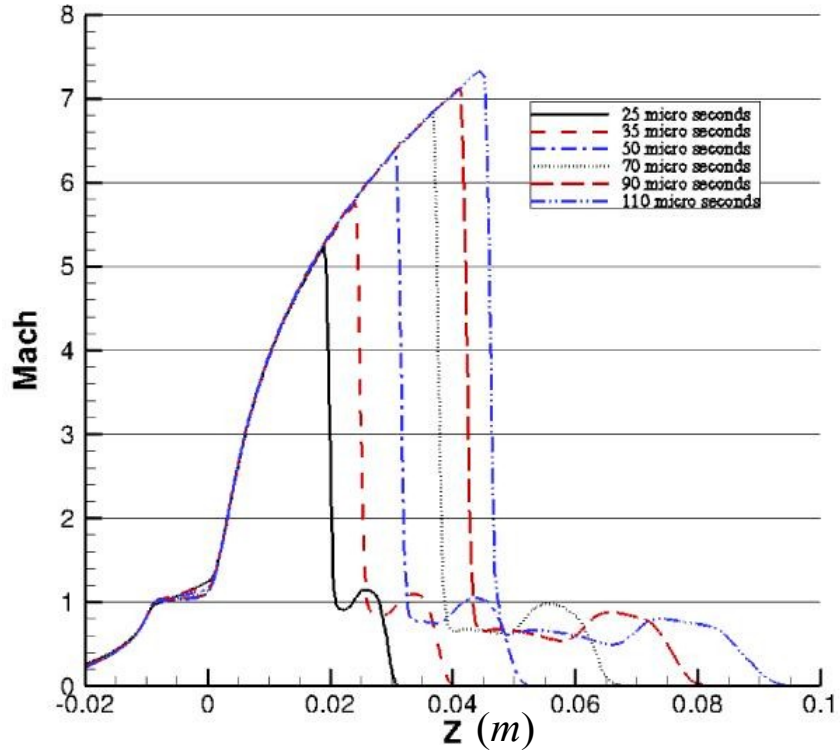

Figure (4-26)- Mach number along the centerline for tank pressure of 34.5 MPa

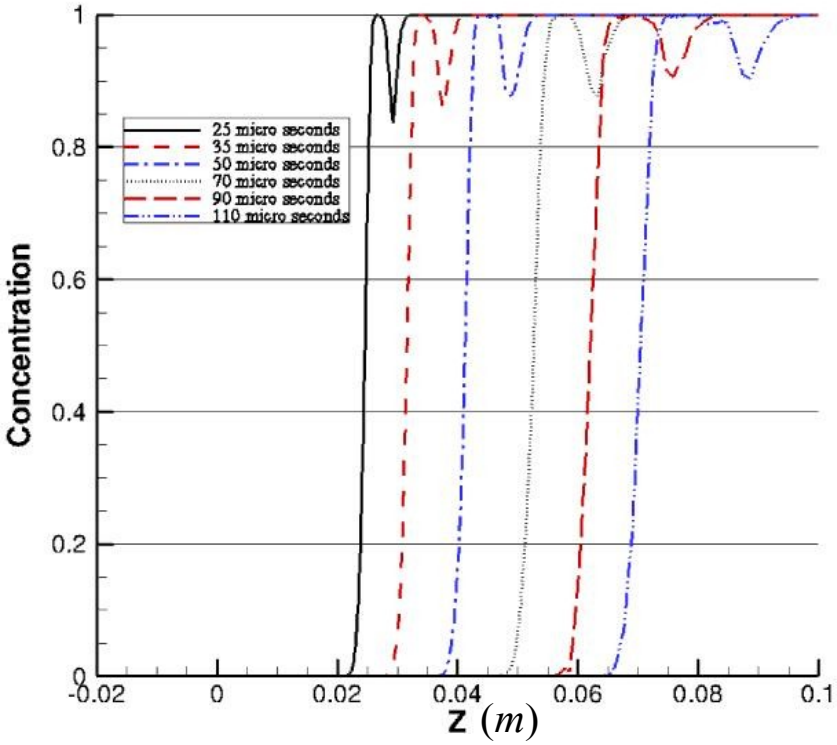

Figure (4-27)- Concentration along the centerline for tank pressure of 34.5 MPa

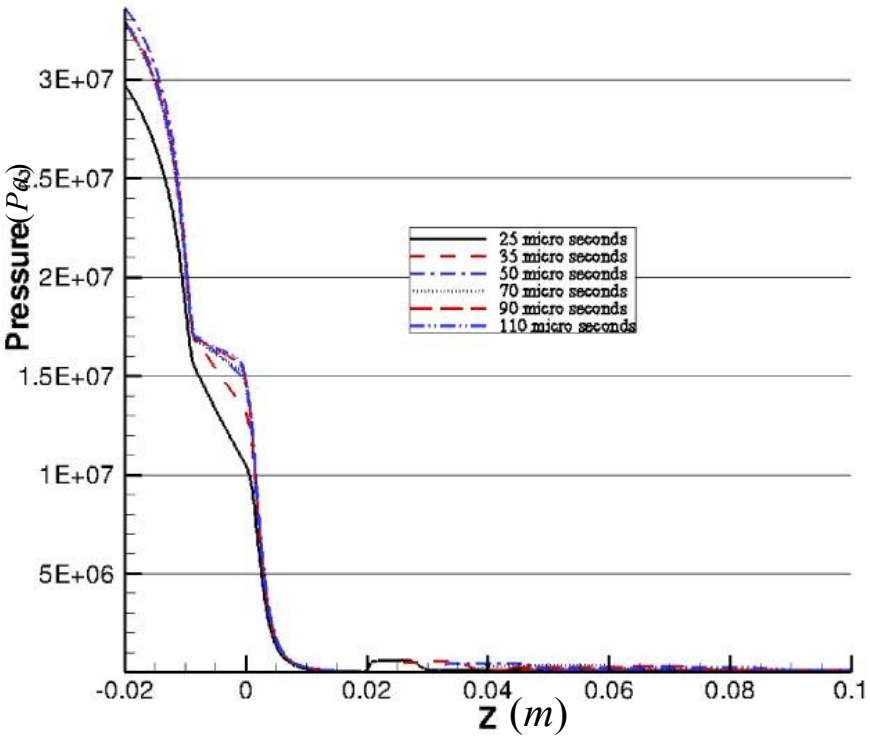

Figure (4-28)- Pressure along the centerline for tank pressure of 34.5 MPa

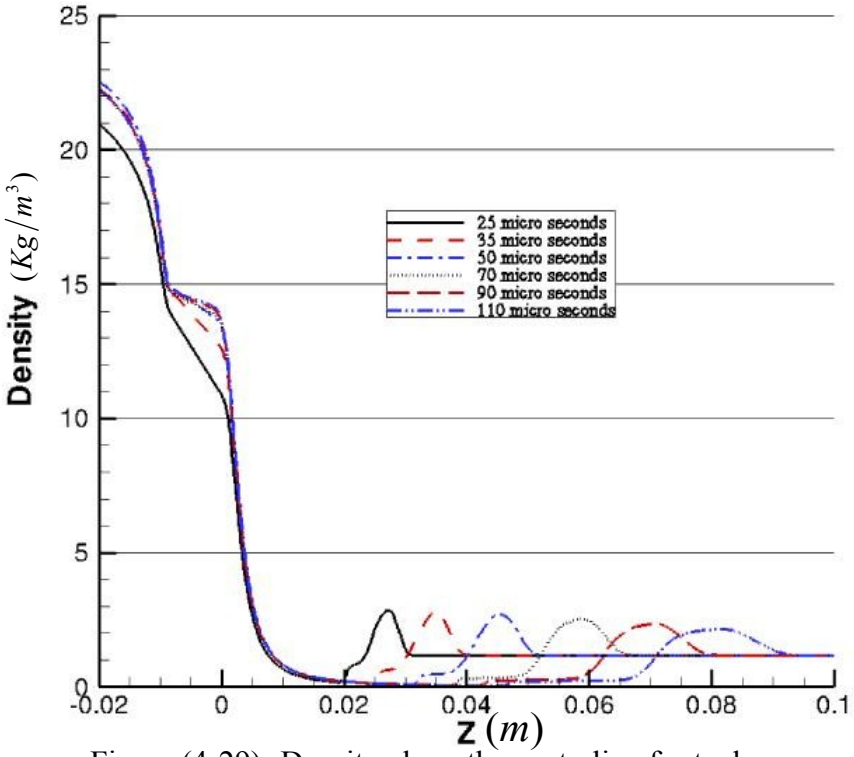

Figure (4-29)- Density along the centerline for tank pressure of 34.5 MPa

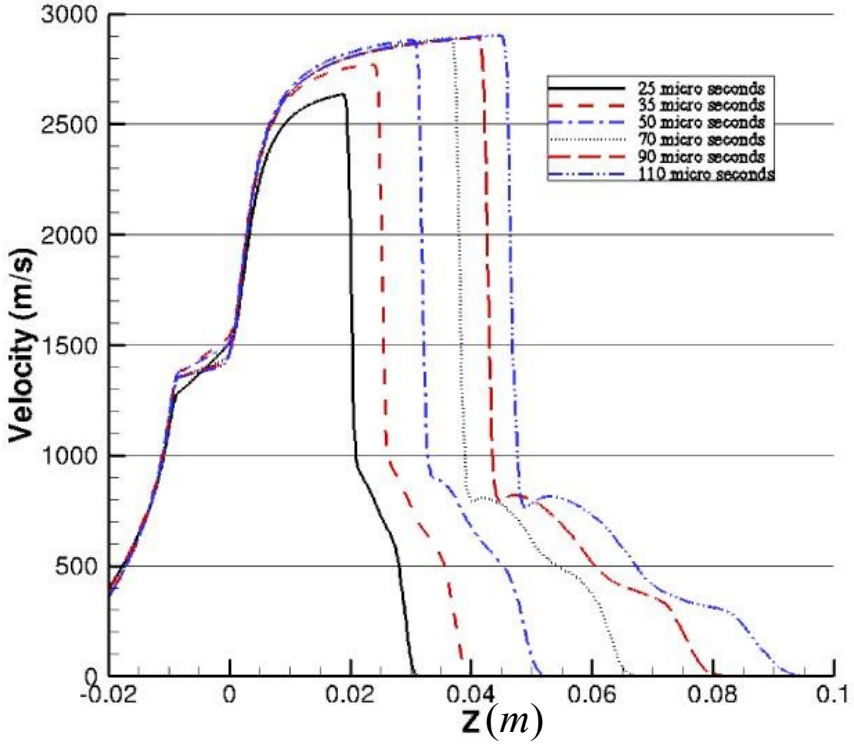

Figure (4-30)- Velocity along the centerline for tank pressure of 34.5 MPa

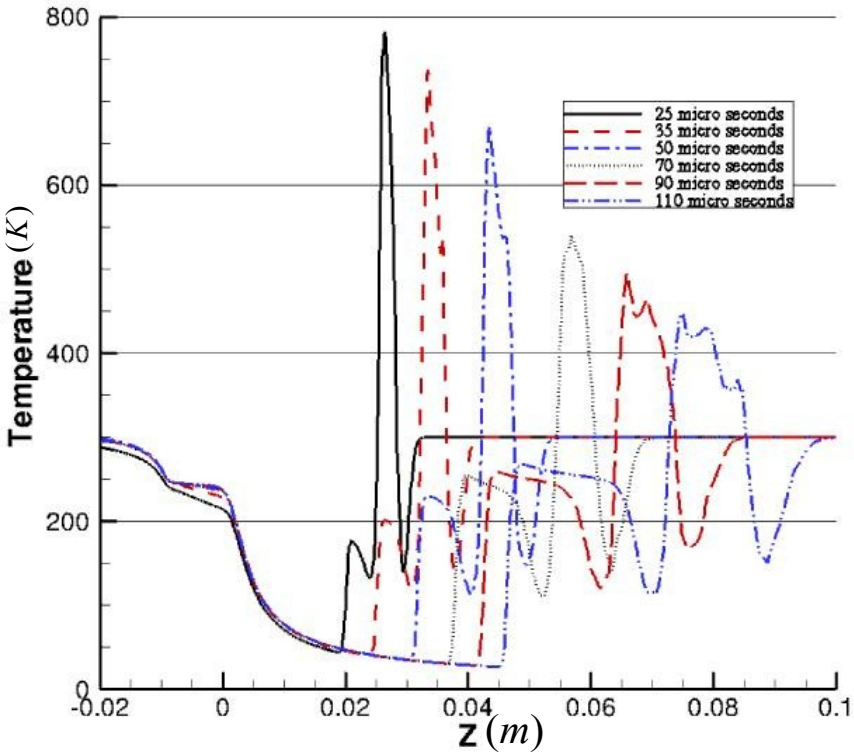

Figure (4-31)- Temperature along the centerline for tank pressure of 34.5 MPa

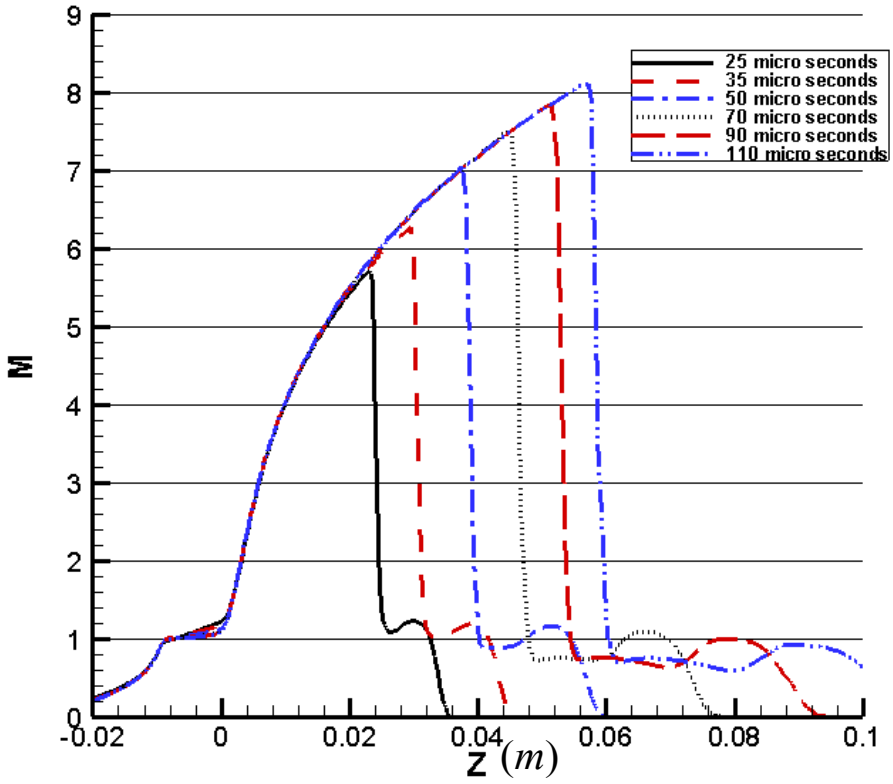

Figure (4-32)- Mach number along the centerline for tank pressure of 70 MPa

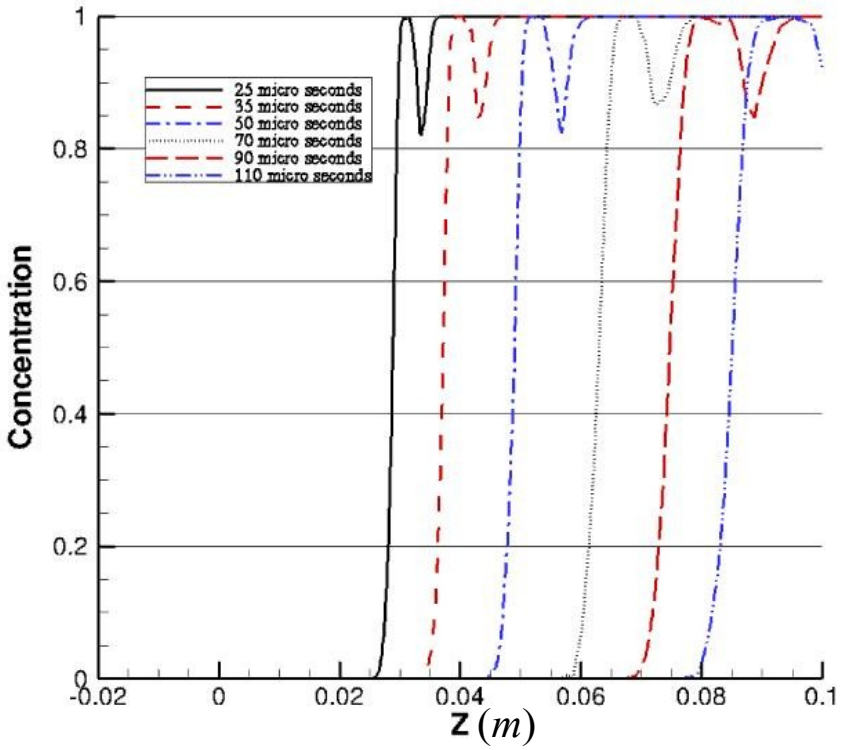

Figure (4-33)- Concentration along the centerline for tank pressure of 70 MPa

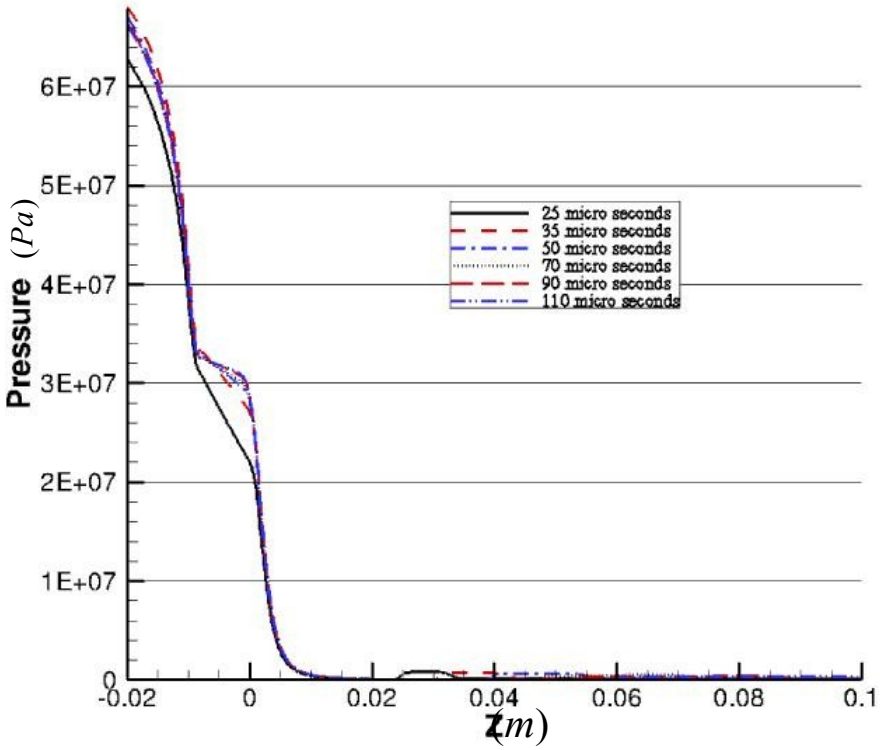

Figure (4-34)- Pressure along the centerline for tank pressure of 70 MPa

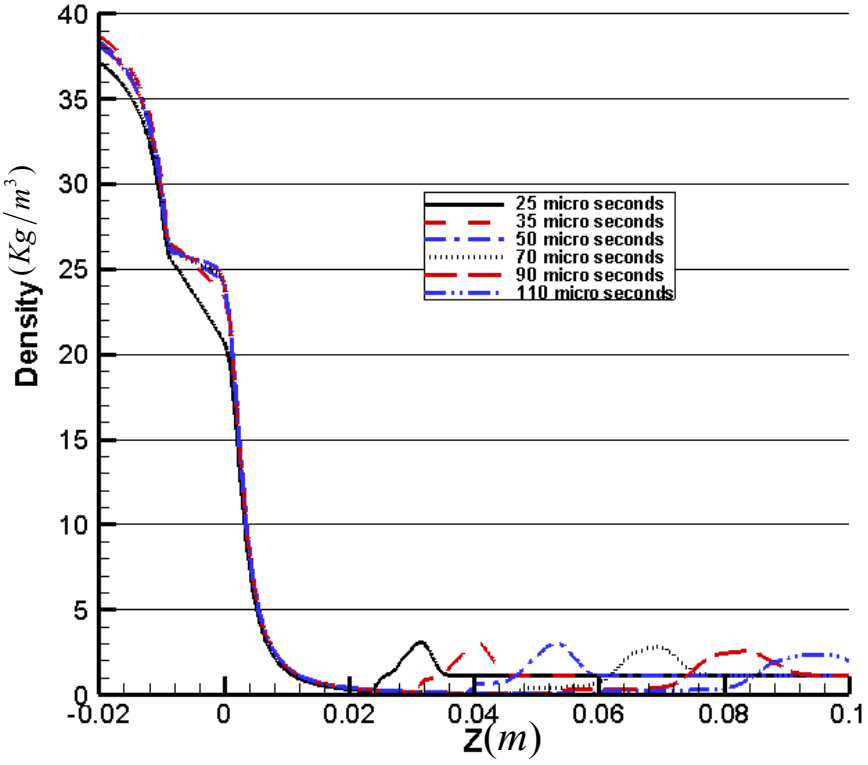

Figure (4-35)- Density along the centerline for tank pressure of 70 MPa

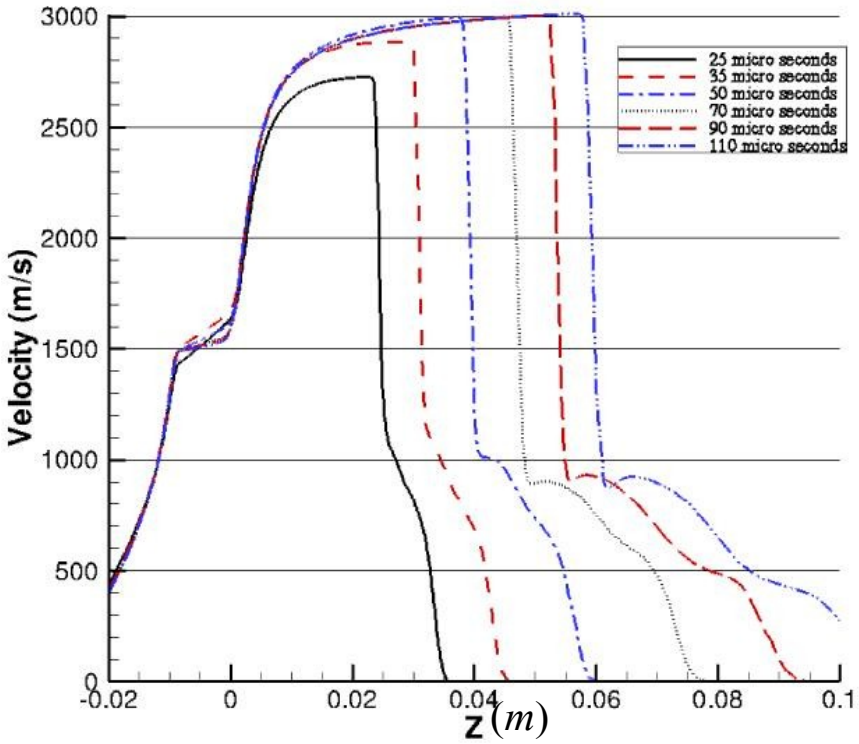

Figure (4-36)- Velocity along the centerline for tank pressure of 70 MPa

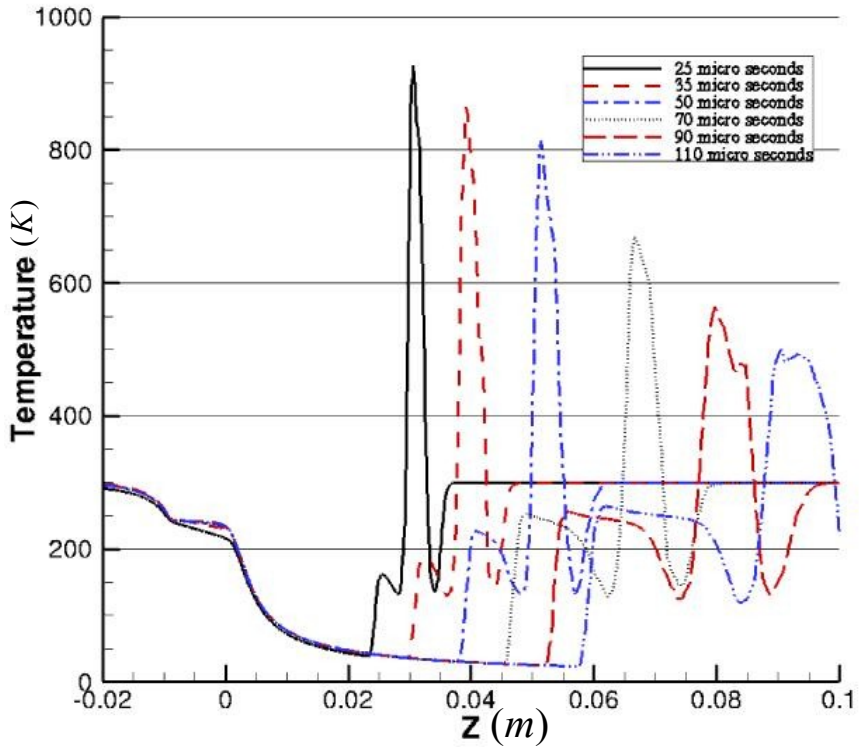

Figure (4-37)- Temperature along the centerline for tank pressure of 70 MPa

In figure (4-38) for the pressure of 70MPa at time of 70 micro seconds, temperature is given next to Mach and concentration contours to find out the location of different features of the flow.

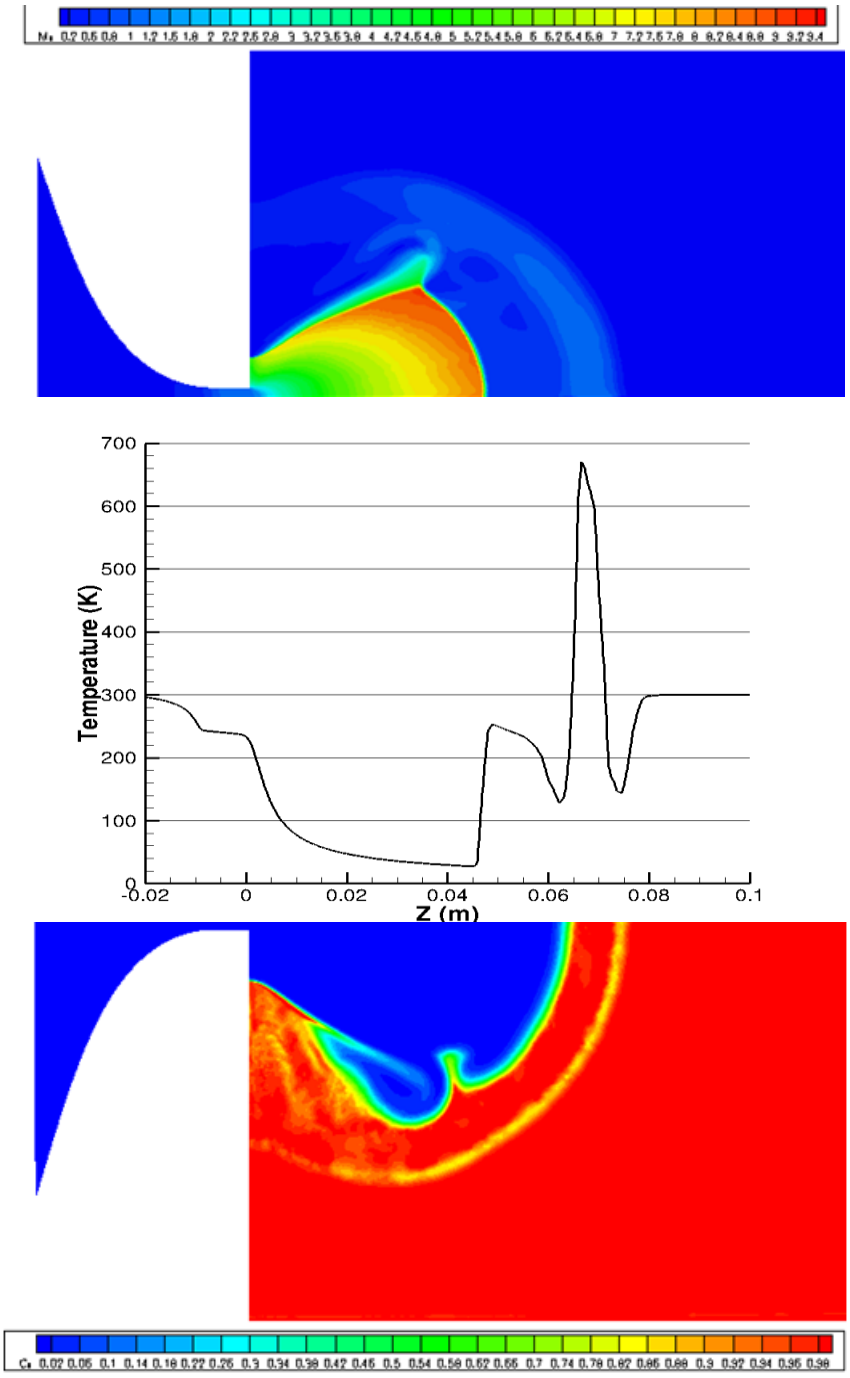

Figure (4-38)- Temperature, Mach number and concentration for tank pressure of 70 MPa

4-2-2 Mesh study

In this section the results of a finer mesh are compared to the previous results. The new mesh includes 3 million nodes which is 1.5 times bigger than the previous mesh. The tank pressure is 70MPa and the results are compared after 25 micro seconds of release. Concentration, density, pressure, velocity and temperature along the centerline are given in figures (4-39) to (4-43). It is noticed the difference is negligible; therefore the mesh of 2 million nodes gives accurate results.

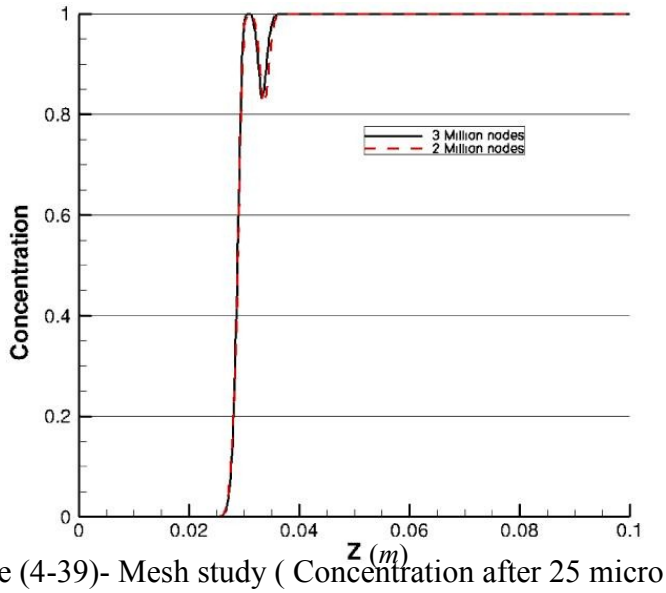

Figure (4-39)- Mesh study (Concentration after 25 micro seconds)

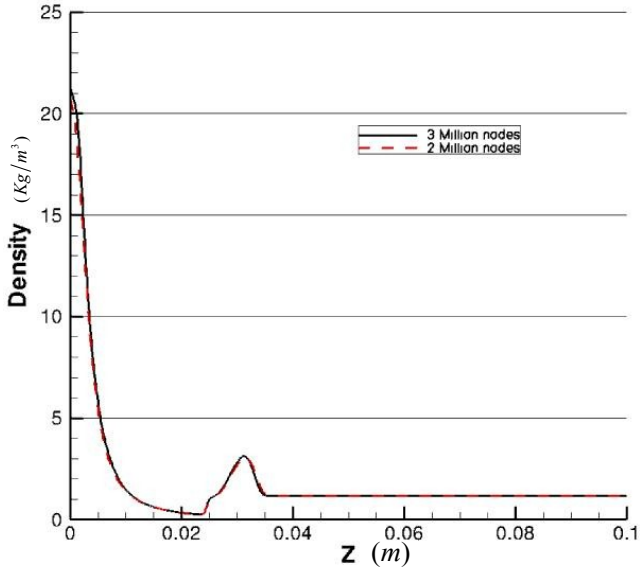

Figure (4-40)- Mesh study (Density after 25 micro seconds)

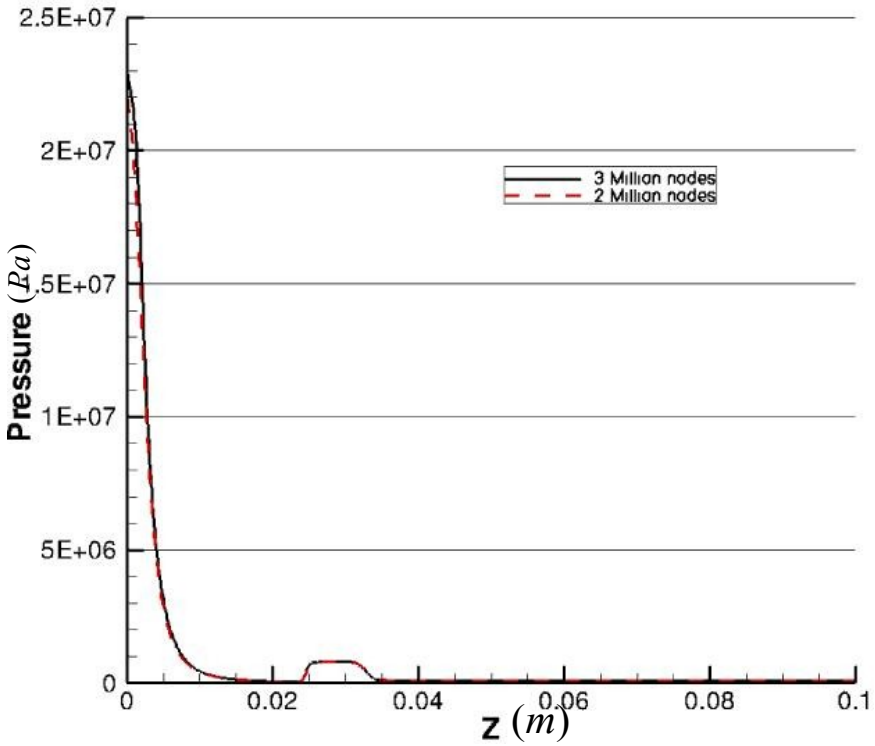

Figure (4-41)- Mesh study (Pressure after 25 micro seconds)

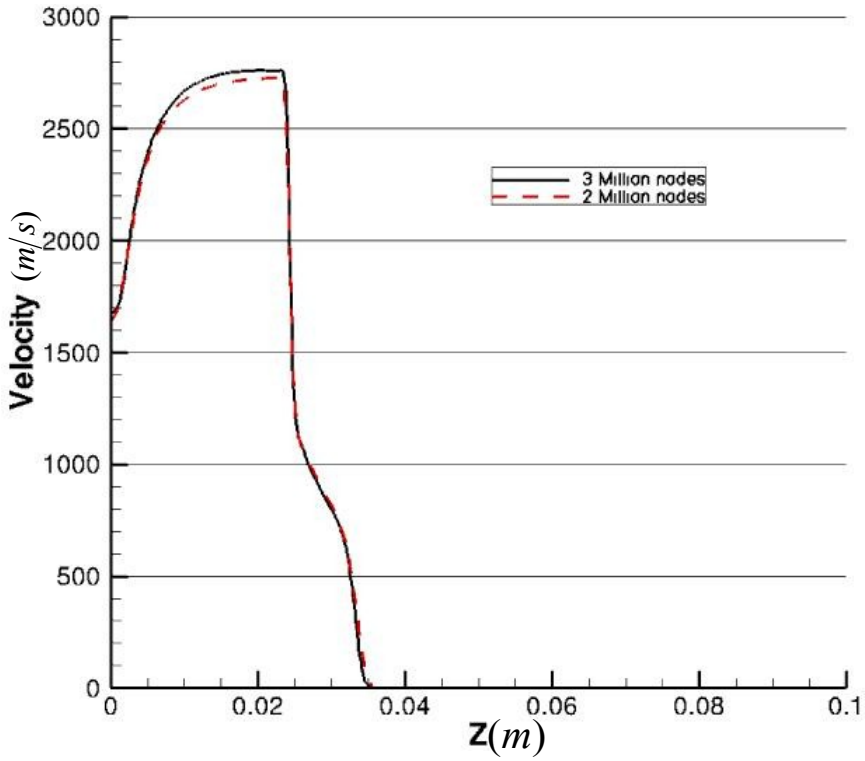

Figure (4-42)- Mesh study (Velocity after 25 micro seconds)

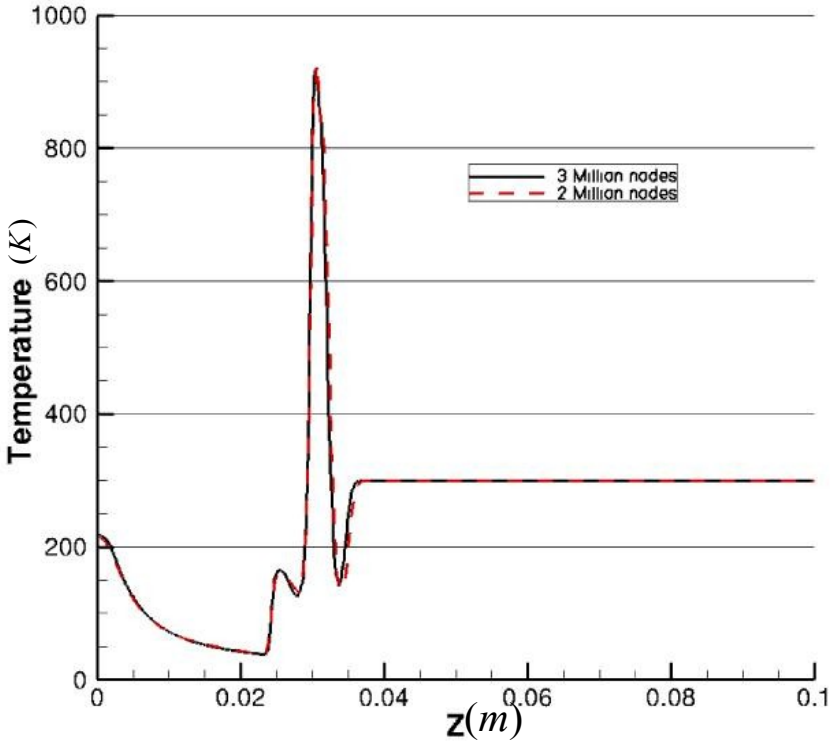

Figure (4-43)- Mesh study (Temperature after 25 micro seconds)

4-2-3 Different tank pressures comparison

In figures (4-44) and (4-45) Mach contours and the concentration contours after 90 micro seconds of release are presented. Once again the initial temperature is 300 K and the low pressure environment is initially at ambient pressure. The flow is getting stronger and faster as the tank pressure is increased, nevertheless the flow pattern is similar in all cases. The Mach disk, the barrel shock and contact surface exist in all cases. The Mach disk always takes place in an area of no air i.e. the hydrogen concentration is 100% in the vicinity of the Mach disk.

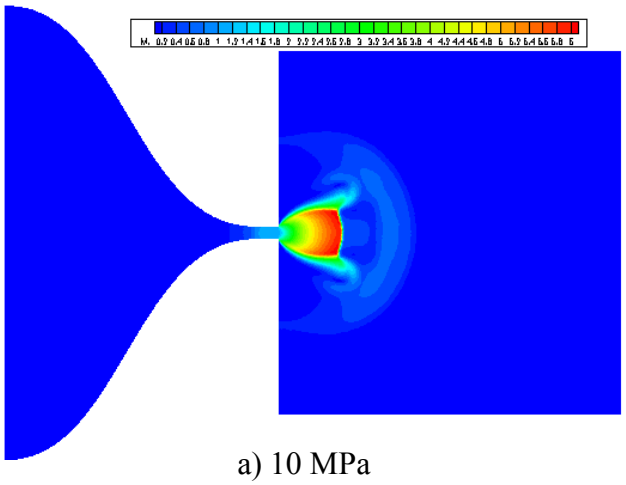

a) 10 MPa

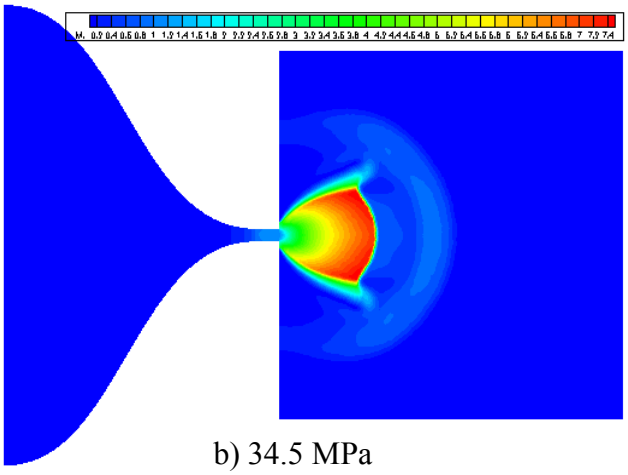

b) 34.5 MPa

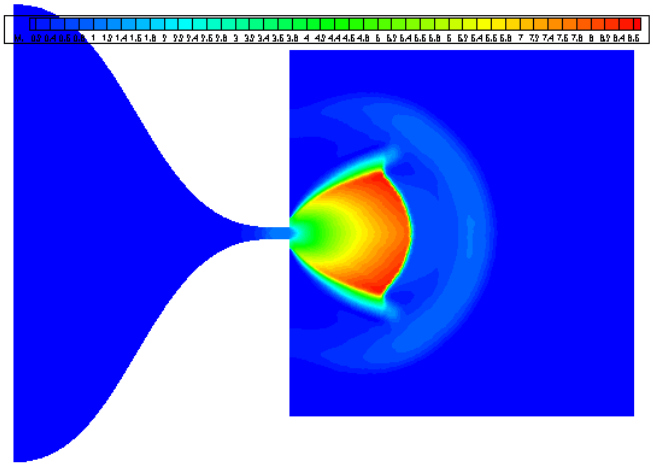

c) 70 MPa

Figure (4-44)- Mach number at time of 90 micro seconds for different tank pressures

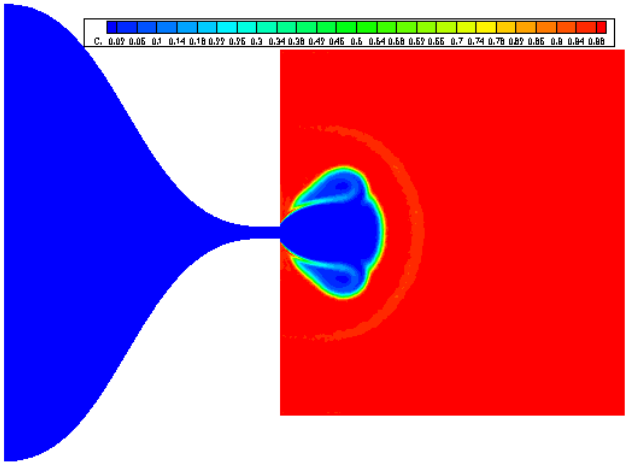

a) 10 MPa

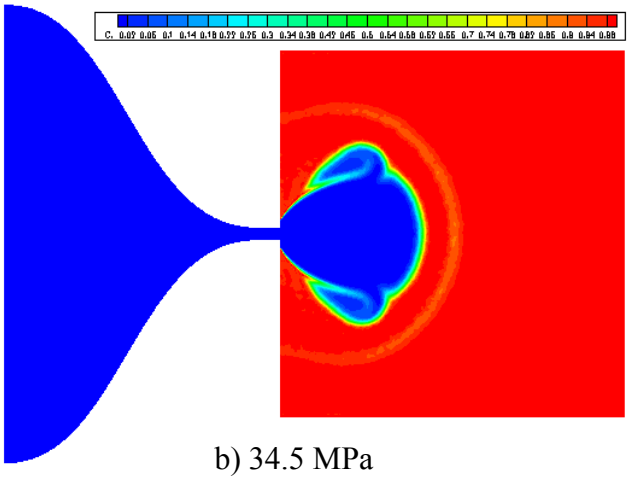

b) 34.5 MPa

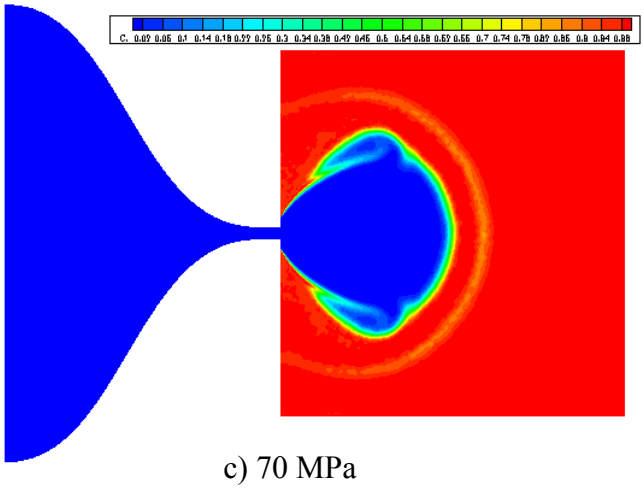

c) 70 MPa

Figure (4-45)- Concentration contours at time of 90 micro seconds for different tank pressures

To investigate the effect of the different tank pressures, in figures (4-46) to (4-51) Mach number, concentration, pressure, density, velocity and temperature along the centerline are reported. A weak shock ahead of the flow is observed. This weak shock is ahead of the contact surface where the Mach number slightly increases. The subsonic flow caused by the Mach disk stays subsonic until it reaches the contact surface. Then the Mach number increases. For the case of 70 MPa, the Mach number becomes more than one and in other cases stays less than one. The weak shock becomes stronger as the tank pressure is increased. The flow does not become supersonic in the cases of 34.5 MPa and 10 MPa since the weak shock diffuses in air very fast. The weak shock is stronger for earlier times since it diffuses in air very fast.

The flow is faster for higher pressures as the Maximum Mach number is higher for higher pressures. The Mach disk and contact surface locations are further for higher pressures. The contact surface is approximately located at z= 70 mm for pressure of 70 MPa, z=60 mm for pressure of 34.5 MPa and z=40 mm for pressure of 10 MPa.

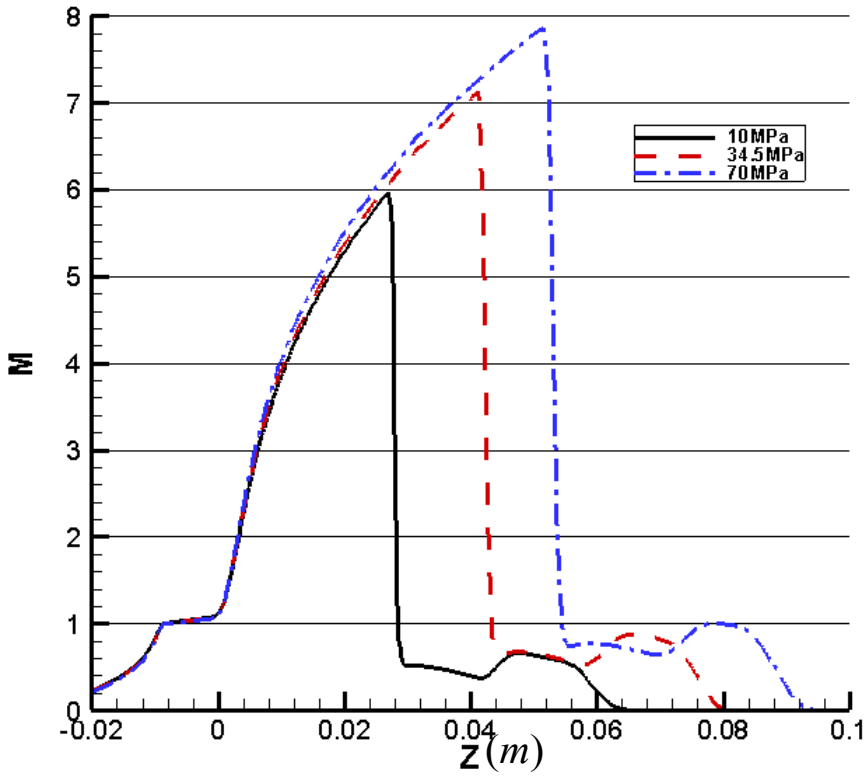

Figure (4-46)- Mach number along the centerline at time of 90 micro seconds

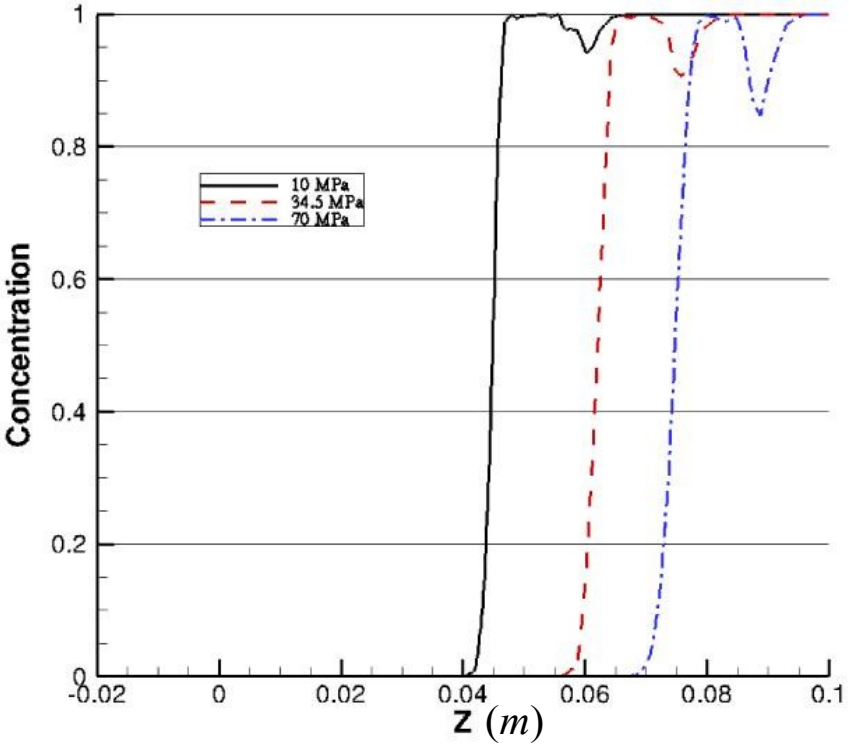

Figure (4-47)- Concentration along the centerline at time of 90 micro seconds

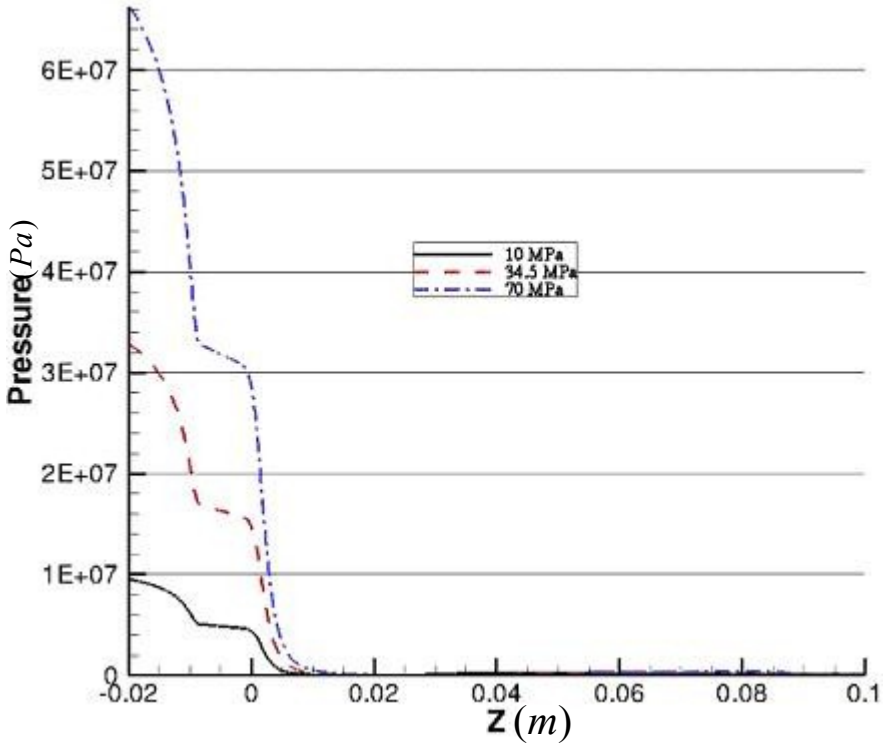

Figure (4-48)- Pressure along the centerline at time of 90 micro seconds

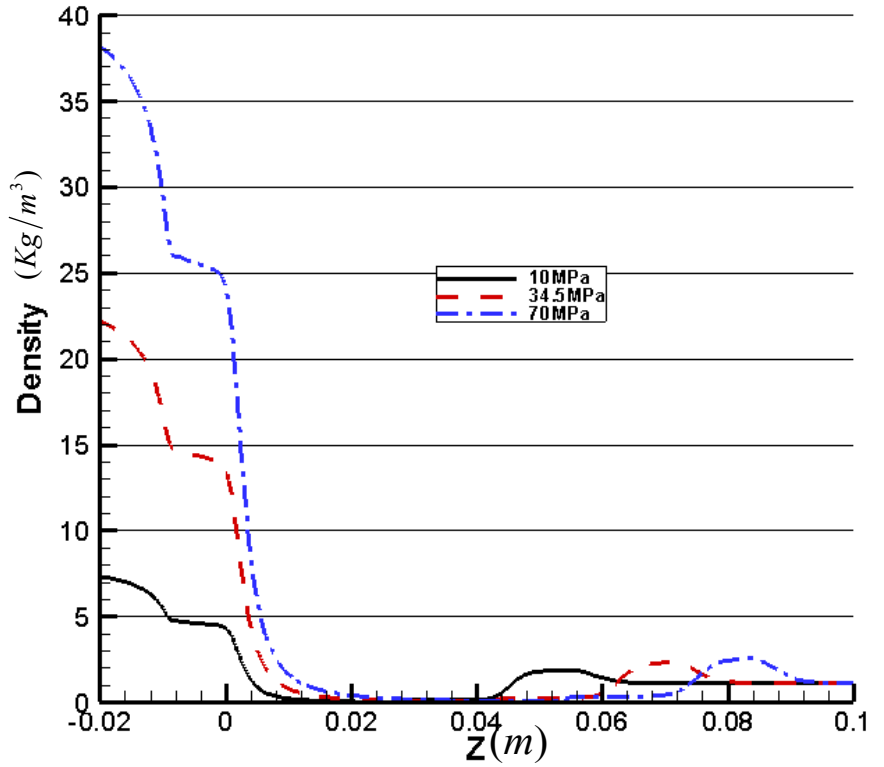

Figure (4-49)- Density along the centerline at time of 90 micro seconds

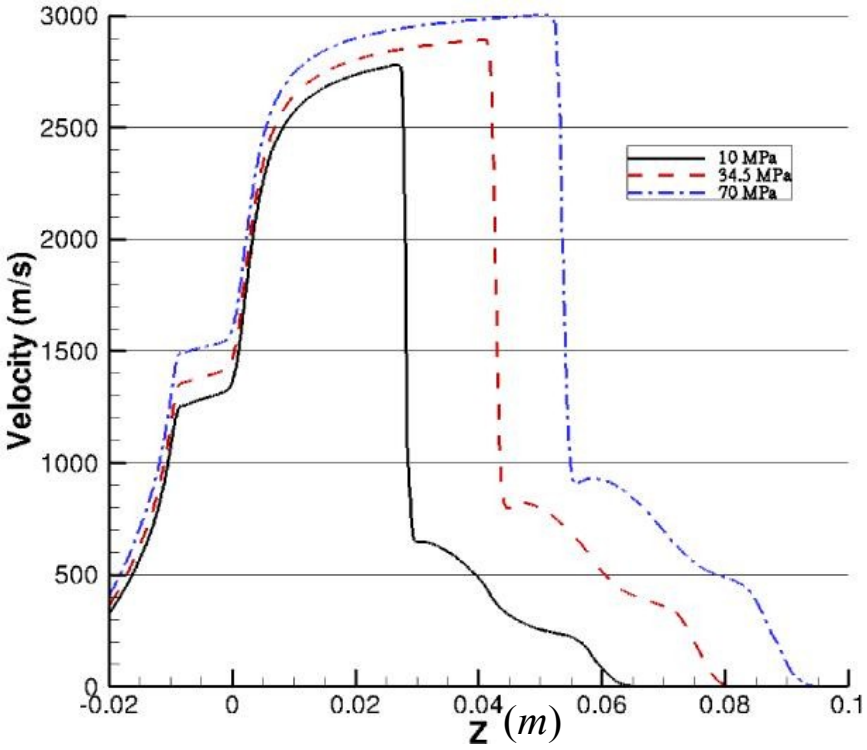

Figure (4-50)- Velocity along the centerline at time of 90 micro seconds

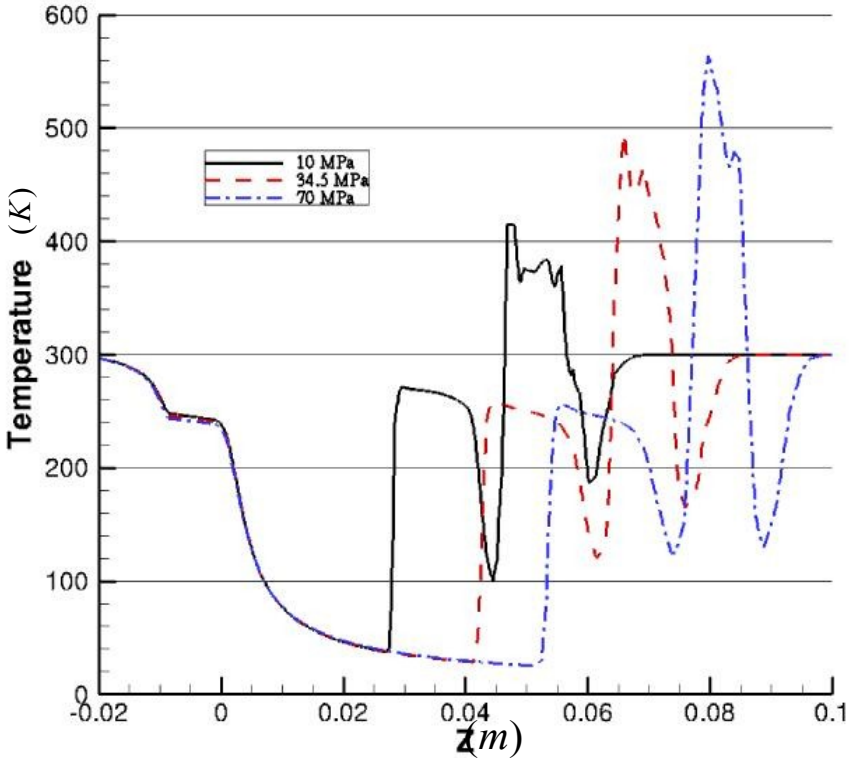

Figure (4-51)- Temperature along the centerline at time of 90 micro seconds

4-2-4 Validation with choked flow analytical solutions

The analytical equations of release properties detailed in section 2-1-3 are used to validate the in-house code results. The code is run to simulate the release of hydrogen in air for three tank pressures: 10 MPa, 34.5 MPa and 70 MPa. In table (4-3), the release density is compared for analytical ideal gas (equation (2-34)), analytical Abel-Noble gas (equation (2-30)) and the Abel-Noble simulation. Note that the release density is increased by increasing the stagnation pressure in the tank. The ideal gas equation overestimates the release density. Although this overestimation may be negligible for the case of 10 MPa, it cannot be ignored for the cases of 34.5 MPa and 70 MPa as it gives an error of almost 30 percents for the pressure of 70 MPa. The real gas model is necessary especially for higher pressures. The simulation results are in good agreement with the results of the analytical Abel-Noble model. In table (4-4), the release temperature is compared for different tank pressures. Release temperature remains the same for the ideal gas since it is only a function of stagnation temperature which is 300 K for all cases. For the results of analytical Abel-Noble (equation (2-31)) and the simulation, release temperature is decreased by increasing the pressure.

Table (4-3)-Release density (Kg/m^3) comparison

	10 MPa	34.5 MPa	70 MPa
Analytical ideal gas	5.1	17.7	35.9
Analytical Abel-Noble gas	4.8	14.2	23.9
Abel -Noble simulation (At 90 micro seconds)	4.6	14.4	25.6

Table (4-4)-Release temperature comparison

	10 MPa	34.5 MPa	70 MPa
Analytical ideal gas	250	250	250
Analytical Abel-Noble gas	247	240	231
Abel -Noble simulation (At 90 micro seconds)	246	244	241

The release velocity, which is the sound velocity, changes with the tank pressure for the real gas model unlike the ideal gas in which the sound velocity remains the same and is only a function of stagnation temperature. In table (4-5) release velocity is given for the analytical ideal gas (equation (2-37)), analytical Abel-Noble (equation (2-33)) and Abel-Noble simulation. The release velocity increases by increasing the pressure except for the ideal gas. Ideal gas underestimates the release velocity and the underestimation is higher for higher pressures. There is a difference of 7 percent between the Abel-Noble analytical and simulation because we believe that the numerical simulation is sensitive to the mesh quality at this location.

Table (4-5)-Release velocity (m/s) comparison

	10 MPa	34.5 MPa	70 MPa
Analytical ideal gas	1201	1201	1201
Analytical Abel-Noble gas	1240	1321	1416
Abel -Noble simulation (At 90 micro seconds)	1280	1380	1515

4-2-5 Numerical real gas vs. Numerical ideal gas

The ideal gas model is not accurate for high pressures as seen by the difference with a real gas model for the hydrogen-air scenario. Table (4-6) represents the release velocity for ideal gas and real gas simulations. The release velocity remains the same in all cases for the ideal gas while it increases by increasing the pressure for the real gas. Table (4-7) gives the release mass flow rate for both ideal gas and real gas cases. As it is expected, for the 10 MPa case, ideal gas is accurate enough and a real gas model may be neglected. The ideal gas model overestimated the release mass flow rate at all pressures. The overestimation reaches almost 10% in the case of 70 MPa. Therefore without a real gas, the results are far from accurate. Figures (4-52), (4-53) and (4-54) show the Mach number, density and velocity along the centerline for the tank pressure of 70 MPa at time of 110 micro seconds. The difference cannot be ignored and it is noticed that this high Mach number and high gradient flow requires a real gas model to accurately capture these features.

Table (4-6)- Release velocity at time of 90 micro seconds

	10 MPa	34.5 MPa	70 MPa
Ideal gas (m/s)	1240	1240	1240
Real gas (m/s)	1280	1380	1515

Table (4-7)- Release mass flow rate at time of 90 micro seconds

	10 MPa	34.5 MPa	70 MPa
Ideal gas (g/s)	119.24	411.26	839.56
Real gas (g/s)	115.55	389.99	761.14

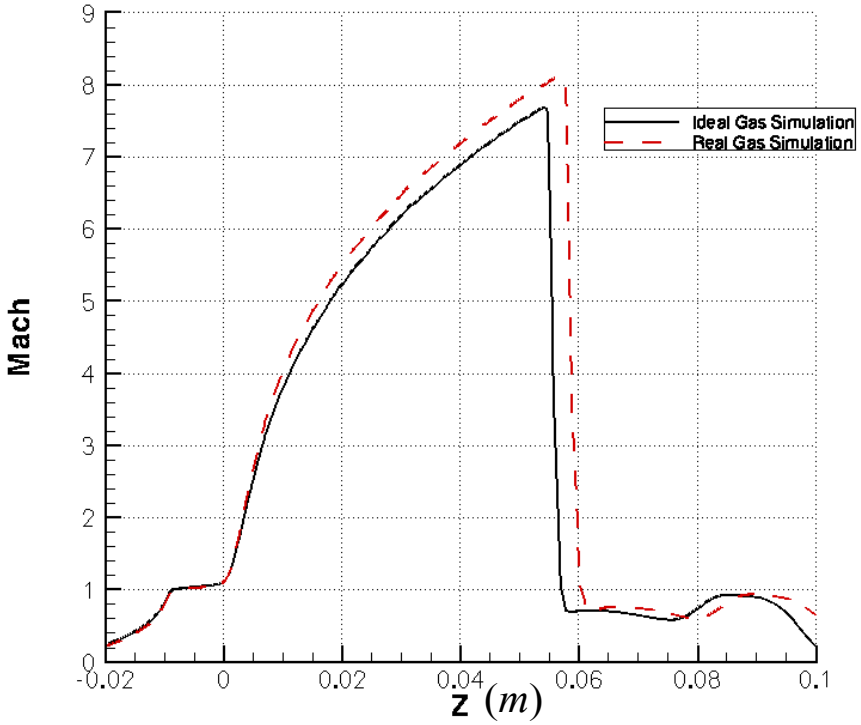

Figure (4-52) - Mach number along the centerline for tank pressure of 70 MPa at time of 110 micro seconds

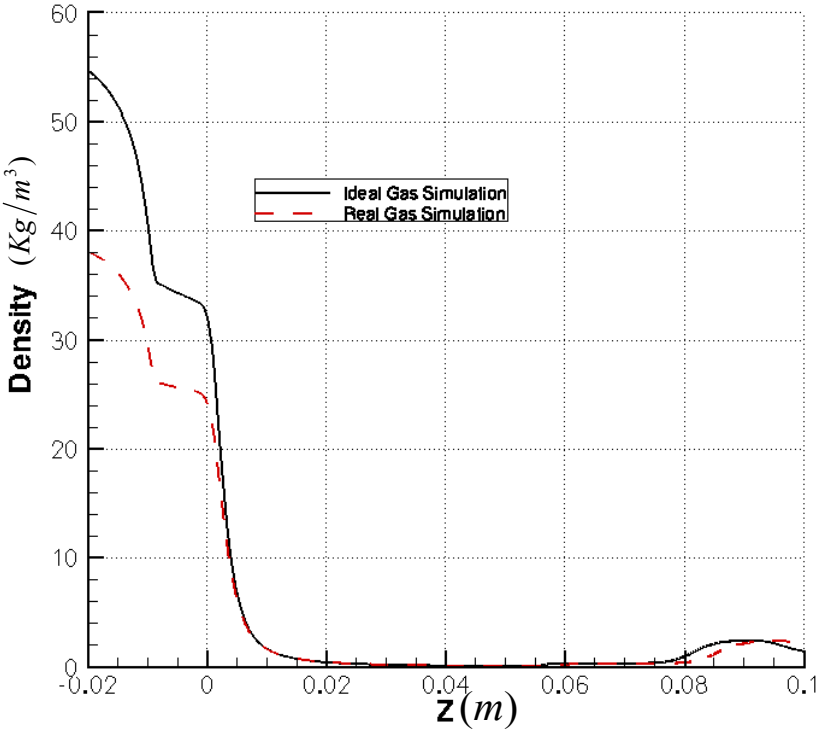

Figure (4-53) - Density along the centerline for tank pressure of 70 MPa at time of 110 micro seconds

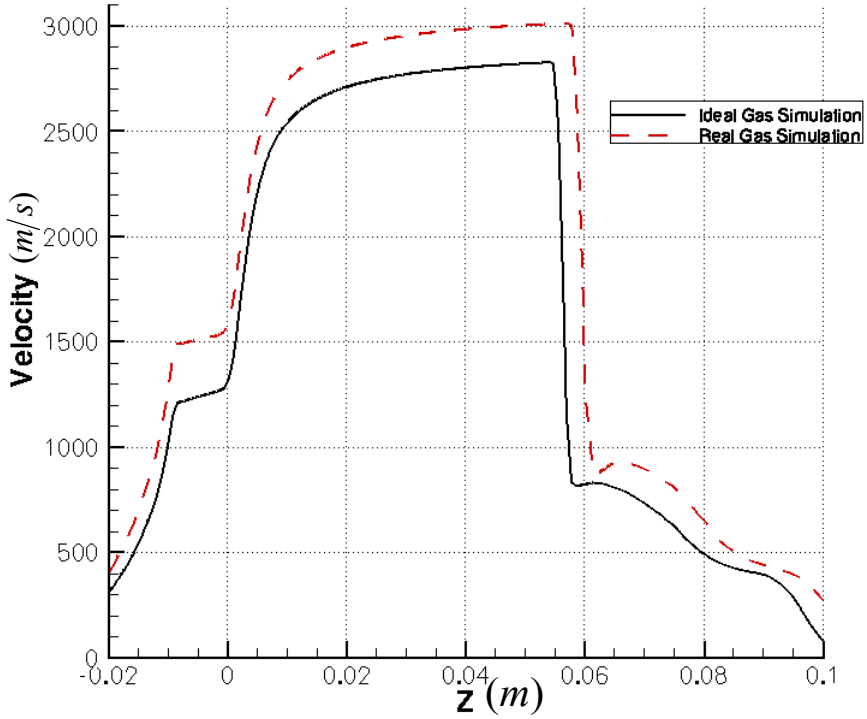

Figure (4-54) - Velocity along the centerline for tank pressure of 70 MPa at time of 110 micro seconds

Figure (4-55) shows the temperature along the centerline for initial tank pressure of 70 MPa at time of 70 micro seconds for ideal gas and real gas simulations. The maximum temperature occurs ahead of the contact surface. The temperature ahead of the contact surface increases by approximately 50 degrees for the real gas model compared to the ideal gas. The temperature comparison shows the necessity of the real gas model to accurately simulate the flow since the difference cannot be neglected.

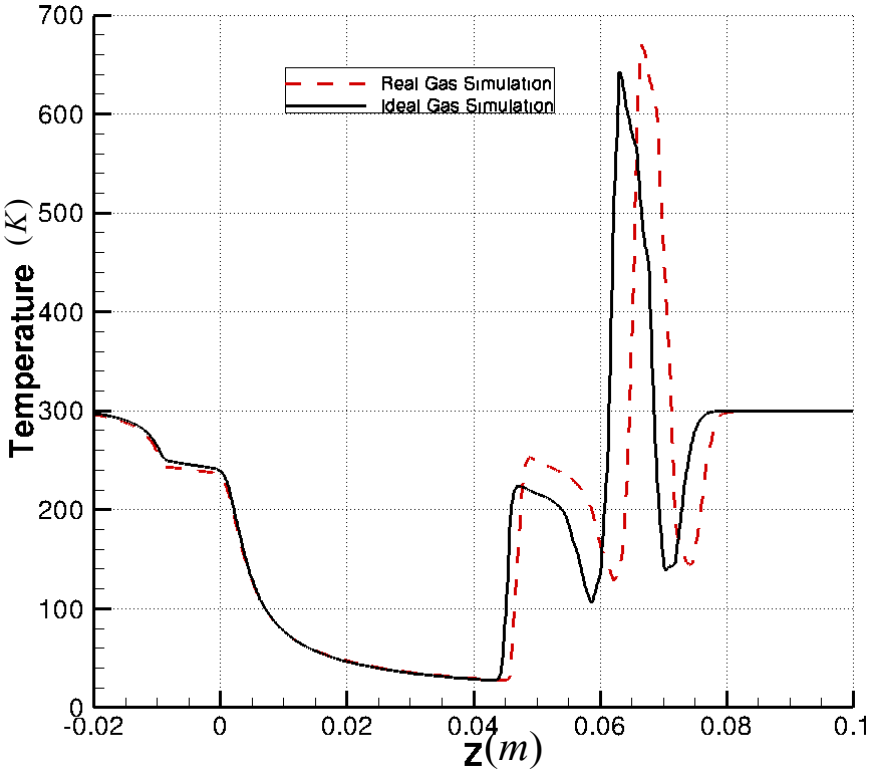

Figure (4-55) - Temperature along the centerline for tank pressure of 70 MPa at time of 70 micro seconds

4-3 Hydrogen in hydrogen vs. hydrogen in air

In this section the release of hydrogen in hydrogen is compared to the release of hydrogen in air. The comparison between these two flows has also been discussed by Peneau et al. [48]. Molecular mass of hydrogen is almost 2 while for air it is 29 so density of air is higher for equal pressure and temperatures. This generates a stronger Mach disk for hydrogen in hydrogen at the same time after release. The flow can advance faster in the case of hydrogen in hydrogen because it is easier to push the lower density hydrogen. In figure (4-56), Mach number along the centerline is viewed for both scenarios for tank pressure of 70 MPa and time of 70 micro seconds.

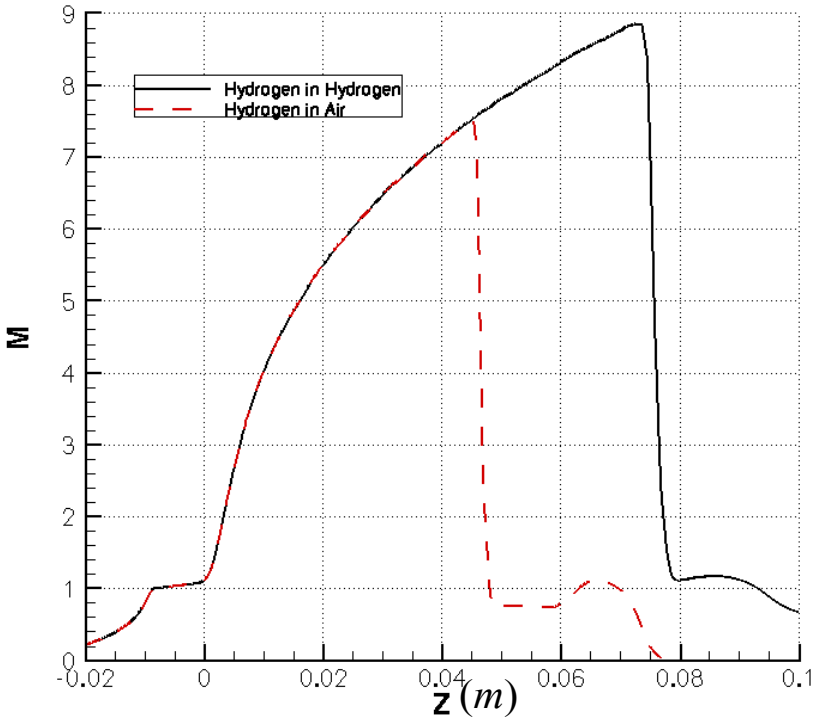

Figure (4-56) - Mach number along the centerline
for tank pressure of 70 MPa at t=70 micro seconds

4-4 Moving Mesh

In this section the release area is expanded to simulate a more realistic scenario. Three initial release area diameters of 1.0mm, 1.5mm and 2.0mm are tested. These diameter values are smaller than for the fixed diameter case because it is believed that this is a more sensitive case. The tank pressure for all cases is 70MPa and the outside has ambient conditions. The initial temperature is 300K everywhere and the initial interface is in the middle of the release area which is 1mm from the end of it. For each case, three opening rates of 80m/s, 200m/s and 500m/s are examined. These opening speeds are less than the choked velocity in the release area which is almost 1250 m/s for the case of 10 Mpa and increases to 1500 m/s for the case of 70 MPa (figure (4-50)). In figure (4-57), for the initial diameter of 1.0mm at the opening rate of 500m/s, the two-dimensional view of the

release area mesh at different times of 1.0, 1.5, 2.0, 2.5 and 3.0 micro seconds after release is given. The mesh is moving based on the spring method and is a very high quality mesh. The final diameter (at time of 3.0 micro seconds) for the initial diameters of 1.0mm, 1.5mm and 2.0mm at the opening rate of 500m/s are 2.5mm, 3.0mm and 3.5mm respectively. In figure (4-58), Mach contours for initial diameter of 1.0mm at the opening rate of 500m/s are given.

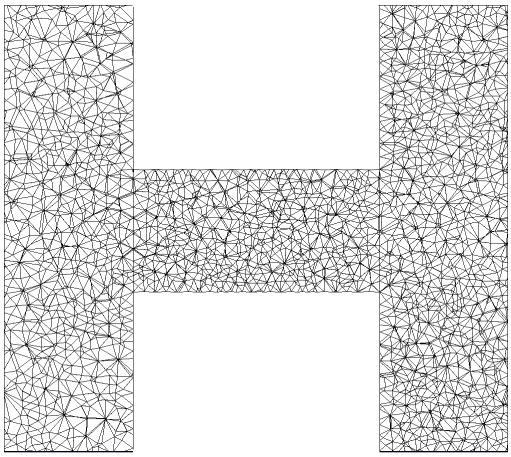

Initial diameter

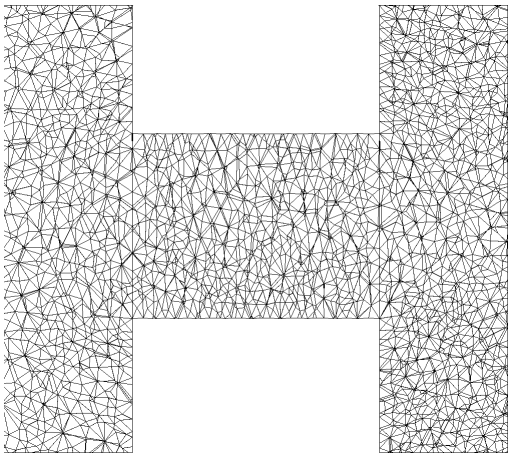

After 1.0 micro

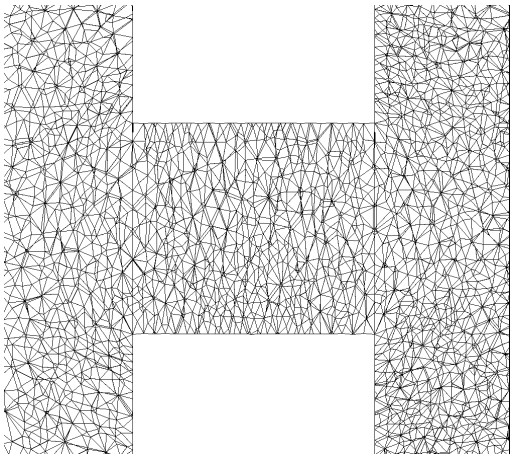

After 1.5 micro

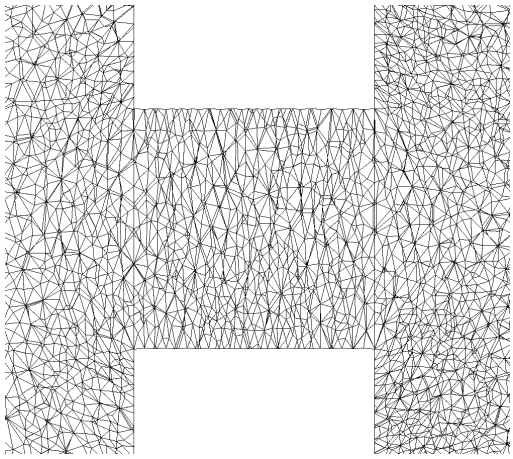

After 2.0 micro

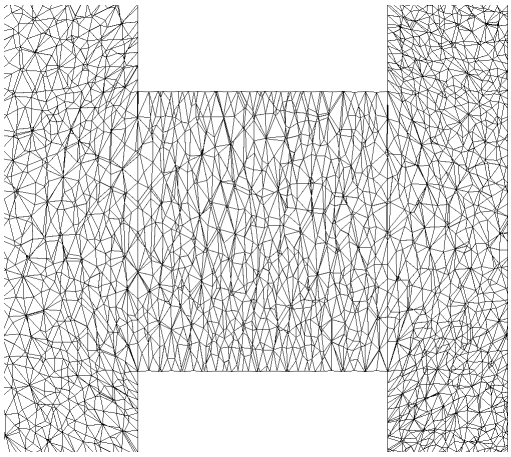

After 2.5 micro

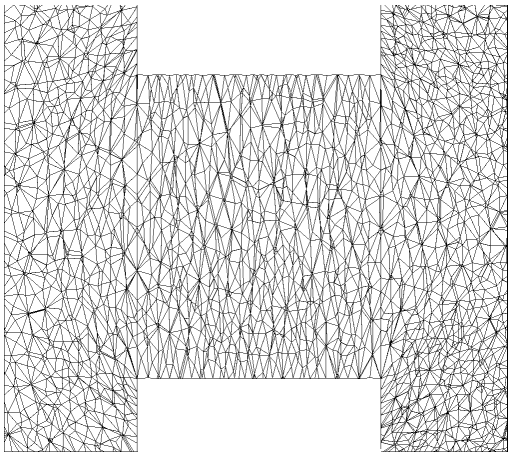

After 3.0 micro

Figure (4-57) – Release area expanding for the initial diameter of 1.0mm at the rate of 500m/s.

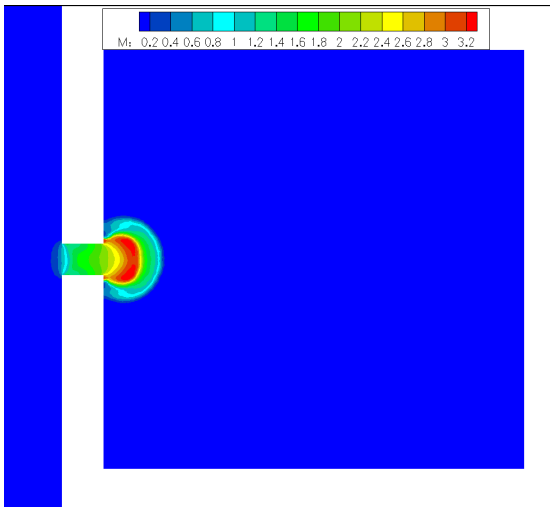

After 1.0 micro seconds

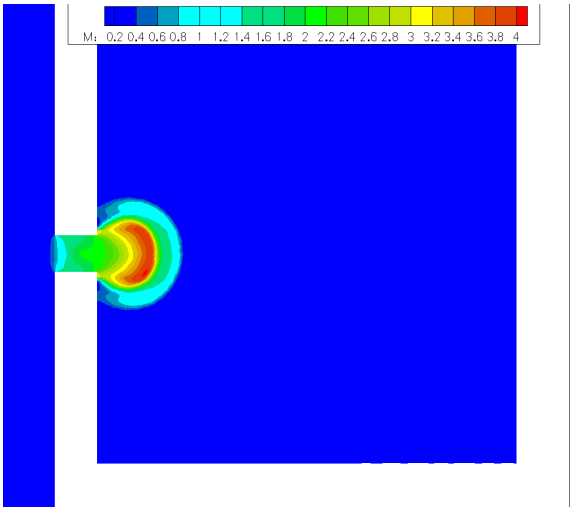

After 1.5 micro seconds

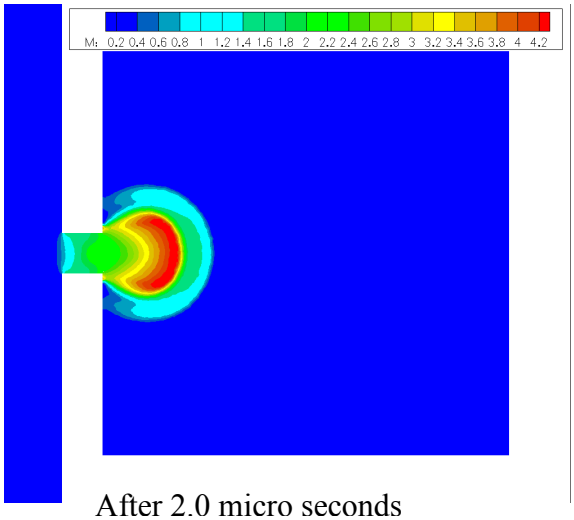

After 2.0 micro seconds

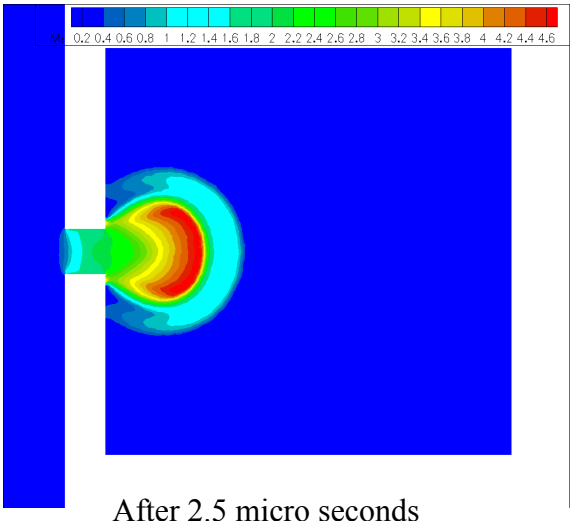

After 2.5 micro seconds

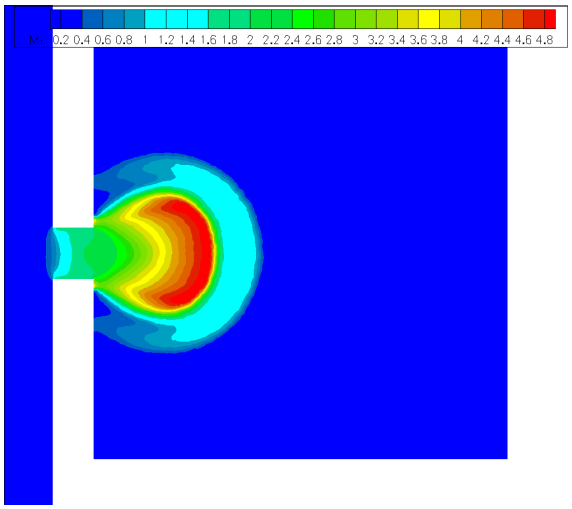

After 3.0 micro seconds

Figure (4-58) – Mach contours for the initial diameter of 1.0mm at the opening rate of 500m/s.

The hydrogen-air mixture ahead of the contact surface is very likely to ignite since oxygen exists and temperature may reach the temperature required for ignition, therefore properties on the contact surface are important for combustion discussion. In fact, if ignition is supposed to happen it is certainly in front of the contact surface which is heated by the lead shock. Combustion models require the pressure as the input. In figure (4-59) Pressure versus time on the contact surface is given for initial release area diameter of 1.0mm at different opening rates and in figure (4-60) contact surface location is given. It is noticed pressure on the contact surface depends on the opening rate. For example, at time of 0.5 micro seconds the pressure is almost 2.0MPa for the opening velocity of 500m/s while it is almost 5.0MPa for the opening velocity of 80m/s. The main difference is noticed in the first micro second. Pressure increases by increasing the opening rate up to the time of 1.5 micro seconds, after that the difference is negligible and it seems the opening rate does not have an impact on the contact surface pressure. There is also a small difference in contact surface location for different opening velocities.

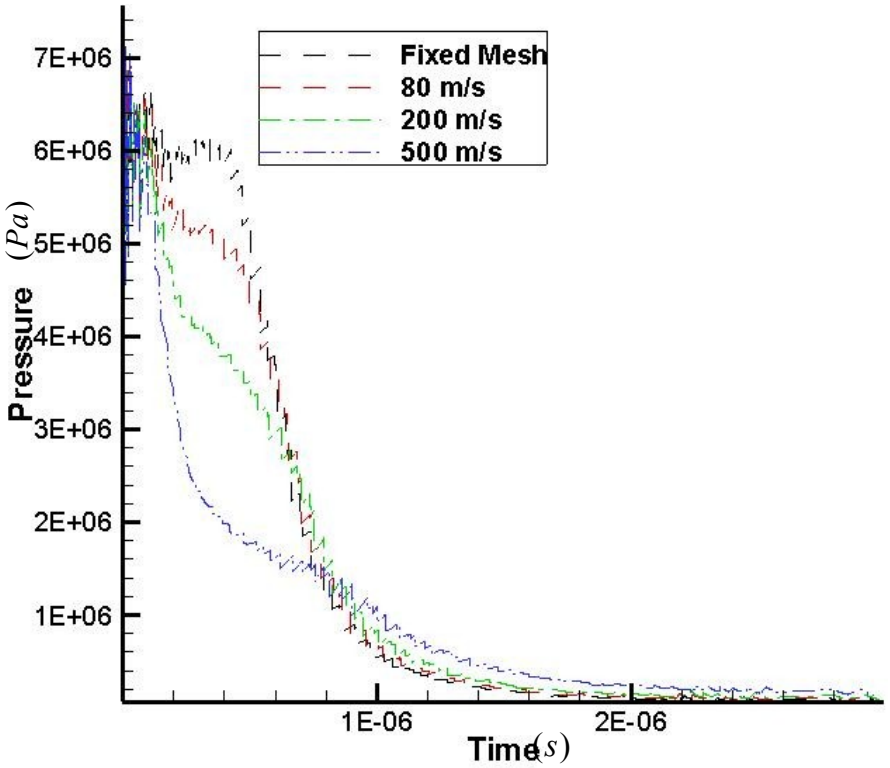

Figure (4-59) – Pressure on the contact surface for the initial diameter of 1.0mm at different opening rates

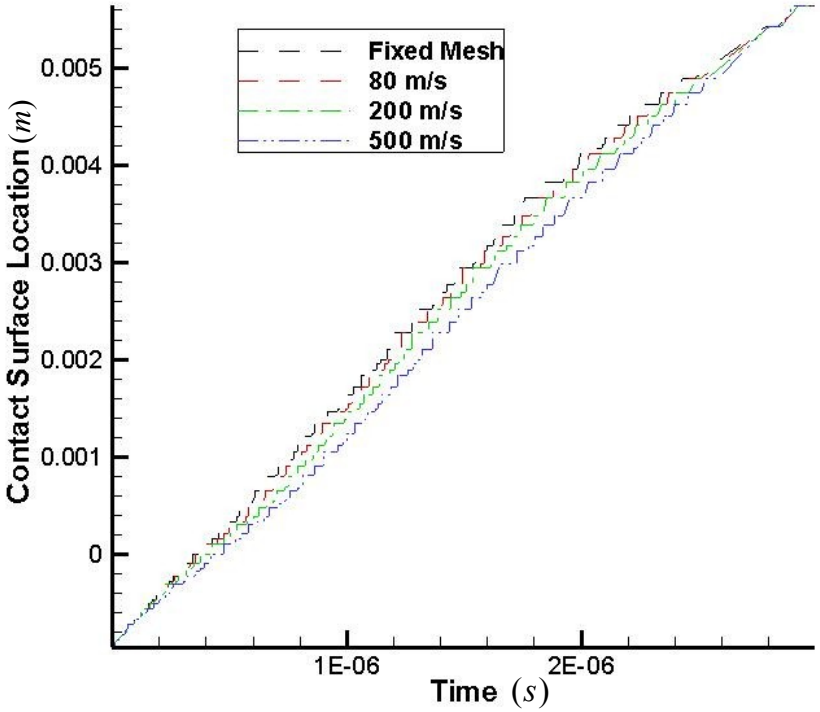

Figure (4-60) – Contact surface location for the initial diameter of 1.0mm at different opening rates

In figures (4-61) and (4-62) pressure and contact surface location versus time at opening rate of 200m/s for the initial release area diameter of 1.0mm, 1.5mm and 2.0mm are given. It is noticed that pressure is higher for higher initial diameters and the difference is not negligible. Contact surface locations are similar up to 2.0 micro seconds and after that the difference appears. After 2.0 micro seconds, the flow advances faster for higher initial diameters.

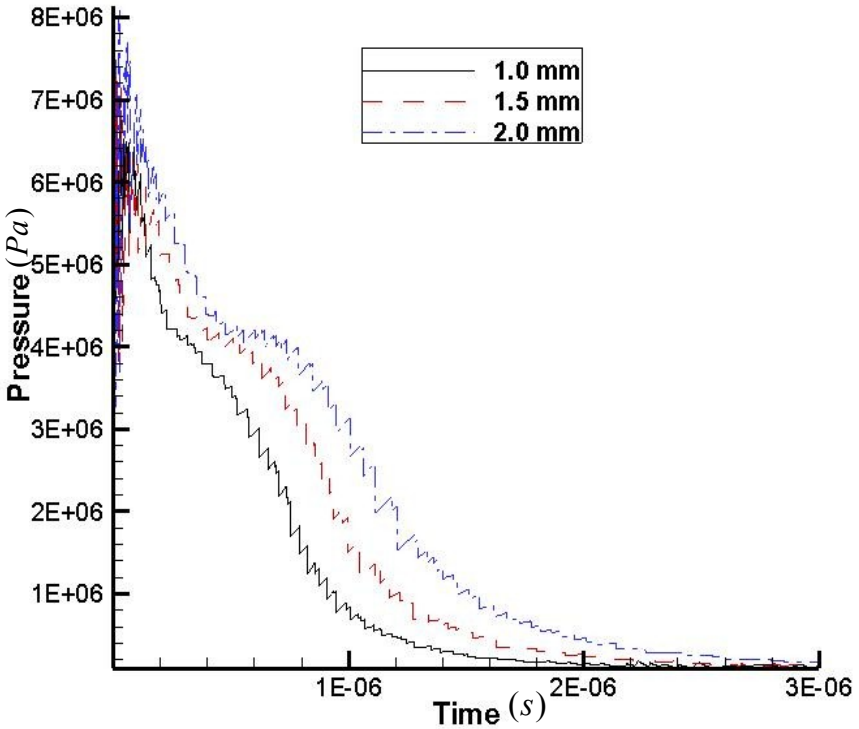

Figure (4-61) – Pressure on the contact surface for different initial diameters at the opening rate of 200m/s

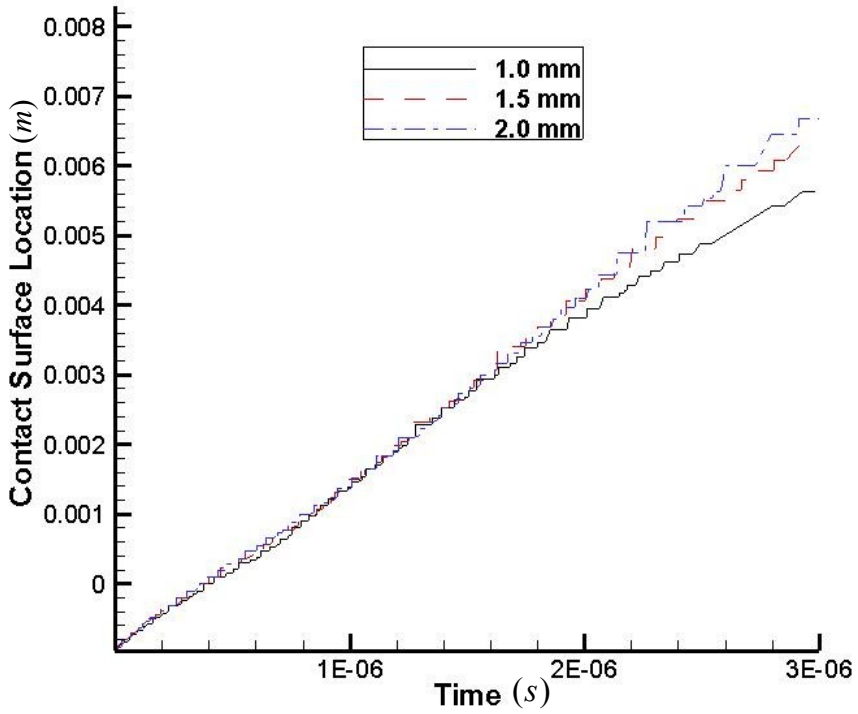

Figure (4-62) – Contact surface location for different initial diameters at the opening rate of 200m/s

A finer mesh is also tested for the moving mesh simulation to see the effect of the mesh quality on the results. This mesh includes almost 2 million node numbers. In figures (4-63) and (4-64) pressure on the contact surface and contact surface location for the coarse and fine meshes and for different opening rates is given. Also in figures (4-65) and (4-66) pressure on the contact surface and contact surface location for the coarse and fine meshes and for different initial diameters is given. It is concluded that the high node number mesh is more accurate. In figures (4-67) and (4-68) pressure on the contact surface and contact surface location for two meshes of 2 and 3 millions nodes are given. The initial diameter is 1 mm and the opening speed is 80 m/s. It is noticed the 2 million nodes mesh is fine enough since the difference in the results is negligible.

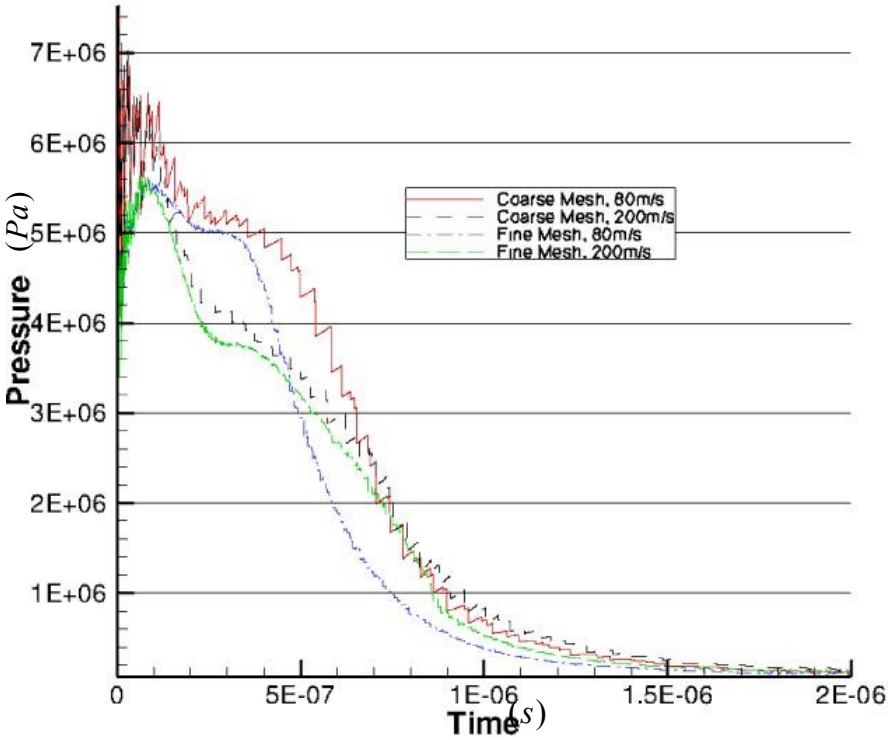

Figure (4-63) – Pressure on the contact surface for two meshes and different opening rates

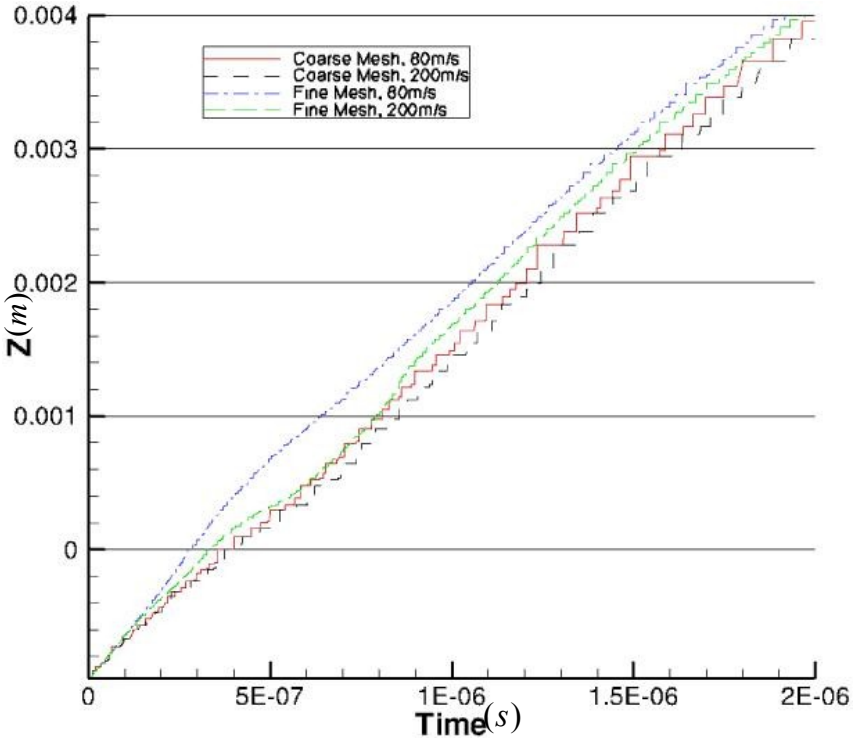

Figure (4-64) – Contact surface location for two meshes and different opening rates

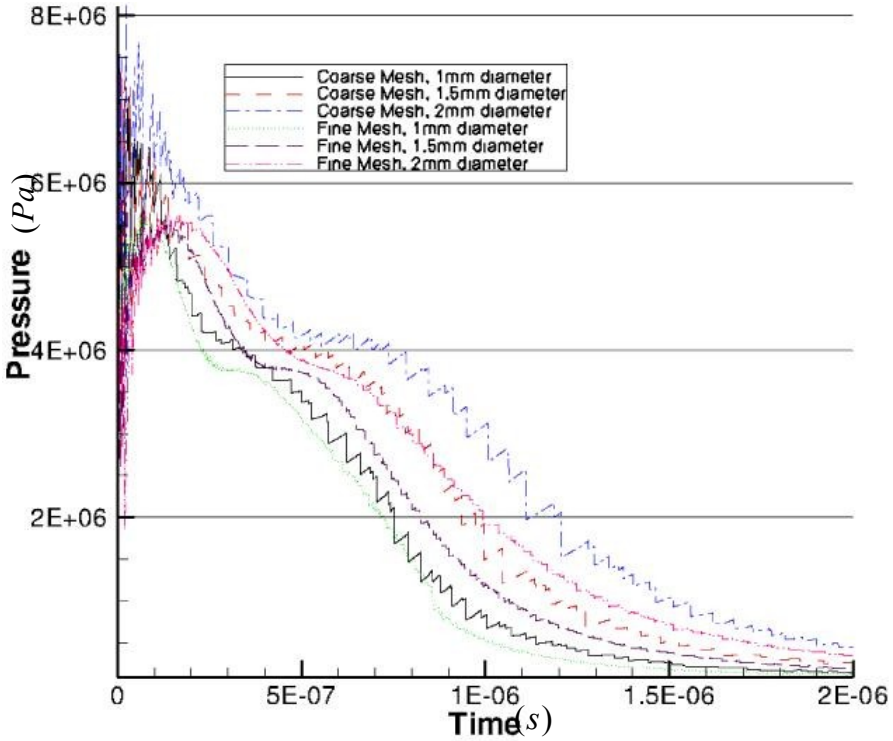

Figure (4-65) – Pressure on the contact surface for two meshes and different initial diameters

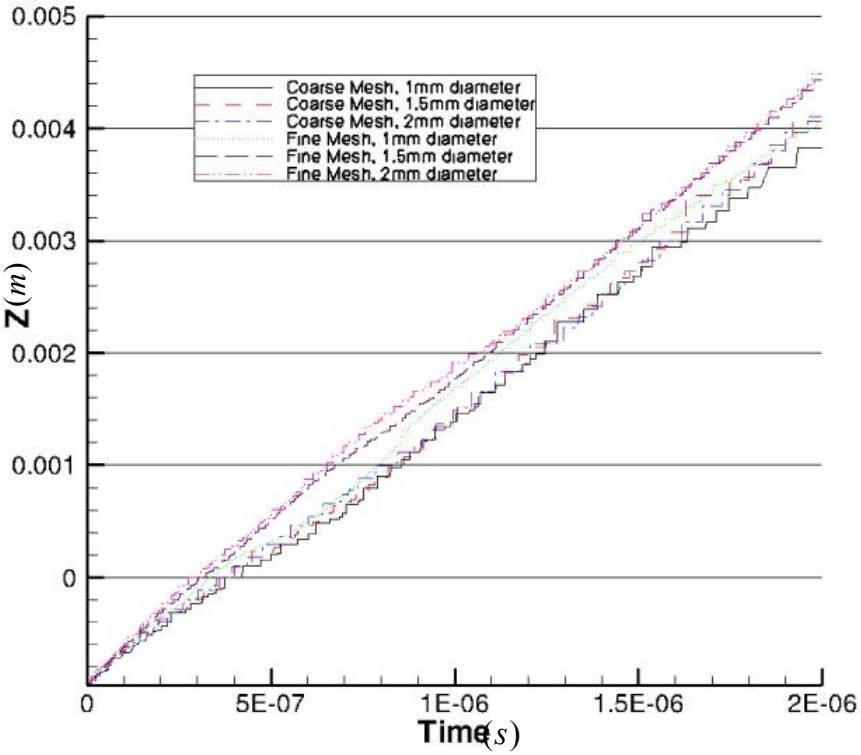

Figure (4-66) – Contact surface location for two meshes and different initial diameters

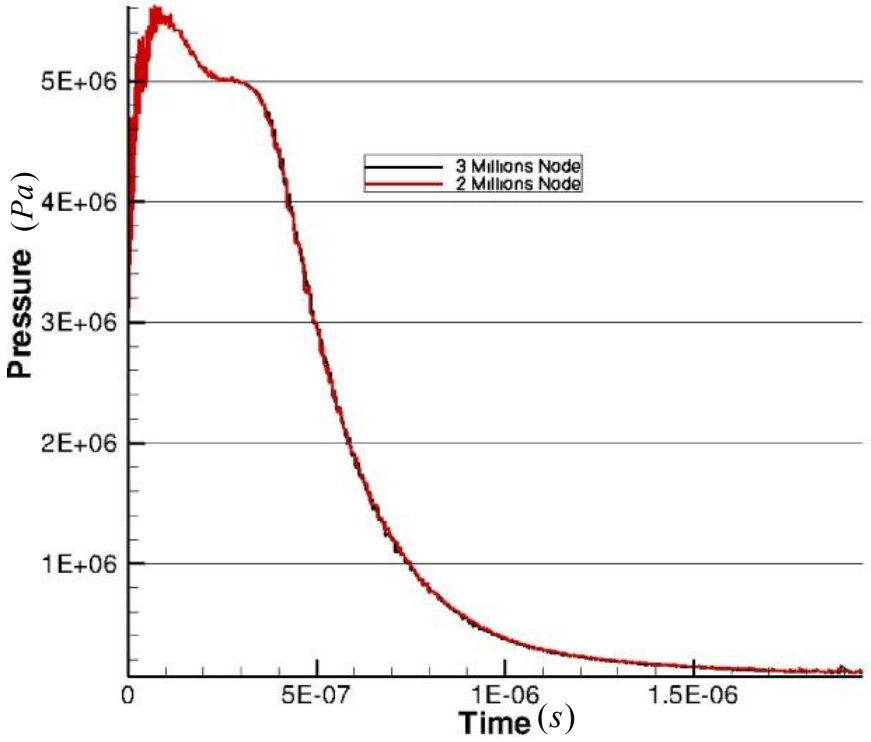

Figure (4-67) – Pressure comparison for fine meshes at opening speed of 80 m/s

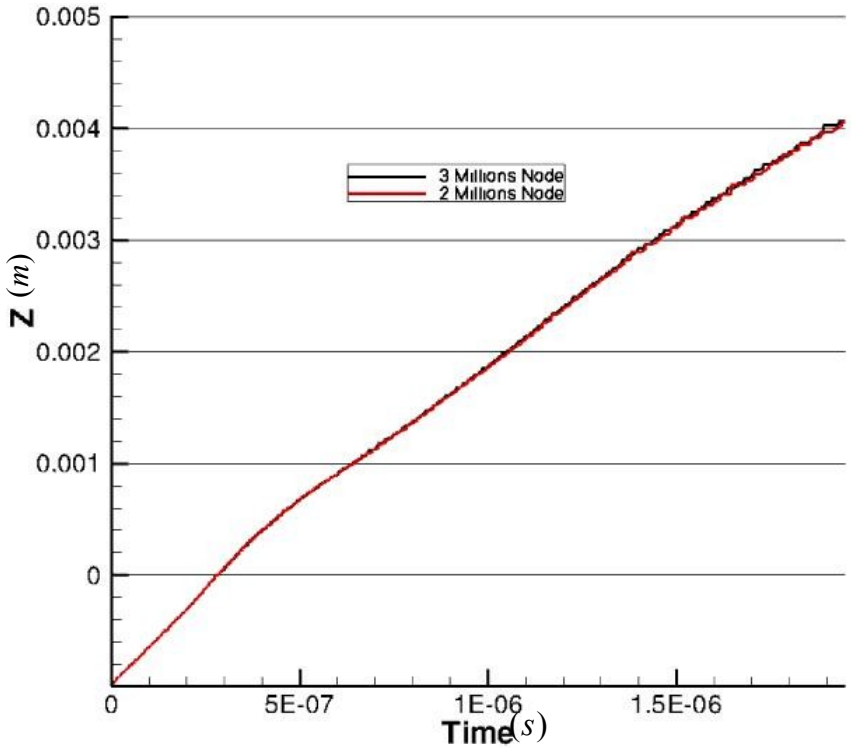

Figure (4-68) – Contact surface comparison for fine meshes at opening speed of 80 m/s

Chapter 5

CONCLUSION AND FUTURE WORK

5-1 Conclusion

Hydrogen release from a high pressure chamber is numerically simulated with computational fluid dynamics. A three dimensional in-house code is developed to investigate all the features of the flow after release.

Hydrogen release into hydrogen is simulated by using the Beattie-Bridgeman and Abel Noble equations. Results show that the difference between the two models is negligible. Hydrogen release in air is only simulated by the Abel Noble model since the Beattie-Bridgeman suffers from stability problems and has shown no advantage over Abel Noble model in case of hydrogen in hydrogen. The release properties are compared with analytical results. Pressures of 10MPa, 34.5MPa and 70MPa are discussed and the results are compared with the ideal gas results. Real gas model is necessary especially for higher pressures as for the initial tank pressure of 70MPa, ideal gas underestimates the release velocity by almost 20 percents while for the initial tank pressure of 10MPa the underestimation is less than 3 percents. The difference between ideal gas and real gas is also observed in the shock location for high pressures. Therefore, based on our test cases, the flow cannot be accurately simulated by ideal gas equation of state for initial tank

pressures of more than 10MPa and a real gas model is required for an accurate simulation.

In reality, the release area expands and does not have a fixed diameter. Three cases of initial release diameter of 1.0mm, 1.5mm and 2.0mm with increasing release area are discussed. Each case is tested for three different opening speeds of 80m/s, 200m/s and 500m/s. Properties on the contact surface are important for combustion discussion, therefore pressure and contact surface location versus time are given for different cases. Each case is investigated until the release time of 3 micro seconds. We conclude that the pressure on the contact surface depends on both opening speed and initial release area diameter. We also note that when the release area is opening faster the pressure decreases faster.

5-2 Contribution

This research results in a tool with following contributions:

- This tool is capable of solving the high pressure hydrogen release using real gas equations of state. Abel Noble equation of state is the real gas model used in this tool. This tool can also be used to simulate the flow using an ideal gas equation of state.
- This tool is able to solve the flow using second order accuracy in space. A modified limiter is employed to apply the second order accuracy. This tool has also the option to switch to first order accuracy.

- This tool has the capability to solve the concentration of hydrogen or air in the hydrogen-air mixture caused after release and finding out the contact surface location at different times.
- This tool uses a moving mesh feature to solve the flow in case of an expanding release area at different speeds. This tool can also be used to solve the flow in case of a fixed mesh.

5-3 Future work

The future work can be divided into two categories:

5-3-1 Algorithm

- Viscous terms are added to the code. Finite element method is used to descritize the viscous terms. Viscous terms are already in the code but they are not tested for this high pressure simulation. This feature is important to capture long term dispersion of hydrogen.
- Large eddy simulation (LES) feature will also be added to the code to consider the turbulence effects. LES is necessary for this high Reynolds number flow. In order to apply LES, the mesh should be of high quality and therefore high number of nodes. More processors are needed for the LES simulation.
- External forces like wind effects and ground effects cannot be neglected for the simulation of this flow. The effect of these forces will be applied for both horizontal and vertical jets. In fact this is the main reason of having a three-dimensional computational domain.

- Muti-species capability will be extended to more than only hydrogen and air. More species will be added and the equations will be changed to couple the equations instead of solving the transport equation at the end of each time step.
- Mesh adaptation is required to increase the number of nodes in critical areas like areas of high gradients. Mesh adaptation will help to save memory by increasing the number of nodes in only the critical areas.
- An ignition model is added to see the possibility of ignition for different tank pressures and different release area diameters.

5-3-2 Application

- The effect of different shapes of the release area including the Irregular shapes can be considered. Various shapes including rectangular shape should be discussed.
- The impact of ground forces on both horizontal and vertical jets is discussed. In reality the ground effects exist and affect the flow pattern. Furthermore, other external forces like wind should be considered.
- The possibility of self-ignition for different scenarios including different tank pressures, different release area shapes and vertical or horizontal jets will be discussed.
- In reality other species in addition to hydrogen and air exist and should be considered in the simulation. The effect of these species is not negligible and should be discussed.

References

[1] M. R. Kameshki, Simulation of Hydrogen Jet Exiting a High Pressure Reservoir, M. Sc. Thesis, Concordia University, 2007

[2] S. Cris, P.M. Sherman, D.R. Glass, Study of Highly Under-Expanded Sonic Jet, AIAA J., 4, pp. 68-71, 1966.

[3] S.M. Dash, D.E. Wolf, and J.M. Seiner, Analysis of turbulent underexpanded jets, part I: parabolized Navier-tokes model, SCIPVIS, AIAA Journal 23, 505-514, 1985.

[4] T.C. Adamson, and J.A. Nicholls, Final Report on the Structure of Jets from Highly underexpanded Nozzles into Still Air, Engineering Research Institute, University of Michigan Ann Arbor, Feb. 1958.

[5] J.A. Wilkes, C.E. Glass, P.M. Danehy, and R.J. Nowak, Fluorescence Imaging of Underexpanded Jets and Comparison with CFD, AIAA paper, 2006-0910, 2006.

[6] S.G. Cheuch, M.C. Lai, and G.M. Faeth, Structure of turbulent sonic underexpanded free jets, AIAA Journal, Vol. 27, 549-559, 1989.

[7] N. L. Lacerda, On the Start up of Supersonic Underexpanded Jets, Ph.D. Thesis, California Institute of Technology, 1987.

[8] A. Martin, M. Reggio, J. -Y. Trépanier, Numerical solution of axisymmetric multi-species compressible gas flow: towards improved circuit breaker simulation, International Journal of Computational Fluid Dynamics, Vol. 22, 259-271, 2008.

[9] M. R. Swain, P. Filoso, E. S. Grilliot and M. N. Swain, Hydrogen leakage into simple geometric enclosures, International Journal of Hydrogen Energy, Vol. 28, 229-248, 2003

[10] W. Breitung, G. Necker, B. Kaup, and A. Veser, Numerical Simulation of Hydrogen Release in a Private Garage, proceedings of Hypothesis IV, p. 368, Strahlsund, Germany, 9-14 September 2001.

[11] S. Mukai, J. Suzuki, H. Mitsuishi, K. Oyakawa, and S. Watanabe, CFD Simulation of Hydrogen Leakage Caused by Fuel Cell Vehicle Accident in Tunnel, Underground Parking Lot and Multistory Parking Garage, Japan Automobile Research Institue, vol. 27, No. 29, 2005.

[12] V. Agranat, Z. Cheng, and A. Tchouvelev, CFD Modelling of Hydrogen Release and Dispersion in Hydrogen Energy Station, Stuart Energy Systems Corporation, Mississauga, Canada, 2004.

[13] A.G. Venetsanos, T. Huld, P. Adams, and J.G. Bartzis, Source, dispesion and combustion modeling of an accidental release of hydrogen in an urban environment, Journal of Hazardous Material, A105, 1-25, 2003.

[14] V.V. Golub, Development of shock wave and vortex structures in unsteady jets, Shock Waves, 3:279-285, 1994.

[15] V. V. Golub, D. I. Baklanov, T. V. Bazhenova, S. V. Golovastov, M. F. Ivanov, I. N. Laskin, N. V. Semin, V. V. Volodin, Experimental and numerical investigation of hydrogen gas auto-ignition, International Journal of Hydrogen Energy 34, 5946-5953, 2009.

[16] R.W. Schefer, W.G. Houf, T. C. Williams, B. Bourne, J. Colton, Characterization of high-pressure, underexpanded hydrogen-jet flames, International Journal of Hydrogen Energy 32, 2081 – 2093, 2007.

[17] L. C. Shirvill, P. Roberts, C. J. Butler, T. A. Roberts, M. Royle, Characterisation of the hazards from jet releases of hydrogen, Proceedings of International Conference on Hydrogen Safety, paper 120005, Pisa, Italy, September 8-10 2005.

[18] J. Dubois, Étude experimentale de jets libres, compressibles ou en precense d'un obstacle, These pour obtenir le titre de Docteur d'Aix-Marseille Université, 2010.

[19] R. Khaksarfard, M. R. Kameshki, M. Paraschivoiu, Numerical simulation of high pressure release and dispersion of hydrogen into air with real gas model, Shock Waves - An International Journal on Shock Waves, Detonations and Explosions, Volume 20, Number 3, 205-216, 2010.

[20] H. Wilkening, and D. Baraldi, CFD Modelling of Accidental Hydrogen Release from Pipelines, The Fisrt International Conference on Hydrogen Safety, Pisa, Italy, Sep. 8-10, 2005.

[21] R. Khaksarfard, M. Paraschivoiu, Numerical Investigation of Hydrogen Dispersion into Air, 18th Annual Conference of the CFD Society of Canada, London, Canada, May 2010.

[22] B. Xu, E. L. Hima, J. X. Wen, S. Dembele, V. H. Y. Tam, T. Donchev, Numerical study of spontaneous ignition of pressurized hydrogen release into air, International Journal of Hydrogen Energy, 34(14), 5954-5960, 2009.

[23] R. Khaksarfard, M. Paraschivoiu, Numerical Investigation of Hydrogen Sonic Jet with Real Gas Model, 17th Annual Conference of the CFD Society of Canada, Ottawa, Canada, May 2009.

[24] Z. Cheng, V. Agranat, A. V. Tchouvelev , W. Houf, S. V. Zhubrin, PRD hydrogen release and dispersion; a comparison of CFD results obtained from using ideal and real

gas law properties, First international conference on hydrogen safety, Pisa, Italy September 8–10, 2005,

[25] B.P. Xu , J. P. Zhang , J. X. Wen , S. Dembele , J. Karwatzki, Numerical study of a higly under-expanded hydrogen jet. Paper presented at the International Conference on Hydrogen Safety, Pisa, Italy, 8-10 September 2005.

[26] Y. –F. Liu, N. Tsuboi, H. Sato, F. Higashino, A. K. Hayashi, Direct numerical simulation on hydrogen fuel jetting from high pressure tank, Proceedings of the 20th international colloquium on the dynamics of explosions and reacting systems, Montreal, Canada, 2005

[27] G. Pedro, F. Peneau, P. Oshkai, and N. Djilali, Computational Analysis of Transient Gas Release from a High Pressure Vessel, Conference CFD, Kingston, Canada, 2006

[28] M. I. Radulescu, C.K. Law, The transient start of supersonic jets, Journal of Fluid Mechanics, Vol. 578, pp. 331-369, 2007.

[29] J.L. Montagne, H.C. Yee, and Vinokur M., Comparative study of high-resolution shock-capturing schemes for a real gas, AIAA Journal, 27(10):1332–1346, 1989.

[30] K. Mohamed, and M. Paraschivoiu, Real gas simulation of hydrogen release from a high-pressure chamber, International journal of hydrogen energy, vol. 30, no8, 903-912, 2005.

[31] P. Wolanski, S. Wojcicki, Investigation into the mechanism of the diffusion ignition of a combustible gas flowing into an oxidizing atmosphere, Proceedings of the Combustion Institute, 14, 1217–1223, 1972.

[32] J. Meguizo-Gavilanes, N. Rezaeyan, M. Tian, L. Bauwens, Shock-induced ignition with single step Arrhenius kinetics, International Journal of Hydrogen Energy, Vol. 36, 2374-2380, 2011.

[33] Z. Liang, L. Bauwens, Detonation structure under chain branching kinetics, Shock Waves, 15, 247-257, 2006.

[34] L. Bédard-Tremblay, L. Fang, J. Melguizo-Gavilanes, L. Bauwens, P. H. E. Finstad, Z. Cheng, A. V. Tchouvelev, Simulation of detonation after an accidental hydrogen release in enclosed environments, International Journal of Hydrogen Energy, Vol. 34, No. 14, 5894-5901, 2009.

[35] J. X. Wen, B. P. Xu, V. H. Y. Tam, Numerical study on spontaneous ignition of pressurized hydrogen release through a length of tube, Combustion and Flame, 156, 2173–2189, 2009.

[36] V. V. Golub, D. I. Baklanov, T. V. Bazhenova, M. V. Bragin, S. V. Golovastov, M. F. Ivanov, V. V. Volodin, Shock-induced ignition of hydrogen gas during accidental or technical opening of high-pressure tanks. Journal of Loss Prevention in the Process Industries, 20, 439-446, 2007.

[37] B. M. Maxwell, One-Dimensional Model for Predicting Ignition During an Accidental Release of Pressurized Hydrogen into Air, M. Sc. Thesis, University of Ottawa, 2010.

[38] F. L. Dryer, M. Chaos, Z. Zhao, J. N. Stein, J. Y. Alpert, C. J. Homer, Spontaneous Ignition of Pressurized Releases of Hydrogen and Natural Gas into Air, Combustion science and technology, 179, 663–694, 2007.

[39] C. Hirsch, Numerical Computation of Internal and External Flows, vol. 2, John Wiley & Sons, 1990.

[40] G. J. Van Wylen, R. E. Sonntag, Fundamental of classical thermodynamics, 2nd ed., New York, John Wiley & Sons, 1976.

[41] K. Mohamed, Hydrogen release from a high-pressure chamber considering real gas effects, M.A.Sc. thesis, Dept. Mechanical Engineering, Concordia University, Montreal, Quebec, 2004.

[42] J.-Y. Trepanier, M. Paraschivoiu, M. Reggio and R. Camarero, A conservative shock fitting method on unstructured grids, Journal of Computational Physics, 126, 421-433,1996.

[43] X. -P. Zhang, D. Zhou, Y. Bao, Mesh motion approach based on spring analogy method for unstructured meshes, Journal of Shanghai Jiaotong University (Science), Volume 15, Number 2, 138-146, 2010.

[44] D. Zenga, C. R. Ethier, A semi-torsional spring analogy model for updating unstructured meshes in 3D moving domains, Finite Elements in Analysis and Design, Volume 41, Issues 11-12, 1118-1139, 2005.

[45] FLUENT 6.1 User's Guide, Chapter 9 - Modeling Flows in Moving and Deforming Zones, Fluent Inc. 2003.

[46] A. Cadiou, NadiaLES : Manuel Theorique, Note Technique CODICIEL-LMFA 2003-01.

[47] H. Ashkenas, F.S. Sherman, The Structure and Utilization of Supersonic Free Jets in Low Density Wind Tunnel, Rarefied Gas Dynamics, Fourth Symposium, Vol. II, Academic, New York, 84-105, 1966.

[48] F. Péneau, G. Pedro, P. Oshkai, P. Bénard, N. Djilali, Transient supersonic release of hydrogen from a high pressure vessel: A computational analysis, International Journal of Hydrogen Energy, Vol. 34, Issue 14, 5817-5827, 2009.

[49] D. Schmidt, U. Krause, U. Schmidtchen, Numerical simulation of hydrogen gas release between buildings, International Journal of Hydrogen Energy 24, 479 – 488 , 1999.

[50] P. Glaister, An approximate linearized Riemann solver for the Euler equations for real gases, Journal of Computational Physics, Vol. 74, 382-408, 1988.

[51] S. Maus, J. Hapke, C. Na Ranong, E. Wüchner, G. Friedlmeier, D. Wenger, Filling procedure for vehicles with compressed hydrogen tanks, International Journal of Hydrogen Energy 33, 4612 – 4621, 2008.

[52] W.S. Young, Derivation of the free-jet Mach-disk location using the entropy-balance principle, Physics of Fluids, vol. 18, 1421-1425, Nov. 1975.

[53] P. Colella, H. M. Glaz, Efficient Solution Algorithm for Riemann Problem for Real Gases, Journal of Computational Physics Vol. 59, pp. 264-289, 1985.

[54] Y. Li, A. Kirkpatrick, C. Mitchell, and B. Willson, Characteristic and Computational Fluid Dynamics Modeling of High-Pressure Gas Jet Injection, ASME J. of Engineering for Gas Turbines and Power, vol. 126, pp. 192-197, 2004.

[55] T.V.R. Rao, R.R. Kumar, and J. Kurian, Near Field Shock Structure of Dual Co-axial Jets, Shock Waves, 6:361-366, 1996.

[56] M. S. Liou, B. Van Leer, J. S. Shuen, Splitting of Inviscid Fluxes for Real gases, Journal of Computational Physics Vol. 87, pp. 1-24, 1990.

[57] J. L. Montagne, H. C. Yee, M. Vinokur, Comparative Study of High-Resolution Shock Capturing Schemes for a Real Gas, AIAA Journal 27(10), 1332-1346, 1989.

[58] J. S. Wallace, A Comparison of Compressed Hydrogen and CNG Storage, International Journal Hydrogen Energy, 9(7), 609-611, 1984.

[59] R. C. Johnson, Real-Gas Effects in Flow Metering, Technical paper-Society of Manufacturing Engineers, 269-278, 1974.

[60] R. Abgrall, An Extension of Roe's Upwind Scheme to Algebraic Equilibrium Real Gas Models, Computers & Fluids 19(2), 171-182, 1991.

[61] J. S. Wallace, C. A. Ward, Hydrogen as a Fuel, International Journal Hydrogen Energy 8(4), 255-268, 1983.

[62] S. Dembele, J. Zhang, J. X. Wen, Exploratory Study of Under-expanded Sonic Hydrogen Jets and Jet Flames, Proceedings of the 5th International Seminar on Fire and Explosion Hazards, Edinburgh, UK, 23-27 April 2007.

[63] B. Xu, E. L. Hima, J. X. Wen, S. Dembele, V. H. Y. Tam, T. Donchev, Numerical study on the spontaneous ignition of pressurized hydrogen release through a tube into air, Journal of Loss Prevention in the Process Industries, 21(2), 205-213, 2008.

[64] Y. L. Liu, J. Y. Zheng, P. Xu, Y. Z. Zhao, H. Y. Bie, H. G. Chen, H. Dryver, Numerical Simulation on the Diffusion of Hydrogen due to High Pressured Storage Tanks Failure, Journal of Loss Prevention in the Process Industries, 22(3), 265-270, 2009.

[65] B. Xu, J. X. Wen, S. Dembele, V. H. Y. Tam, S. J. Hawksworth, The effect of pressure boundary rupture rate on spontaneous ignition of pressurized hydrogen release, Journal of Loss Prevention in the Process Industries, 22(3), 279-287, 2009.

[66] B. Angers, A. Hourri, P. Benard, P. Tessier, J. Perrin, Simulations of Hydrogen Releases from a Storage Tank: Dispersion and Consequences of Ignition, The Fisrt International Conference on Hydrogen Safety, Pisa, Italy, Sep. 8-10, 2005.

[67] A. O. Hector, A. R. Choudhuri, Numerical simulation of hydrogen diffusion in the vicinity of a cubical building instable stratified atmospheres, International Journal of Hydrogen Energy, 31, 2356–2369, 2006.

[68] K. Takeno, K. Okabayashi, A. Kouchi, T. Nonaka, K. Hashiguchi, K. Chitose, Dispersion and explosion field tests for 40MPa pressurized hydrogen, International Journal of Hydrogen Energy, 32, 2144–2153, 2007.

[69] T. Tanaka, T. Azuma, J. A. Evans, P. M. Cronin, D. M. Johnson, R. P. Cleaver, Experimental study on hydrogen explosions in a full-scale hydrogen filling station model, International Journal of Hydrogen Energy, 32, 2162–2170, 2007.

[70] B. Maté, I. A. Graur, T. Elizarova, I. Chirokov, G. Tejeda, J. M. Fernandez, S. Montero, Experimental and numerical investigation of an axisymmetric supersonic jet. Journal of Fluid Mechanics, 426, 177-197. 2001.

[71] I.O. Sand, K. Sjoen, and J.R. Bakke, Modeling of Release of Gas from High-Pressure Pipelines, International Journal for Numerical Methods in Fluids, vol. 23, 953-983, 1996.